Aus dem Department für Augenheikunde Tübingen,

Forschungsinstitut für Augenheilkunde,

Sektion für Experimentelle Vitreoretinale Chirurgie

A mouse model of advanced Stargardt disease and its application in preclinical assessment of a new pharmacological therapy

Inaugural-Dissertation

zur Erlangung des Doktorgrades

der Medizin

der Medizinischen Fakultät

der Eberhard Karls Universität

zu Tübingen

vorgelegt von

Fang, Yuan

2020

Dekan: Professor Dr. I.B. Autenrieth

1. Berichterstatter: Professor Dr. U. Schraermeyer
2. Berichterstatter: Professor Dr. F. Ziemssen

Tag der Disputation: 10.12.2019

Table of contents

List of Figures

List of tables

List of Abbreviation

11c-N-ret-PE	N-11-cis-retinylidene-PE
11cRDH	11-cis-retinol dehydrogenase
A2-DHP-PE	A2-dihydropyridinephosphatidylethanolamine
A2E	N-retinylidene-N-retinylethanolamine
A2PE	di-retinoid-pyridinium-phosphatidylethanolamine
all-trans-RE	all-trans-retinyl esters
all-trans-ROL	all-trans-retinol
BCVA	Best-corrected visual acuity
BM	Bruch’s membrane
CC	choriocapillaris
CNV	choroidal neovascularization
CRPs	complement regulatory proteins
CRRY	complement receptor 1-like protein y
cSLO	confocal scanning laser ophthalmoscopy
DHA	Docosahexaenoic Acid
DMSO	Dimethyl sulfoxide
ELM	external limiting membrane
EOG	electro-oculogram
ERG	electroretinogram
EZ	ellipsoid zone
FAF	fundus autofluorescence
FERG	focal electroretinogram
FFERG	full-field electroretinogram
GA	geographic atrophy
GC	ganglion cell
HE	Hematoxylin and Eosin
hESCs	Human embryonic stem cells

i.p.	intraperitoneal
INL	inner nuclear layer
IPL	inner plexiform layer
iPSCs	induced pluripotent stem cells
IS	inner segment
IS/OS	inner segment/outer segment of photoreceptors
IZ	interdigitation zone
MAC	membrane attack complex
NIR-AF	near-infrared autofluorescence
N-ret-PE	N-retinylidene-PE
ONH	optic nerve head
ONL	outer nuclear layer
OPL	outer plexiform layer
OS	outer segment
O_SO_4	Osmiun tetraoxide solution
PE	phosphatidylethanolamine
PERG	pattern electroretinogram
PUFAs	polyunsaturated fatty acids
RNFL	retinal nerve fiber layer
ROS	reactive oxygen species
RPE	retinal pigment epithelium
SD	standard deviation
SD-OCT	spectral-domain optical coherence tomography
SW-AF	short-wavelength autofluorescence
TEM	transmission electron microscopy
UAC	uranyl acetate
VCMs	visual cycle modulators

1. Introduction

1.1 Stargardt disease

Stargardt disease (STGD1, OMIM #248200), known as the most prevalent form of inherited macular dystrophy, was first described by Stargardt (Stargardt, 1909). One of the hallmarks of the disease is the premature accumulation of lipofuscin, an autofluorescent pigment increasing with aging in RPE cells. The onset age of Stargardt disease and the progression of vision deterioration is widely variable between individuals. The onset of most patients is commonly in the first two decades. Early-onset Stargardt has been defined as age at onset<10 years old (Lambertus et al., 2015), while late-onset Stargardt can be diagnosed at age>45 years old (Lambertus et al., 2016). It has been suggested that better prognosis of visual acuity is related to a later age of onset (Rotenstreich et al., 2003). In most patients, Stargardt disease initially manifests with bilateral central vision impairment, including dyschromatopsia and central scotomata, then develop into a poor vision outcome over time (Blacharski, 1988). The diagnosis of Stargardt disease dominantly depends on fundus examination, electrophysiological investigations (including full-field electroretinogram (FFERG), pattern electroretinogram (PERG), focal electroretinogram (FERG) and electro-oculogram (EOG)), fundus autofluorescence (FAF), spectral-domain optical coherence tomography (SD-OCT). The ophthalmoscopy reveals the presence of macular and/or peripheral round or pisciform-shaped yellowish-white flecks (Blacharski, 1988). Macular involvement is observed as either a “beaten-bronze” appearance, macular granularity, a bull’s-eye appearance, or retinal pigment epithelium (RPE) depigmentation with atrophy (Glazer and Dryja, 2002). According to fundus appearance, Stargardt disease has been classified into four stages (Table 1) (Fishman, 1976).

Table 1: Based on fundus appearance, a clinical classification of Stargardt disease proposed by Fishman. (Fishman, 1976)

Stage I	Fundus pigmentary lesion including irregular pigment speckles, “beaten-bronze” appearance and atrophy. The presence of round or pisciform-shaped ring of flecks within one disk diameter around fovea with normal ERG and normal EOG.
Stage II	Flecks distribute more widely (> one-disc diameter) even extend beyond temporal arcades and the optic disc with subnormal cone/rod response and delayed dark adaption
Stage III	Resorbable flecks and choriocapillaris (CC) atrophy diffuse in the fundus with cone/rod dysfunction in ERG and subnormal ratio in EOG. Impairment can be observed in the posterior pole and peripheral retina.
Stage IV	Resorbable flecks with extensive CC and RPE atrophy diffuse in the whole fundus. Further decrease in cone and rod amplitudes.

Based on electrophysiological phenotypes, Stargardt disease has also been classified into distinct subtypes, as shown in Table 2 (Lois et al., 2001). As described by Lois et al., the patients in Group 1 usually have fundus flecks and atrophy confining to macular and better visual acuity. While the patients in Group 3 have macular atrophy with widespread fundus flecks and worst visual acuity (Lois et al., 2001). A longitudinal study of Stargardt disease has determined that FFERG can be an indicator of visual prognosis (Fujinami et al., 2013a). The patients in Group 1 were likely to have a better visual prognosis, only 22% of them turned out to significant ERG deterioration. 47% of patients in Group 2 progressed to Group 3 during the follow-up period. All patients in Group 3 with worst prognosis showed significant ERG deterioration (Fujinami et al., 2013a).

Table 2: Based on electrophysiological assessments, patients with Stargardt disease has been classified into three groups. (Lois et al., 2001)

Group 1	Severe abnormal PERG and FERG show macular dysfunction.

	Normal scotopic and photopic amplitudes in FFERG.
Group 2	Severe abnormal PERG and FERG. Abnormally loss of photopic amplitudes but normal scotopic amplitude in FFERG. Abnormal EOG in some patients.
Group 3	Severe abnormal PERG and FERG. Loss of photopic and scotopic amplitudes in FFERG. Abnormalities in EOG.

Autofluorescence techniques used to visualize the distribution of two major pigments in RPE cells: lipofuscin, and melanin. FAF as an imaging tool for evaluation of lipofuscin is performed by illuminating the retina with a wavelength of 488 nm. It facilitates to understand pathophysiology, diagnosis, prognosis of retinal disease and monitoring of novel therapies (Schmitz-Valckenberg et al., 2008). In Stargardt disease, three major features have been found among FAF abnormalities. The first feature appeared as the area with decreased FAF fusing into multiple patches. Second, some abnormalities of AF showed as flecks with increased FAF. Additionally, the yellow/white flecks observed with funduscopy corresponded to flecks with increased or decreased FAF. The third feature appeared as dark patched of FAF loss at the posterior pole, which correlated to RPE and choriocapillaris atrophy (Kellner et al., 2009). The longitudinal study has classified Stargardt patients into three subtypes based on FAF evaluation, as shown in Table 3. The observation of FAF patterns is suggested to provide advice on prognosis (Fujinami et al., 2013b).

Table 3: Based on FAF findings, Stargardt patients have been classified into three subtypes. (Fujinami et al., 2013b)

Type 1	Hypo-AF confined to the fovea and surrounded by a homogeneous background, with/without perifoveal flecks of hyper-AF or hypo-AF
Type 2	Hypo-AF confined to the macula and surrounded by a heterogeneous background, with diffuse flecks of hyper-AF or hypo-AF extending to the vascular arcades
Type 3	multiple patches with hypo-AF at the posterior pole with a

	heterogeneous background, with/without flecks of hyper-AF or hypo-AF

Near-infrared autofluorescence (NIR-AF) imaging with the excitation of 788nm wavelength is used to visualize melanin in RPE and choroid. Abnormalities in NIR-AF have been observed with three features as well (Kellner et al., 2009). The predominant feature was the patch with decreased NIR-AF signal. The second feature was areas of absent NIR-AF signal which also corresponded to areas of FAF loss. The third feature, few foci with increased NIR-AF were observed corresponding to foci of increased FAFs (Kellner et al., 2009). Compared to FAF findings, NIR-AF abnormalities were more widespread. It is suggested that NIR-AF sensitively monitoring early fundus changes in Stargardt patients has advantages over short-wavelength autofluorescence (SW-AF) (Greenstein et al., 2015, Anastasakis et al., 2011).

SD-OCT as a noninvasive technique, provides optical cross-sectional images of the retinal laminar structure. For Stargardt disease, SD-OCT is used to detect the different morphology of retinal flecks as well as the structural integrity of RPE and photoreceptor layers. Five distinct groups of retinal flecks in Stargardt disease have been distinguished by SD-OCT, as shown in Table 4 (Voigt et al., 2010). Furthermore, central foveal thickness detected by OCT has been associated with visual acuity loss (van Huet et al., 2014).

Table 4: Based on SD-OCT scans, five groups of retinal flecks in Stargardt patients have been distinguished. (Voigt et al., 2010)

Group A	Various extents and shapes of accumulation of hyper-reflective material limited to the outer segment (OS) of the photoreceptors.
Group B	Increased accumulation of hyper-reflective material starting in the OS and expanding further through the junction of the inner segment (IS)/OS, up to the external limiting membrane (ELM).
Group C	Resemble the lesions in Group B but protrude into the outer nuclear layer (ONL).

Group D	An accumulation of hyper-reflective material confined to ONL the outer nuclear layer.
Group E	Drusen-like small pigment epithelium detachments associated with an accumulation of hyper-reflective material protruding into different layers to the varying level.

1.2 *ABCA4* gene mutation & accumulation of lipofuscin

Mutations in the *ABCA4* gene, a member of ATP-binding cassette (ABC) transporter gene superfamily A, are responsible for distinct phenotypes of STGD1. ABCA4 protein, a 2,273-amino-acid protein encoded by *ABCA4* gene, is a membrane-associated protein mainly localized in the outer segments (OS) of rod and cone photoreceptors (Allikmets et al., 1997, Molday et al., 2000). All-trans-retinal (produced after photo absorption by visual pigment) and excess 11-cis-retinal (not required for visual cycle) react with phosphatidylethanolamine (PE) to form the Schiff base conjugate N-retinylidene-PE (N-ret-PE) and N-11-cis-retinylidene-PE (11c-N-ret-PE) in the disk membrane, respectively (Wald, 1968, Boyer et al., 2012). Biochemical evidence illustrates that ABCA4 protein, acting as a flippase, translocates N-ret-PE and 11c-N-ret-PE from lumen side to the cytoplasmic side of the disk membrane. 11c-N-ret-PE could be isomerized to N-ret-PE. Then all-trans-retinal, dissociating from hydrolysis of N-ret-PE, is reduced to all-trans-retinol (all-trans-ROL) for the further steps of the visual cycle on the cytoplasmic side (Weng et al., 1999, Quazi and Molday, 2014). Lack of functional ABCA4 protein induces accumulation of N-ret-PE which further forms di-retinoid-pyridinium-phosphatidylethanolamine (A2PE) in the disk. The material accumulating in the OS is transferred to the RPE cells because of phagocytosis after several days. After outer segment shedding and phagocytosed by retinal pigment epithelium (RPE) cells, A2PE is hydrolyzed in acidic phagolysosomes and result in formation of N-retinylidene-N-retinylethanolamine (A2E) and other bisretinoids, the main constituents of lipofuscin that accumulates in lysosome

system (Fig.1) (Mata et al., 2000, Sparrow et al., 2012). Bisretinoids are the best-characterized components of retinal lipofuscin, including A2E and other fluorophores such as the isomers A2E and isoA2E, oxidized derivatives of A2E, A2-dihydropyridinephosphatidylethanolamine (A2-DHP-PE), A2-dihydropyridine-ethanolamine which forms from phosphate hydrolysis of A2-DHP-PE and all-trans-retinal dimer-phosphatidylethanolamine (Parish et al., 1998, Wu et al., 2009). Recently, *ABCA4* gene is found to express in RPE cells. ABCA protein in RPE endolysosomes is proposed to perform a similar function for clearance of all-trans-retinal and 11-cis-retinal by translocating both isomers of N-ret-PE from phagolysosome to the cytoplasmic surface, where all-trans-retinal and 11-cis retinal are reduced to their respective retinols. The lack of ABCA4 protein in RPE endolysosomes also leads to accumulation of bisretinoids in RPE cells (Lenis et al., 2018).

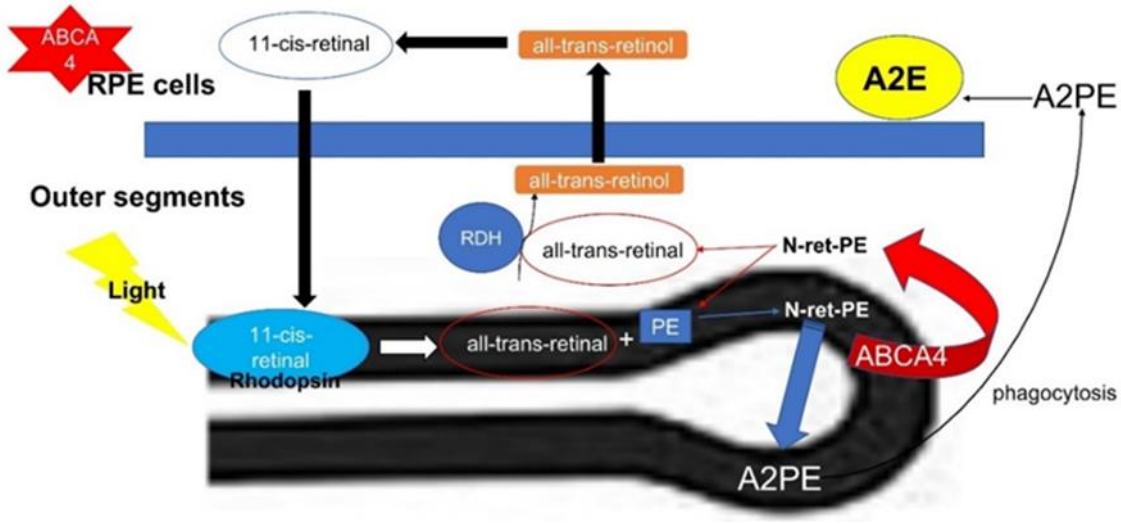

Figure 1: The role of ABCA4 in the clearance of all-trans-retinal.

Abnormal accumulation of lipofuscin disrupts RPE cellular function and causes secondary photoreceptor degeneration. *In vitro* study has proved that A2E alone can induce RPE cell death even in low concentrations (Mihai and Washington, 2014). The accumulation of A2E can cause the alkalinization of lysosomes (Holz et al., 1999). Lipofuscin in RPE is proved to photoinducedly generate reactive

oxygen species (ROS) such as singlet oxygen and superoxide anion, cause lipid peroxidation, enzyme inactivation, protein oxidation, DNA damage, and impairment of lysosome integrity. The photoreactivity of lipofuscin leads to RPE cells dysfunction and atrophy, followed by photoreceptor degeneration (Wassell et al., 1999, Sparrow and Boulton, 2005). A2E and its photo-oxidized products, subsequent to photoactivation and cleavage activate complement system contributing to the chronic inflammatory processes and retinal degeneration in RPE (Zhou et al., 2009, Zhou et al., 2006).

A2E is considered to be an initiator in the process of blue light-induced apoptosis and necroptosis of RPE cells (Sparrow et al., 2000). Upon exposure to blue light, A2E and iso-A2E generate excessive ROS which directly damages cells. A2E epoxides and oxiranes, formed by photooxidation of bisretinoids, damage DNA in RPE cells (Sparrow et al., 2003, Radu et al., 2004). Photooxidation of bisretinoids in RPE cells is shown to activate the complement system and alter the transcription of genes for stress response, apoptosis and the immune response (Zhou et al., 2006, van der Burght et al., 2013). Products of blue light-induced A2E photooxidation leads to modifications of intrinsic proteins in Bruch's membrane (BM) and is suggested to contribute to BM thickening (Thao et al., 2014, Zhou et al., 2015). Besides, the formation of A2-PE, the A2E precursor which is susceptible to the same photooxidation can be modulated by light intensity (Ben-Shabat et al., 2002, Kim et al., 2006). Recent studies suggested 415–455 nm blue-violet light that generates the highest amount of ROS and produces the highest level of mitochondrial dysfunction is toxic to A2E-loaded RPE cells (Marie et al., 2018). In normal life, one source of blue light is the digital screen. Studies suggested that *in vivo*, periodic exposure to smartphone-mimic low-luminance blue light induces retinal damage including decreased total retinal thickness, atrophy of photoreceptors, and injured neuron transduction in the retina(Lin et al., 2017). Additionally, the RPE of STGD1 patients is suggested at

increased risk of photo-oxidative stress with 3-fold higher oxygen uptake and light absorption by lipofuscin granules compared to age-matched controls (Teussink et al., 2017).

1.3 Animal models for STGD1

The Pigmented *Abca4*$^{-/-}$ mouse was first generated by Weng et al.as an animal model of Stargardt disease (Weng et al., 1999). This animal model has been characterized with 1) delayed rod dark adaptation resulted from transient accumulation of the opsin/all-trans-RAL photoproduct in the disc, 2) delayed clearance of all-trans-RAL and transient depletion of all-trans-ROL and all-trans-retinyl esters (all-trans-RE) after a photobleach, 3) increased PE in OS and RPE, 4) containing protonated N-ret-PE instead of nonprotonated form, 5) lipofuscin (A2E&iso-A2E) accumulation in RPE (Weng et al., 1999). Even though there is an early elevation of 488nm-excited fundus AF intensity contributed by the accumulation of lipofuscin, no sign of photoreceptor degeneration can be observed in pigmented *Abca4*$^{-/-}$ mouse according to ERG test and histological analysis (Charbel Issa et al., 2013). This mouse model has been considered to mainly reflect the early stages of ABCA4-related retinopathy. However, a mild retinal degeneration could be caused in 3-month old *Abca4*$^{-/-}$ mice by 10,000-lux white fluorescent light exposure for 60 min (Maeda et al., 2008).

The Albino *Abca4*$^{-/-}$ mouse has been generated by crossing the *Abca4*$^{-/-}$ mutation onto an albino background (Radu et al., 2004). Besides the higher levels of all-trans-retinal, albino *Abca4*$^{-/-}$ mouse shows similar high A2E/iso-A2E levels and 1.5-fold higher oxiranes compared with pigmented ones (Radu et al., 2004). By the age of 7 months, albino *Abca4*$^{-/-}$ mouse starts to show a mild retinal degeneration (Radu et al., 2011). Then, by 11 months, albino ones showing thinning of OS are approximately 40% degenerate with OS shortening (Radu et al., 2008). Albino *Abca4*$^{-/-}$ mouse is also observed with higher expression of oxidative-stress genes, elevated complement-activation products and lipid

peroxidation products, but lower complement regulatory proteins (CRPs) and thickening of Bruch's Membrane (Radu et al., 2011).

The Mice carrying a double knock-out of the Rdh8 and Abca4 genes has been reported as another animal model for Stargardt disease (Maeda et al., 2008). RDH8 is an enzyme that contributes to clearance of all-trans-retinal in rod and cone OS (Rattner et al., 2000). Besides disrupted all-trans-retinal clearance, accumulation of A2E, A2E-precursors and retinal dimer conjugates, *Abca4*$^{-/-}$ *Rdh8*$^{-/-}$ mice has been described with dramatic retinal degeneration including cone/rod dysfunction, RPE/photoreceptor atrophy, basal laminar deposits, increased thickness of Bruch's membrane and even choroidal neovascularization by 10 month-age (Maeda et al., 2008). The retinal degeneration in this mouse model progresses with age.

The comparison of the age-dependent ultrastructural changes in above three mouse models for Stargardt disease has been studied (Taubitz et al., 2018). It is suggested that albino *Abca4*$^{-/-}$ mouse shows the earliest onset among the Stargardt mice with OS shortening, disordered disk membranes, damaged IS. These three kinds of Stargardt's mice show different morphology of lipofuscin. In pigmented *Abca4*$^{-/-}$ mice lipofuscin with clearly defined margin shows clearly defined AF. In albino *Abca4*$^{-/-}$ mice, lipofuscin with not defined margin exhibited blurry AF, indicating loss of the lysosomal membrane. While in *Abca4*$^{-/-}$*Rdh8*$^{-/-}$ mice, the lipofuscin shows both clearly defined and blurry lipofuscin autofluorescence (Taubitz et al., 2018). Cideciyan et al. have proposed six stages of ABCA4-related retinopathy according to fundus AF patterns, AF intensity and electrophysiological assessments, as shown in Table 5 (Cideciyan et al., 2004). There are still many challenges in generating mice model to reflect stages of ABCA4-related retinopathy (Cideciyan et al., 2015). The Pigmented *Abca4*$^{-/-}$ mouse containing melanin which has been suggested to be involved in Stargardt pathology and substantial accumulation of lipofuscin shows no sign of retinal

degeneration (Charbel Issa et al., 2013, Taubitz et al., 2018). Albino *Abca4*$^{-/-}$ mice without the presence of melanin show a mild retinal degeneration with further lipofuscin accumulation but do not match the normal retinas of human heterozygote carriers (Radu et al., 2004, Radu et al., 2008). The *Abca4*$^{-/-}$*Rdh8*$^{-/-}$ mice show retinal degeneration and hypersensitivity to acute light damage (Maeda et al., 2008). However, mutation of RDH8 gene is not associated with the pathology of Stargardt disease in patients.

Table 5: Six stages of ABCA4-related retinopathy have been defined by Cideciyan et al. (Cideciyan et al., 2004)

Stage Ⅰ	normal retinal structure and function of photoreceptors and RPE with normal AF intensity and texture.
Stage Ⅱ	The only abnormality is increased AF intensity which indicates the first pathophysiological process in human ABCA4-related retinopathy.
Stage Ⅲ	Besides abnormal increased AF intensity, the fundus is observed with an abnormal increase of AF texture.
Stage Ⅳ	The declined function of photoreceptors and slowing of the retinoid cycle, in addition, to increase of mean AF intensity and texture.
Stage Ⅴ	Further functional deficiency of photoreceptors and a decline of mean AF intensity.
Stage Ⅵ	Retinal regions with complete degeneration of photoreceptors and RPE with undetectable visual function and fundus AF.

Additionally, lack of macular, the mouse model is suggested that it might mimic the pathophysiology in the peripheral human retina (Charbel Issa et al., 2013). A canine model carrying homozygous ABCA4 loss-of-function mutation has been developed as a large animal model of human STGD (Makelainen et al., 2019).

1.4 Current therapeutic options for STGD1

Currently, there is still no effective therapy for STGD1 available in the clinic. However, the experimental and clinical trials for the treatment of STGD1 never

cease. The therapeutic researches of STGD1 include modulating visual cycle to inhibit the generation of vitamin A toxic dimers (ALK-001, isotretinoin, VM200, emixustat, and A1120), complement inhibition, gene therapy, stem cell therapy.

1.4.1 Stem cell transplantation

Given that RPE degeneration and the secondary photoreceptors degeneration are hallmarks of Stargardt disease, stem cell therapy also has been studied as a therapeutic option to restore RPE function and visual outcomes. Human embryonic stem cells (hESCs) are the best at differentiating into a variety of cell types (Amit et al., 2000). A prospective phase I/II study has been done to evaluate the safety and tolerability of subretinal transplantation of hESC-derived RPE in Stargardt patients (age >18 years) (ClinicalTrials.gov, Identifier: NCT01345006) (Schwartz et al., 2015). Another phase I/II open-label dose-escalation clinical trial has been conducted to assess survival of transplanted cells, retinal structure and function after subretinal injection of 200,000 hESC-derived RPE cells (clinicaltrials.gov identifier: NCT01469832) (Mehat et al., 2018).

1.4.2 Gene Therapy

In accordance with the pathogenesis of STGD1, gene replacement therapy by delivering a functioning copy of the *ABCA4* gene is one of the potential treatment options. Adeno-associated viruses (AAV) vectors with high capability of photoreceptor transduction are commonly used for gene therapy of inherited retinal diseases. Even though the AAV vector is not capable of *ABCA4* delivery, because the size of ABCA4 cDNA (6.8kbp) is beyond the packaging capacity of AVV vector (5 kbp). A Phase I/II clinical trial of gene therapy (SAR422459) based on lentivirus vector has been conducted to deliver ABCA4 gene by subretinal injection based on lentivirus vector (ClinicalTrials.gov Identifier: NCT01367444) (Parker et al., 2016). The results of this clinical trial are still unknown. Recently, the potential of dual AAV vectors for ABCA4 delivery has been warranted to have efficient photoreceptor transduction and rescue effect on retinal degeneration

(Trapani et al., 2015). Nonviral DNA nanoparticles (NPs) with the capability of packaging genes with large size have been developed to deliver ABCA4 by subretinal injection to ABCA4-deficient mice (Han et al., 2012).

1.4.3 pharmacotherapeutic options

It is known that in STGD1 patients and *Abca4*$^{-/-}$ mice, augmented complement activation resulting from bisretinoid-containing lipofuscin accumulation in the RPE cells (Zhou et al., 2009). Thus, modulation of the complement system has been considered as a therapeutic option of Stargardt disease. Lenis, T. L. et al. have subretinally injected AAV carrying the complement receptor 1-like protein y (CRRY) coding sequence (AAV-CRRY) in 4-week-old *Abca4*$^{-/-}$ mice (Lenis et al., 2017). By increasing expression of CRRY in RPE cells, complement factors C3/C3b and bisretinoids accumulation reduced in the RPE, retinal degeneration also got retarded (Lenis et al., 2017). Avacincaptad pegol (Zimura®, Ophthotech Corporation), a C5 complement inhibitor has been explored to inhibit MAC formation as a therapeutic option of STGD1. A Phase 2b randomized, double-masked, controlled trial has been recently conducted to evaluate the safety and efficacy of Zimura™ in STGD1 patients (ClinicalTrials.gov Identifier: NCT03364153).

Isotretinoin (13-cis-retinoic acid), a drug for the treatment of acne, has been found to inhibit 11-cis-retinol dehydrogenase (11cRDH), thus slow rhodopsin regeneration and recovery of rod sensitivity after light exposure in rats, but cause no photoreceptor degeneration (Sieving et al., 2001). Fenretinide (N-(4-hydroxyphenyl) retinamide, 4-HPR) is known to compete with retinol for binding sites on retinol-binding protein 4 (RBP4) and thus reduce serum retinol potently and reversibly (Berni and Frarte, 1992). The inhibitory effect of fenretinide on the formation of A2E and lipofuscin in RPE has been validated in *Abca4*$^{-/-}$ mice (Radu et al., 2005). However, fenretinide has a dose- and time-dependent apoptotic effect on ARPE-19 cells and increases the generation of reactive oxygen species

(ROS) (Samuel et al., 2006). The reported side effect of fenretinide treatment include decreased visual acuity, night blindness and visual disturbance (Hussain et al., 2018). A1120, a nonretinoid RBP4 antagonist, also induces a dramatic reduction in serum RBP4 and significantly suppresses accumulation of lipofuscin bisretinoids in the *Abca4*$^{-/-}$ mice (Dobri et al., 2013). ALK-001, C20-D3-vitamin A, containing deuterium atoms instead of C20 hydrogen atoms of vitamin A slows in vitamin A dimerization (Kaufman et al., 2011). Slowed A2E biosynthesis has been proved in wild-type rodents treated with C20-D3-vitamin A (Kaufman et al., 2011). Administration of C20-D3-vitamin A also slows A2E biosynthesis in albino *Abca4*$^{-/-}$ mice, thus attenuates lipofuscin accumulation and delays deterioration of retinal function (Ma et al., 2011).

11-cis-retinoid are absent in *Rpe65*$^{-/-}$ mice lacking rhodopsin (Redmond et al., 1998). It supports that RPE65 protein is essential in the visual pigment regeneration pathway (Redmond et al., 1998). Nonretinoid mRPE65 antagonists inhibiting regeneration of 11-cis-retinal after bleaching, profoundly suppresses the formation of A2E in *Abca4*$^{-/-}$ mice. These antagonists can be candidates of treatment of Stargardt disease (Maiti et al., 2006). Emixustat (also known as ACU-4429) is a non-retinoid derivative of retinylamine (Ret-NH2) that inhibits the activity of RPE65 and prevent A2E accumulation. Emixustat is originally developed as an oral tablet formulation for the treatment of GA secondary to AMD (KUBOTA et al., 2014).

Additionally, other supplements aiming at anti-oxidation and anti-inflammation have been investigated to treat Stargardt disease. Supplement of lutein or zeaxanthin has a potential protective effect by anti-oxidation and inhibition of A2E formation (Bhosale et al., 2009). Supplement of omega-3 polyunsaturated fatty acids (PUFAs) (eicosapentaenoic acid (EPA, C20:5n-3): docosahexaenoic acid (DHA, C22:6n-3) =5:1) suppresses A2E and lipofuscin accumulation, reduces C3

level, limiting a complement-related inflammation thus prevents photoreceptor degeneration in *Abca4*$^{-/-}$ mice (Prokopiou et al., 2018).

1.5 Aim of the study

1.5.1 Establish an animal model of advanced STGD-1 by illuminating *Abca4*$^{-/-}$ mice with blue light

In consideration of the deleterious effect of the combination of excessive blue light and lipofuscin on the retina, studying clinical ophthalmic photography, retinal function and structure in blue light-irradiated pigmented *Abca4*$^{-/-}$ mice may provide more implications for researches of lipofuscin-related human retinal disease such as advanced stage of Stargardt disease and age-related macular degeneration (AMD). The *Abca4*$^{-/-}$ mice were illuminated with blue light to establish a mouse model that reflect advanced stages of STGD1. For comparison, the peri-macular tissue of a Stargardt patient and blue light-illuminated *Abca4*$^{-/-}$ mice were investigated as well.

1.5.2 photoreceptor rescue effect of Remofuscin® treatment in blue light illuminated *Abca4*$^{-/-}$ mice

Accumulation of lipofuscin in the RPE cells, as a cytologic hallmark of Stargardt disease, results in the progressive deterioration of the retina, leading to vision loss.

There have been many therapeutic options for STGD1 aiming to slow or prevent the formation of lipofuscin. However, none of the above can remove the existing lipofuscin. Removal of the existing lipofuscin from the RPE is a potential strategy to ameliorate the clinical symptoms and slowing the progression of Stargardt disease. Remofuscin® [(7R,8R,9R)2, 3-dimethyl-8-hydroxy-7 (2-methoxyethoxy)-9-phenyl7,8,9,10-tetrahydro-imidazo-[1,2-h][1,7]-naphthyridine] (Katairo, Kusterdingen, Germany), belongs to tetrahydropyridoether class of compounds is introduced as an inhibitor of H, K-ATPase for therapy of gastroesophageal reflux disease previously (Simon et al., 2007). It also has been

reported to reduce lipofuscin by stimulating the exocytosis of the RPE cells (Julien and Schraermeyer, 2012). In primates, oral treatment of Remofuscin® (24 mg/kg/day) for one year resulted in the reduction of lipofuscin with no adverse effects (Julien and Schraermeyer, 2012).

Remofuscin® is the only one known to remove existing lipofuscin efficiently. In this study, the pigmented *Abca4*$^{-/-}$ mice were treated with Remofuscin® by intravitreal injection to assess the protective effect of Remofuscin® on retina against blue light damage.

2. Materials and Methods

2.1 Mice

All experiments concerning animals were designed to conform to the German laws governing the use of experimental animals. All procedures were conducted with the approval of the local agency for animal welfare (Einrichtung für Tierschutz, Tierärztlichen Dienst und Labortierkunde der Eberhard Karls Universität Tübingen, Tuebingen, Germany) and the local authorities (Regierungspräsidium Tübingen, Tuebingen, Germany). The pigmented *Abca4*$^{-/-}$ mice (129S4/SvJae-Abca4tm1Ght) were purchased from The Jackson Laboratory (Bar Harbor, Maine, US). Albino *Abca4*$^{-/-}$ mice (BALB/c-Abca4 tm1Ght) were kindly donated by G. Travis and R. Radu (University of California, Los Angeles, CA). The mice were housed in a 12:12-h light (approximately 50 lux in cages)–dark cycle with food and water ad libitum.

2.2 Blue-light illumination

Pigmented and albino *Abca4*$^{-/-}$ mice, aged 9 months, were intraperitoneal (i.p.) anesthetized with a three-component narcosis consisting of 0.05mg/kg Fentanyl, 5 mg/kg Midazolam and 0.5mg/kg Medetomidine. Pupils got dilated with a mixture of 0.5% tropicamide and 2.5% phenylephrine hydrochloride. Methocel® (Omni Vision, Puchheim, Germany) was applied to moisten the cornea. During light

illumination, a glass slip was placed on the cornea of the exposed eye, while the fellow eye was covered by tinfoil to avoid irradiation. The distance from the cornea surface to the lamp was kept as 1.3±0.1 cm to ensure the light intensity is 50 mW/cm^2. The settings of the lamp and the mice were shown in Fig. 2. Both eyes were exposed to blue light (wavelength: 430nm) at an intensity of 50 mW/cm^2 for 15min successively. After light illumination, the mice were hypodermic injected with the antidote, a mixture of 1.2mg/kg naloxone, 0.5mg/kg flumazenil and 2.5mg/kg atipamezole. The mice were kept in the dark room for seven days before the further assessments

Figure 2. The settings of the mice and the lamp for blue light illumination.

2.3 Treatment with Remofuscin®

To assess the protective effect of Remofuscin® on the retina, part of the pigmented *Abca4*$^{-/-}$ mice were treated with Remofuscin® or vehicle solution 28 days before they were exposed to blue light. The mice were anesthetized by Isoflurane (Isoflurane CP®, CP-Pharma, Germany) inhalation (3.5% isoflurane and 25% oxygen). Pupils were fully dilated with Medriaticum drops (Pharmacy of the University of Tuebingen, Tuebingen, Germany). One drop of Novesine (OmniVision, Puchheim, Germany) was applied as topical anesthetics before

injection. The mice were positioned under a surgical microscope. Remofuscin® was dissolved in Dimethylsulfoxide (DMSO, Merck, Darmstadt, Germany) at a concentration of 2g/ml. A Hamilton syringe with a 26-gauge cannula was used for intravitreal injection. Intravitreal injection was performed by inserting the tip of the syringe into eyes at a 45° angle through the sclera and reached into the vitreous body without damaging the lens or posterior retina, as shown in Fig.3. The right eyes of the mice were injected with 2µl sterile phosphate buffered saline (PBS, Gibco®, Darmstadt, Germany) containing 40µg Remofuscin® and 1% DMSO. The right eyes of another group of mice were intravitreally injected with 2µl vehicle solution (sterile PBS containing 1%DMSO). The left eyes of these mice were kept untreated. After injection, antibiotic eye drops (Gentamicin-POS®, URSAPHARM, Saarbrücken, Germany) were applied for protection. Then the mice were looked after carefully till recovery from anesthesia. The timeline of Remofuscin® treatment was shown in Fig. 4.

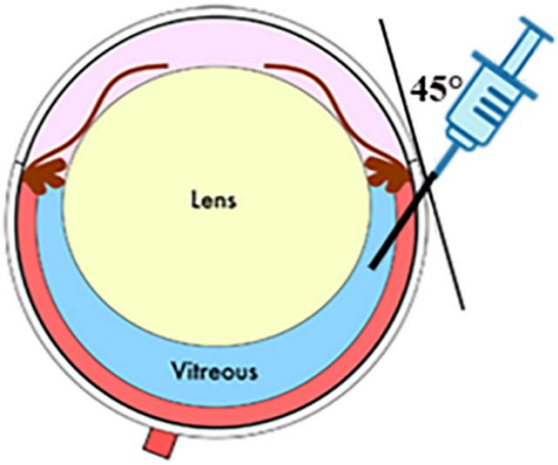

Figure 3. Intravitreal injection. The tip of the syringe was inserted into eyes at a 45° angle through the sclera and reached into the vitreous body of mice.

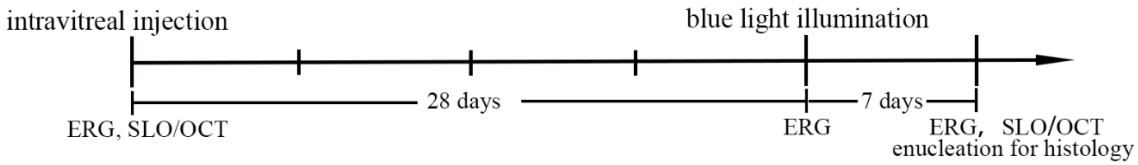

Figure 4. Experimental timeline. The right eyes of the mice were intravitreal injected with Remofuscin®/vehicle. 28 days later, the mice were illuminated by blue light (430 nm,

15min, 50 mW/cm^2). The mice were investigated by ERG and OCT before and seven days after blue light illumination. Seven days after blue light illumination, the mice were sacrificed, and the eyes were enucleated for histological analysis

2.4 Electroretinography

Full-field Electroretinogram (ERG) was performed before blue light illumination and seven days after blue light illumination. Mice were dark adapted for more than 16 hours before ERG investigation. All procedures were completed in a dark room with a dim red light. Mice were intraperitoneally injected with ketamine (100 mg/kg) and xylazine (5mg/kg). Pupils were fully dilated. Methocel® was dropped onto the surface of the cornea to protect the eyes from drying out. The mice were placed in the middle of the platform. A pair of gold wire ring as the positive electrodes were lightly placed onto the cornea of the mice. The reference electrode was inserted into the skin of the forehead and the ground electrode was placed subcutaneously near the tail, as shown in Fig.4.

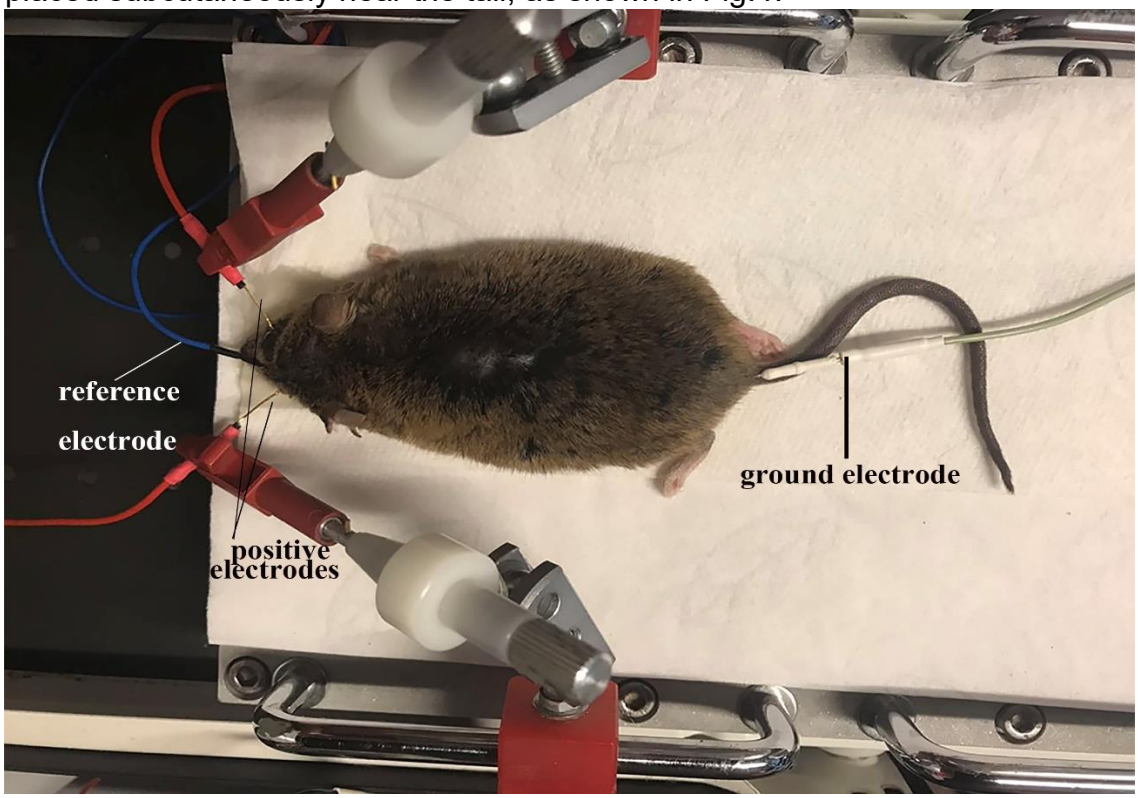

Figure 5. The mice were placed in the middle of the platform. A pair of gold wire ring as the positive electrodes were placed onto the cornea of the mice. The reference electrode was inserted into the skin of the forehead and ground electrode was placed subcutaneously near the tail

For the evaluation of rod photoreceptor function (scotopic ERG), seven strobe flash stimuli were presented in a Ganzfeld with flash intensities from 0.0003 cds/m^2 to 25 cds/m^2 (0.0003, 0.00095, 0.0095, 0.095, 3, 10, 25 cds/m^2). After 10 min of light adaption (30 cds/m^2 white-light), the function of cone photoreceptors (photopic ERG) was investigated with 3 and 10 cds/m^2 white-flash stimuli. The amplitude of the ERG a-wave was measured from the baseline to the maximum a-wave peak, and the ERG b-wave was measured from the trough of the a-wave to the maximum b-wave peak. The a-wave reflects the function of the photoreceptors, while the b-wave reflects the function of bipolar cell and Müller cell.

2.5 Fundus autofluorescence images acquisition

Before blue light illumination and seven days after blue light illumination, a confocal scanning laser ophthalmoscopy (cSLO; SpectralisTM HRA+OCT, Heidelberg Engineering, Heidelberg, Germany) was used for fundus AF images acquisition as reported previously (Charbel Issa et al., 2012). The mice were anesthetized with an intraperitoneal injection of the three-component narcosis. Methocel® was applied on the surface of the cornea after full dilation of pupils (diameters>2mm). For the application of the Spectralis® to the analysis of mouse retina, a 78 dpt non-contact slit lamp lens (Volk Optical, Inc., Mentor, OH 44060, USA) was fixed directly in front of the device. Additionally, a custom-made contact lens (100 dpt) was positioned onto the cornea. The mouse was placed on a three-dimensional platform which is adjustable to acquire clear scanning images.

Near-infrared reflectance (NIR-R) mode was performed first to align the camera and acquire well-focused images centered on the optic nerve head (ONH). SW-AF and NIR-AF images were recorded simultaneously with the excitation of 488 nm laser and 788 nm laser, respectively. All the fundus fluorescence images were recorded with 55°and 30°angle of view, 768*768 pixels image size, the detector sensitivity setting at 100 after the fundus was exposed to blue laser for 20

seconds. Automatic real-time (ART) function was activated for images capture. 15 consecutive frames were captured in video format, and then the averaged-images were also saved in “non-normalization” mode for quantitation of fundus AF. Normalized images as the average of 100 successive frames were captured as well. For correlative analysis, the normalized SW-AF images were coded with green color, and the normalized NIR-AF images were coded with red color. The color-coded SW-AF and NIR-AF images were merged by Image J software.

2.6 Images analysis

The quantification of fundus AF was performed by Image J software according to the published method (Charbel Issa et al., 2012). Non-normalized images recorded with 55°angle of view and same sensitivity were used for quantitative analysis. Briefly, the mean grey value of each raw non-normalized image was measured in entire fundus subtracted the area of optic nerve head. The area for quantitative measurement of the mean grey value was defined within an annular area, concentric to the optic disc center. The radius of the inner circle and outer circle were defined as 50 and 200 pixels, respectively, as shown in Fig.6. The grey value of zero signal which is affected by ambient light was recorded automatically for each image and showed as “offset” in the “information panel”. For the calculation of the corrected mean grey value of fundus AF images, “grey value offset” was subtracted from the grey value measured from the area of interest. The corrected grey value was used to represent AF intensity of fundus AF image.

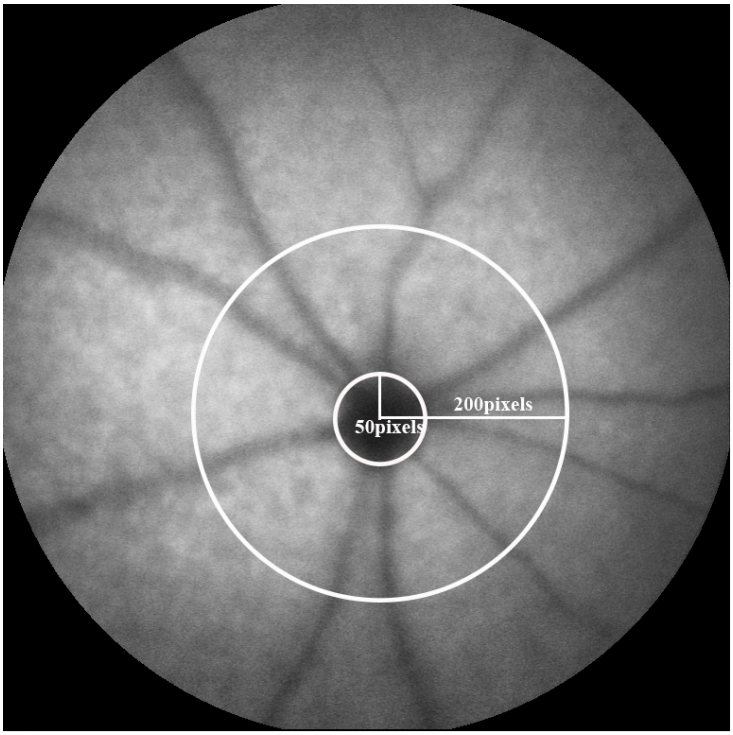

Figure 6. Quantification of mean intensity of fundus AF. The annular area for quantitative measurement of the mean grey value was defined as the area between one inner circle (radius:50 pixels) and one outer circle (radius: 200 pixels).

2.7 OCT and retinal thickness measurement in OCT images

Spectralis^{TM} HRA+OCT was performed for OCT scans as well. All the OCT images were recorded in the 30°field of view. To measure the retinal thickness *in vivo*, line scans were performed vertically through the ONH. The OCT images for quantification were recorded as the averaging of 100 B-scans. Volume scans centered at optic nerve head were recorded in both horizontal and vertical directions. At least 32 B-scans were acquired for volume scan and registered to NIR-R images or SW-AF images, which were simultaneously recorded, for correlation of SW-AF images, NIR-AF images and OCT scans.

Total retinal thickness was measured as the distance from the retinal nerve fiber layer (RNFL) to the inner segment/outer segment of photoreceptors (IS/OS). The retinal thickness was measured every 200μm interval beginning from ONH to superior and inferior along the vertical axis in OCT images for statistic analysis, as shown in Fig.7.

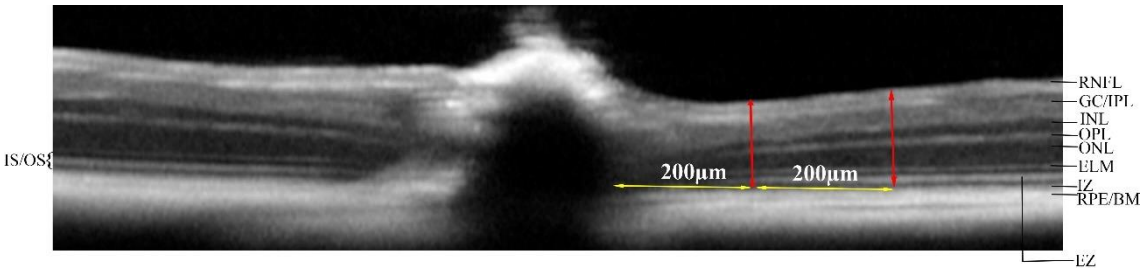

Figure 7. Measurement of retinal thickness in OCT images. Retinal thickness was measured from the retinal nerve fiber layer (RNFL) to the inner segment/outer segment of photoreceptors (IS/OS) and measured every 200μm interval beginning from ONH to superior and inferior along the vertical axis in OCT images. RNFL: retinal nerve fibre layer; GC: ganglion cell; IPL: inner plexiform layer; INL: inner nuclear layer; OPL: outer plexiform layer; ONL: outer nuclear layer; ELM: external limiting membrane; EZ: ellipsoid zone; IS: inner segment; OS: outer segment; IZ: interdigitation zone; RPE: retinal pigment epithelium; BM: Bruch's membrane.

2.8 Preparation samples for Light Microscopy and Transmission Electron Microscopy (TEM)

2.8.1 Embedding of samples

For the histological analysis, the *Abca4*$^{-/-}$ mice were sacrificed seven days after blue light illumination. The age-matched, non-treated *Abca4*$^{-/-}$ mice were used as control. Before enucleation, the eyes were marked with the stitches at the position of 12 o'clock, then they were fixed in 5% glutaraldehyde overnight at 4℃. The corneas and lens were removed. Then the eyecups were hemisected into halves through the ONH along the vertical axis of the eyecups. The half embedded for the ultra-thin section was post-fixed with 1% OsO_4 in 0.1 M cacodylate buffer (pH 7.4), then stained with saturated uranyl acetate (UAC). The chemical reagents for Epon embedding are listed in Table 6. The procedures and details of embedding the eyecups with Epon are shown in Table.7. Epon was made from Glycid ether 100 (53.6%), 2-Dodecenylsuccinic acid anhydride (6.7%), Methylnacid anhydride (38.28%), 2,4,6-Tris (dimethyl aminomethyl) phenol (1.5%). To prepare usable Epon, all the reagents should be added in the indicated order and mixed for 10min in the dark place.

Table 6. The chemical reagents for Epon embedding.

Reagents	Company	
Glutaraldehyde (25%)	AppliChem, Darmstardt, Germany	
Dimethylarisinic acid sodium salt	Merck, Darmstadt, Germany	
Osmiun tetraoxide solution (O_SO_4) 4%	Carl Roth, Karlsruhe, Germany	
Ethanol (absolute for analysis EMSURE®)	Merck, Darmstadt, Germany	
UAC	Electron Microscopy Science, Hatfield, USA	
Propylenoxid	Serva, Heidelberg, Germany	
Glycid ether 100 for electron microscopy	Preparation of Epon	Serva, Heidelberg, Germany
2-Dodecenylsuccinic acid anhydride		
Methylnacid anhydride		
2,4,6-Tris(dimethylaminomethyl)phenol		

Table 7. The procedures of embedding the eyecups with Epon for electron microscopy.

Procedure	Reagent	time
Fixation	5% glutaraldehyde in 0.1M cacodylate buffer (Dimethylarisinic acid sodium salt in distilled water)	Overnight at 4℃
Washing	0.1M cacodylate buffer	10 min*3 times
Post-fixation	2% O_SO_4 in 0.1 M cacodylate buffer	2 hours
Washing	0.1 M cacodylate buffer	10 min*3 times
Dehydration	30% ethanol	15 min

	50% ethanol	15 min
	70% ethanol	15 min
Block staining	UAC in 70% ethanol	Overnight at 4℃
Dehydration	70% ethanol	15 min
	80% ethanol	15 min
	95% ethanol	15 min
	absolute ethanol	20 min
	absolute ethanol	20 min
intermedium	propylenoxid	20 min*2 times
Resin	propylenoxid:Epon=1:1	2 hours
	Epon	2 hours
	Epon	1 hour
Polymerization	60℃	48 hours

Another half for fluorescence microscopy was only washed with 0.1 M cacodylate buffer without OsO_4 post-fixation or UAC staining. Both halves were dehydrated with a graded series of ethanol and propylene oxide. The specimens were then embedded in Epon. The procedures of embedding sample for fluorescence microscopy are listed in Table 8.

Table 8. The procedures of embedding samples for fluorescence microscopy.

Procedure	Reagent	time
Fixation	5% glutaraldehyde in 0.1M cacodylate buffer (Dimethylarisinic acid sodium salt in distilled water)	Overnight at 4℃
Washing	0.1M cacodylate buffer	10 min*3 times
Dehydration	30% ethanol	15 min
	50% ethanol	15 min
	70% ethanol	15 min

Dehydration	70% ethanol	15 min
	80% ethanol	15 min
	95% ethanol	15 min
	Ethanol (absolute for analysis)	20 min
	Ethanol (absolute for analysis)	20 min
intermedium	propylenoxid	20 min*2 times
Resin	propylenoxid:Epon=1:1	2 hours
	Epon	2 hours
	Epon	1 hour
Polymerization	60℃	48 hours

2.8.2 Preparation of semi-sections for light microscopy

The glass slides were coated with 0.01% Poly-L-lysine solution (Sigma-Aldrich, Schnelldorf, Germany) in advance. The semi-thin and ultra-thin sections were prepared with a Reichert-Jung Ultracut E ultramicrotome (Leica Biosystems, Nussloch, Germany). Firstly, I trimmed the Epon blocks to get a flat trapezoid-shapes surface with sloping sides by using a razorblade. Then, the blocks and a diamond knife were fixed in the cantilever arm and the knife holder of the ultramicrotome, respectively. After orienting the block and adjusting the distance from the block to the diamond knife, the ultramicrotome started to make the semi-thin sections in the thickness of 700nm. Before transferring the sections, I placed a drop of distilled water onto the glass slide. Then the floating sections were transferred from the boat of the knife to the drop of water by using a glass stick with the end mounted a metal loop. The slide then was placed on a warm hot plate to evaporate the water and make the section adhere to the slide. The semi-thin sections were stained with toluidine blue (0.5% toluidine blue in 2.5% $NaHCO_3$). Epon was dropped onto glass slides as a mounting medium. After covered by a coverslip, the glass slide was kept in a 60℃ oven overnight.

2.8.3 Preparation of ultra-sections and Image acquisition for TEM

Ultra-thin sections were sectioned with a thickness of 70nm by using an ultra-diamond knife. The ultra-thin sections were collected by formvar-coated grids and then kept in room temperature till water evaporating from the grids. Post-staining with Lead Citrate is needed to enhance the contrast of biological materials and acquire images with high resolution in TEM (WATSON, 1958b). Staining after embedding could avoid distorting structure (WATSON, 1958a). I post-stained the ultra-thin sections with lead citrate (0.1g/25ml) by placing the grid onto the surface of a droplet of lead citrate for 1 min. Importantly, the side with the samples of the grid should be facing the staining droplet. Then the grids with ultra-thin sections should be kept in air overnight to get dry again.

The sections were examined by transmission electron microscope (Zeiss, EM 902, Jena, Germany). The electron microscope consists of three parts: the illumination system (the electron gun and condenser lenses), the specimen stage, the imaging system (lenses that determine the magnification and the spatial resolution of the TEM images) (Egerton, 2005b). Variation of the intensity of TEM images results from the transmitting electrons scattered by the atoms of the specimen. (Egerton, 2005a). Bright-field images were acquired by the TEM. The dark area of the bright field image is attributed to elastic electron scattering by the regions of higher atomic number and subsequent absorption of scattered electrons at the objective diaphragm (Egerton, 2005a).

2.9 Quantification of RPE nuclei and photoreceptor nuclei

Semi-thin sections (700 nm) stained with toluidine blue were investigated by light microscope (Zeiss Axioplan2 imaging, Zeiss, Jena, Germany) and used for histological analysis and nuclei quantification. The images of semi-thin sections through the ONH were recorded with a 63× oil objective for quantification of RPE nuclei and photoreceptor nuclei. The multiple images from the same eye were composited to show the entire retina by the Image Composite Editor software. The number of nuclei was quantified within each 200μm-interval starting next to

the optic nerve head and continuing superiorly and inferiorly along the vertical meridian. The area from 2mm superior to 2mm inferior was included for the analysis. The average of the data from three sections of each eye was obtained as the mean value of each interval. The quantification was performed by using Image-Pro® Plus 6.0 software (Media Cybernetics, Rockville, USA).

2.10 Fluorescence microscopy

Post-fixation with OsO_4 or staining with other heavy metals weakens retinal AF. The hemisphere without OsO_4 fixation or UAC staining was used to examine retinal AF. The semi-thin sections (500 nm) were photographed with a 63× oil objective by using a Zeiss Axioplan2 imaging microscope (Zeiss, Jena, Germany). The images were obtained using a lipofuscin filter set (excitation 360 nm, emission 540 nm) (Taubitz et al., 2018) and a Cy7 filter set (excitation 672.5-747.5nm, emission 765-855 nm) for NIR-AF (Taubitz et al., 2018, Oguchi et al., 2018). Fluorescence images were merged by using Image J software.

2.11 Preparation for paraffin sections

To prepare paraffin sections for immunofluorescence staining, eyes (with cornea and lens) were kept in 4.5% formaldehyde (Carl Roth, Karlsruhe, Germany) for fixation after enucleation. Dehydration of eyes was accomplished by an automated tissue processor (Leica TP1021, Leica Biosystems, Germany). The whole process was listed in Table 9.

Table 9. The process of dehydration of eyes before paraffin embedding.

1. 70% Ethanol—1 hour	2. 96% Ethanol—1 hour
3. 96% Ethanol—1 hour	4. 96% Ethanol—1 hour
5. 99% Ethanol—1 hour	6. 99% Ethanol—1 hour
7. 99% Ethanol—1-hour	8. xylene—1 hour
9. xylene—2 hour	10. xylene—2 hour
11. Paraffin—2 hour	12. Paraffin—2 hour

The eyes were embedded with paraffin wax by using a paraffin embedding station

(Leica EG 1140H, Leica Biosystems, Germany). Paraffin sections were cut with a thickness of 4μm by using a manual microtome (Leica RM2235, Leica Biosystems, Germany). Then the sections were placed gently onto the surface of 50℃ water long enough to flatten and then collected by glass slides. The glass slides (SuperFrost Ultra Plus™) were coated with 0.01% Poly-L-lysine solution in advance as well to avoid tissue falling from the slides in the process of immunofluorescence staining and Hematoxylin and Eosin (HE) staining. The slides with sections were dried at 30℃ overnight.

2.12 HE-staining of paraffin sections

The paraffin sections were deparaffinized in ethanol before stained with HE. The sections were investigated under the light microscope with a 40× and a 63× oil objective. The procedures of HE staining are listed as below:

1. Deparaffinize the sections: xylene for 4 times, 5min each time.
   99% Ethanol 2 times, 1 min each time.
   96% Ethanol 2 times, 1 min each time.
   70% Ethanol for 2 times, 1 min each time.
   Wash slides in distilled water for 2 times.
2. Immerse the slides in Harris hematoxylin solution for 10min.
3. Wash the slides with distilled water.
4. Differentiate the slides in HCL-alcohol for 3 seconds.
5. Wash the slides with running tap water until the water is clear.
6. Immerse the slides in distilled water for another 10min.
7. Immerse the slides Stain in Eosin Y for 2 minutes.
8. Dehydrate the slides in increasing concentration of Ethanol
   70% Ethanol for 1 min.
   96% Ethanol 2 times, 1 min each time.
   99% Ethanol 2 times, 1 min each time.

Xylene for 4 times, 1min each time.

9. The slides were mounted with Eukitt® mounting medium (Merck, Darmstadt, Germany).

2.13 Immunofluorescence staining

Paraffin sections (4 μM) of the entire retina, with the ONH, were deparaffinized, dehydrated as showed in 2.13. Then the slides were heated for 2 min in citrate buffer at pH 6 for antigen retrieval. Then sections were incubated with goat anti-RPE65 (1:100; Santa Cruz Biotechnology Inc., Santa Cruz, CA, USA) and rabbit anti-Iba1 (1:1000; FUJIFILM Wako, Japan) (1:1000, Wako) at 4◦C overnight. Cy3 rabbit anti-goat IgG (H+L) antibody and Cy3 goat anti-rabbit IgG (H+L) anti-rabbit (Jackson ImmunoResearch, Ely, UK) were applied as secondary antibodies for anti-RPE65 and anti-Iba1, respectively. 4', 6-diamidino-2-phenylindole (DAPI) was used to counterstain the cell nucleus. The slides were cover-slipped with fluorescence mounting medium (Dako Omnis, Denmark) and analyzed with a Zeiss Axioplan2 imaging microscope (Zeiss, Jena, Germany).

2.14 Human Tissue

The peri-macular tissue of a 72-year-old human donor with clinically diagnosed Stargardt disease obtained from Foundation Fighting Blindness (Columbia, MD, USA), as previously described (Taubitz et al., 2018), was prepared into semi-thin sections (500 nm, without OsO4 fixation or UAC staining). The use of the tissue in medical research was approved by Institutional Review Board of the University of Tuebingen (Ethik-Kommission an der Medizinischen Fakultät der Eberhard-Karls Universität und am Universitätsklinikum Tübingen, Tuebingen, Germany, approval number 462/2009BO2) and written informed consent was obtained from the donor. To investigate the lipofuscin AF and NIR-AF, I examined the sections under a fluorescence microscope with the lipofuscin filter set and the Cy7 filter set, respectively. All experiments were conducted according to the Declaration of

Helsinki.

2.15 Statistical analysis

All the results were presented as the means (standard deviation (SD)). For comparison the mice before and after blue light illumination, the grey value of fundus AF, retinal thickness and the amplitudes of the ERG test were studied by paired t-test. While for comparison between non-treated and blue light illuminated mice, the number of nuclei from each group was compared with unpaired t-test. One-way ANOVA with Bonferroni correction for multiple comparisons was applied for statistical analysis among non-treated, vehicle-treated and Remofuscin®-treated mice. Statistical analysis was performed with SPSS25.0 software (SPSS, Chicago, USA) and GraphPad Prism 7.0 (GraphPad Software, San Diego, CA, USA). Statistical significance was set at $P < 0.05$ for all tests.

3. Results

3.1 Retinal degeneration was caused by blue light in *Abca4*$^{-/-}$ mice

3.1.1 Retinal dysfunction after blue light illumination (BLI) in pigmented *Abca4*$^{-/-}$ mice

Scotopic and photopic ERG were performed before and seven days after BLI (Fig. 8A-B). The results showed blue light decreased the amplitude of a-wave in the intensity of 9.49 cds/m^2 and 25 cds/m^2 of scotopic ERG significantly (n=10 eyes, $P<0.05$, paired t-test) (Fig. 8C). Similarly, b-wave amplitudes of scotopic ERG were reduced dramatically (n=10 eyes, $P<0.05$, paired t-test) in the intensity from 0.095 cds/m^2 to 25 cds/m^2 after BLI (Fig. 8D). In photopic ERG, compared to the data before BLI, the amplitude of b-wave was diminished at the intensity of 3 cds/m^2 and 9.49 cds/m^2 markedly (n=10 eyes, $P<0.05$, paired t-test) after BLI (Fig. 8F). Whereas, the difference of photopic a-wave was not statistically significant (Fig. 8E). The function of photoreceptors of pigmented *Abca4*$^{-/-}$ was damaged by

blue light significantly, and rods are more susceptible to blue light than cones.

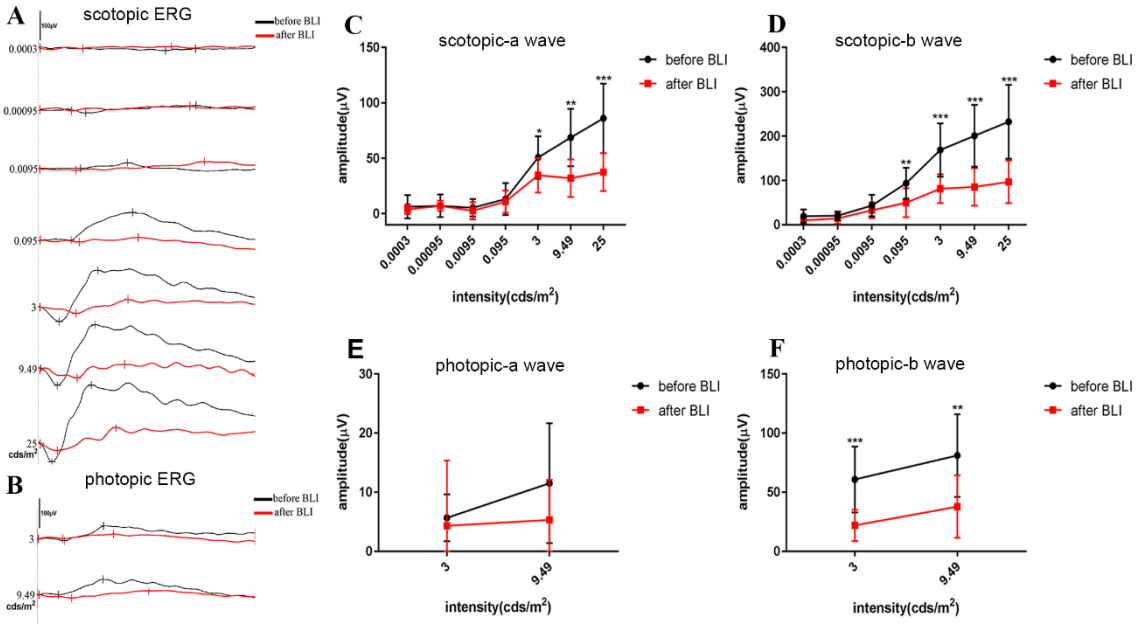

Figure 8. Retinal dysfunction seven days after BLI in pigmented *Abca4*$^{-/-}$ mice. (**A**) Representative waveforms of scotopic ERG in increasing intensities of flash were recorded in pigmented *Abca4*$^{-/-}$ mice before and seven days after blue light illumination (BLI). (**B**) Representative waveforms of photopic ERG were recorded in pigmented *Abca4*$^{-/-}$ mice before and seven days after BLI. Quantification of (**C**) scotopic a-wave amplitudes and (**D**) scotopic b-wave amplitudes before and seven days after BLI. (**E**) Mean amplitudes of a-wave in photopic ERG and (**F**) mean amplitudes of b-wave in photopic ERG were calculated in pigmented *Abca4*$^{-/-}$ mice before and seven days after BLI. The data are expressed as the mean (SD), n=10 eyes. Significant differences were calculated with paired t-test. *P<0.05, **P<0.01, ***P<0.001, before BLI vs. after BLI.

3.1.2 Findings in SW-AF and NIR-AF images

SW-AF (488 nm) and NIR-AF (788 nm) were investigated concurrently by using cSLO. SW-AF imaging is a non-invasive technique to visualize the accumulation of lipofuscin (Delori et al., 1995). NIR-AF is known to originate predominantly from melanin in the RPE (Keilhauer and Delori, 2006). Before BLI, the signal of fundus SW-AF was homogeneous in pigmented *Abca4*$^{-/-}$ mice. Differently, in NIR-AF images, a mottling AF pattern distributed uniformly in the fundus of all mice (Fig. 9A). Seven days after illumination, SW-AF images showed that the optic nerve head (ONH) was surrounded by a demarcated area with the simultaneous

presence of hyper-autofluorescence (hyper-AF, relative to background) and hypo-autofluorescence (hypo-AF, relative to background). Additionally, the area was discovered to incline to the superior part of the fundus in all mice. Meanwhile, a corresponding area exhibiting irregular flecks with hyper-AF or hypo-AF was observed in NIR-AF images (Fig. 9B).

To analyze the correlation of AF alterations on SW-AF and NIR-AF imaging after blue light illumination, green-coded SW-AF images and the corresponding red-coded NIR-AF images were merged (Cukras et al., 2012). It was revealed that a greater part of AF alterations was markedly hyperautofluorescent on SW-AF while being hypoautofluorescent on NIR-AF, which appeared green in the merged images. Nevertheless, some AF abnormalities were found to be hyperautofluorescent patches in both modalities and appeared orange or yellow on image composition. Furthermore, dark patches of absent AF in SW-AF images corresponded with dark patches in NIR-AF images, indicating geographic atrophy (GA), as typically seen in patients with AMD and SD. No area exhibiting hypo-AF on SW-AF but hyper-AF on NIR-AF was observed (Fig. 10). These observations suggested that blue light-induced abnormalities of fundus AF manifesting varying AF intensity in different modalities of fundus AF imaging.

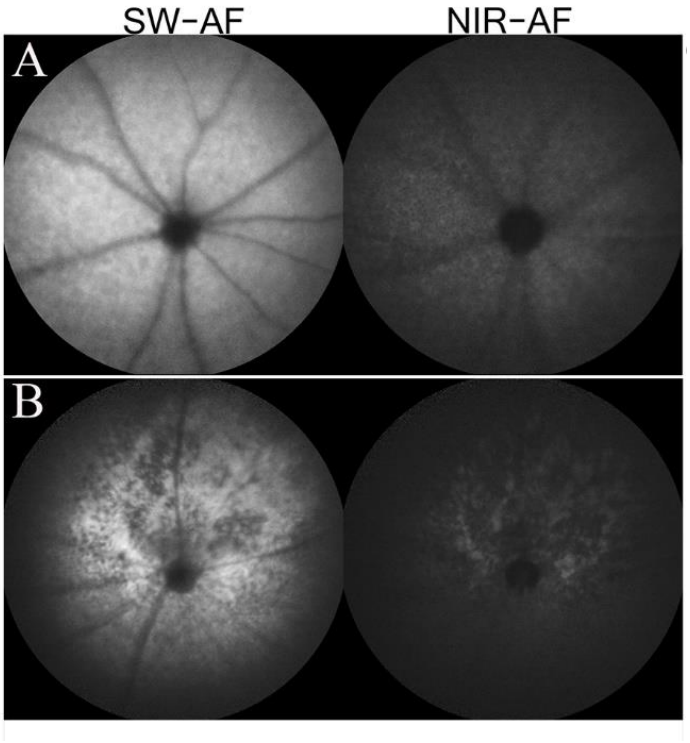

Figure 9. Blue light-induced AF abnormalities on SW-AF and NIR-AF imaging in 9-month pigmented *Abca4*$^{-/-}$ mice. (**A**) Representative non-normalized fundus SW-AF (left) and NIR-AF (right) images from a pigmented *Abca4*$^{-/-}$ mouse before BLI. (**B**) Representative fundus SW-AF (left) and NIR-AF (right) non-normalized images were recorded from a pigmented *Abca4*$^{-/-}$ mouse seven days after BLI.

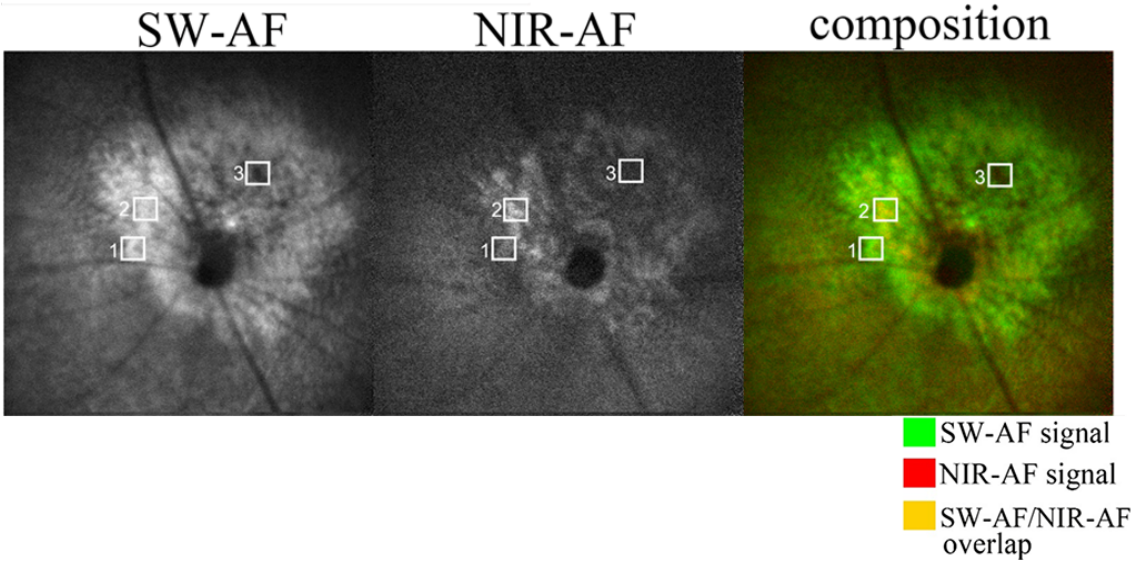

Figure 10. Correlation between SW-AF and NIR-AF after blue light illumination. The green-coded SW-AF image and red-coded NIR-AF image were composited. Boxes 1: AF alterations are markedly hyperAF on SW-AF while being hypoAF on NIR-AF, which appeared green in composite images. Boxes 2: AF abnormalities are hyperAF patches in both modalities and appeared yellow on image composition. Boxes 3: Dark patches

are found in both SW-AF and NIR-AF images, indicating geographic atrophy. No area exhibiting hypoAF on SW-AF but hyperAF on NIR-AF was observed.

3.1.3 Intensities of fundus SW-AF and NIR-AF were reduced by blue light in pigmented *Abca4*$^{-/-}$ mice

To evaluate the effect of blue light on the distribution of retinal pigments, mean grey value of nonnormalized SW-AF and NIR-AF images was measured and corrected for quantitative analysis of fundus AF. As shown in Fig. 11, quantified AF intensity in SW-AF images decreased dramatically (n=8 eyes, P=0.001, paired t-test) after blue light illumination. Similarly, blue light reduced AF intensity on NIR-AF distinctly (n=8 eyes, P=0.007, paired t-test).

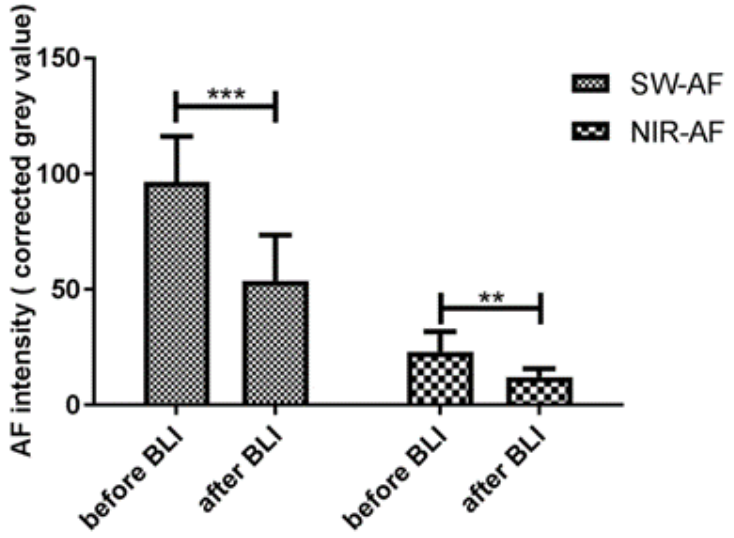

Figure 11. Mean intensity of fundus SW-AF and NIR-AF were reduced after BLI in pigmented Abca4-/- mice. The data are expressed as the means (SD), n=8 eyes. Significant differences are analyzed using the paired t-test. *P<0.05, **P<0.01, ***P<0.001, before BLI vs. after BLI.

3.1.4 Reduction of retinal thickness after blue light in pigmented *Abca4*$^{-/-}$ mice

Total retinal thickness (the distance from the retinal nerve fiber layer (RNFL) to the inner segment/outer segment of photoreceptors (IS/OS)) was measured and plotted every 200μm interval beginning from ONH to superior and inferior along the vertical axis in OCT images. The plot showed that the lesion area caused by blue light was from 400μm inferior position to ONH and 700μm superior position

to ONH along vertical meridian (n=9 eyes, P<0.05, paired t-test) (Fig. 12). Acute blue light reduced the thickness of the superior retina more significantly. The decrease in retinal thickness was 14.85-21.27% inferiorly and 17.14-34.78% superiorly.

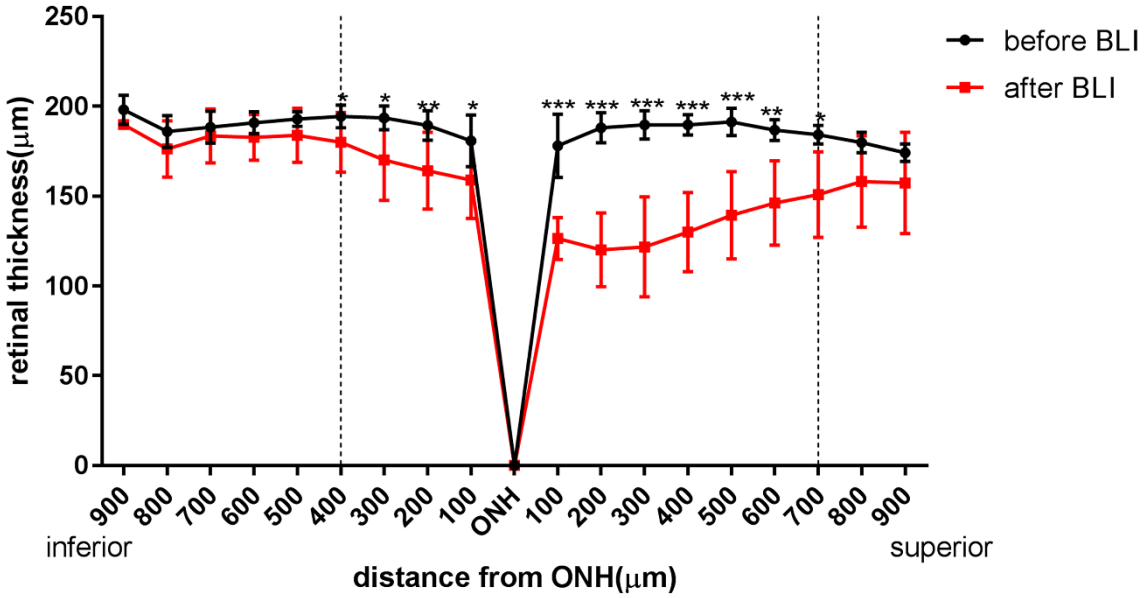

Figure 12. Reduction of the retinal thickness after BLI in pigmented *Abca4*$^{-/-}$ mice. Total retinal thicknesses are measures (from RNFL to IS/OS, including both layers) and plotted in pigmented *Abca4*$^{-/-}$ mice before and seven days after BLI. The data are expressed as the means (SD), n=9 eyes. Significant differences are analyzed using the paired t-test. *P<0.05, **P<0.01, ***P<0.001, before BLI vs. after BLI.

3.1.5 Findings in OCT

OCT images recorded on volume scan were used to analyze the alterations of the retinal structure after blue light illumination. 5 Categories of lesion invading different retinal layers were highlighted by OCT imaging.

As revealed by Fig. 13A, hyper-reflective material accumulated within the area of IS/OS from RPE to the external limiting membrane (ELM), which was classified as Category 1. Category 1 lesions corresponded to hyper-AF in both AF modalities, appeared as yellow flecks in merged AF images (Fig. 13B-C). Analysis of OCT images revealed that Category 2 lesions, which can be described as disruption of IS/OS with loss of ellipsoid zone (EZ) and ELM,

corresponded to hyper-AF only in SW-AF (green-colored in merged AF images) (Fig. 13D-F). Category3 lesions were observed as disruption of IS/OS and the accumulation of hyper-reflective material located from the RPE layer and extending to ONL, with thinning of ONL (Fig. 13G). Importantly, some lesions in Category 3 correlated to green patches on AF image composition, and others appeared yellow (Fig. 13H-I). Category 4 lesions appeared disruption of IS/OS, hyper-reflective material accumulated around RPE layer and distributed in ONL, infoldings of OPL expanding to INL (Fig. 13J). Concerning the corresponding fundus AF, lesions in Category 4 appeared as hyper-AF in SW-AF and NIR-AF, resulting in orange-colored in merged AF images (Fig. 13K-L). The lesions with loss of ONL, disruption of IS/OS and disruption of RPE in OCT images were classified as Category 5 lesions (Fig. 13M), which corresponded to the loss of fundus AF and appeared dark patches in SW-AF and NIR-AF images. Nevertheless, some of Category 5 lesions exhibited increased fundus AF in both modalities and orange-colored in merged AF images, when a high amount of hyper-reflective material accumulated around the RPE layer simultaneously. Additionally, Category5 lesions with less amount of hyper-reflective material showed hyper-AF in SW-AF and appeared as green-colored in AF composite image (Fig. 13N-O).

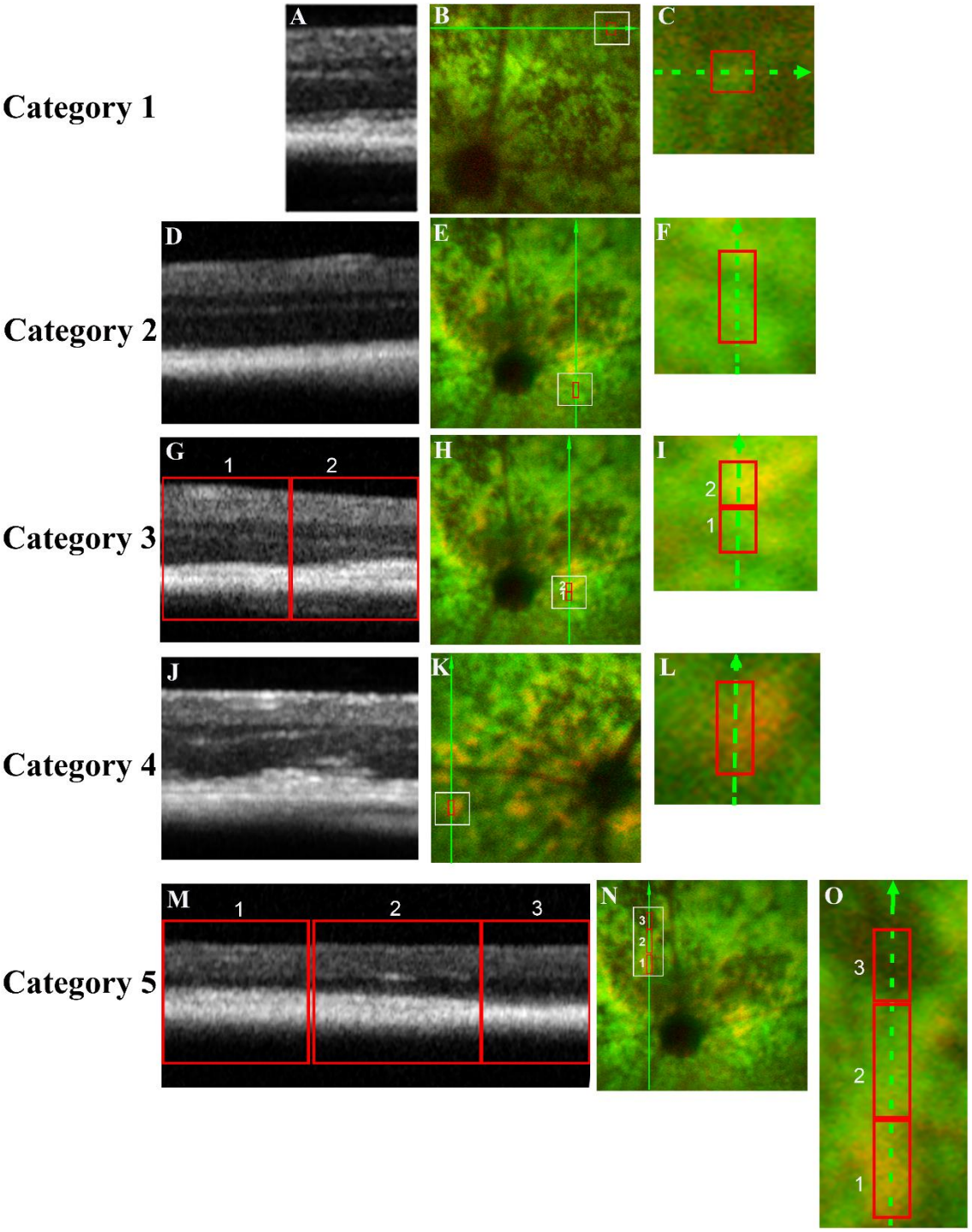

Figure 13. Correlation between OCT and fundus AF imaging from 9-month pigmented *Abca4*$^{-/-}$ mice seven days after BLI. (**A**) Cross-sectional OCT image of Category 1 lesions (hyperreflective material located in the IS/OS) (**B**) appeared as yellow flecks in color composite AF image. (**D**) Cross-sectional OCT image of Category 2 lesions (disruption of IS/OS with loss of EZ and ELM) (**E**) corresponded to the green-colored area in color composite AF image. (**G**) Category 3 lesions (disruption of IS/OS and hyperreflective material locating from the RPE layer and extending to ONL and thinning of ONL) are recorded in OCT image. (**H**) Category 3 lesions correlated to green

patch (red box 1) or yellow-color patch (red box 2) on AF image composition. (**J**) Category 4 lesions (disruption of IS/OS, hyperreflective material accumulating around the RPE layer and distributing into ONL, infoldings of OPL expanding to INL) in OCT image (**K**) appeared as orange-colored in color composite AF image. (**M**) Category 5 lesions (loss of ONL, disruption of IS/OS and disruption of RPE) in OCT image (**N**) appeared as an orange-colored patch (red box 1), green-colored patch (red box 2) or dark patch (red box 3) in color composite AF image. (**C, F, I, L, O**) Higher magnification of the white boxed area in B, E, H, K, N, respectively.

3.1.6 Reduction of RPE nuclei number and photoreceptor nuclei number after BLI in pigmented *Abca4*$^{-/-}$ mice

RPE monolayers and photoreceptor nuclei were counted as a function of distance within each 200 μm interval from ONH to 2 mm inferiorly and 2 mm superiorly along the vertical axis. Blue light diminished RPE cell numbers pronouncedly in the area from 400 μm inferior to ONH and 800μm superior to ONH (n=8 eyes, $P<0.05$, unpaired t-test) (Fig. 14A). The decrease of RPE nuclei number was 66-69% inferiorly and 50-88% superiorly. Meanwhile, photoreceptor nuclei in ONL were reduced in light-illuminated eyes, with the statistically significant differences from 200 μm inferior position to 600 μm superior position (n=8 eyes, $P<0.05$, unpaired t-test) (Fig. 14B). The reduction of photoreceptor cells reached 36% in the inferior hemiretina and 26-49% in the superior hemiretina.

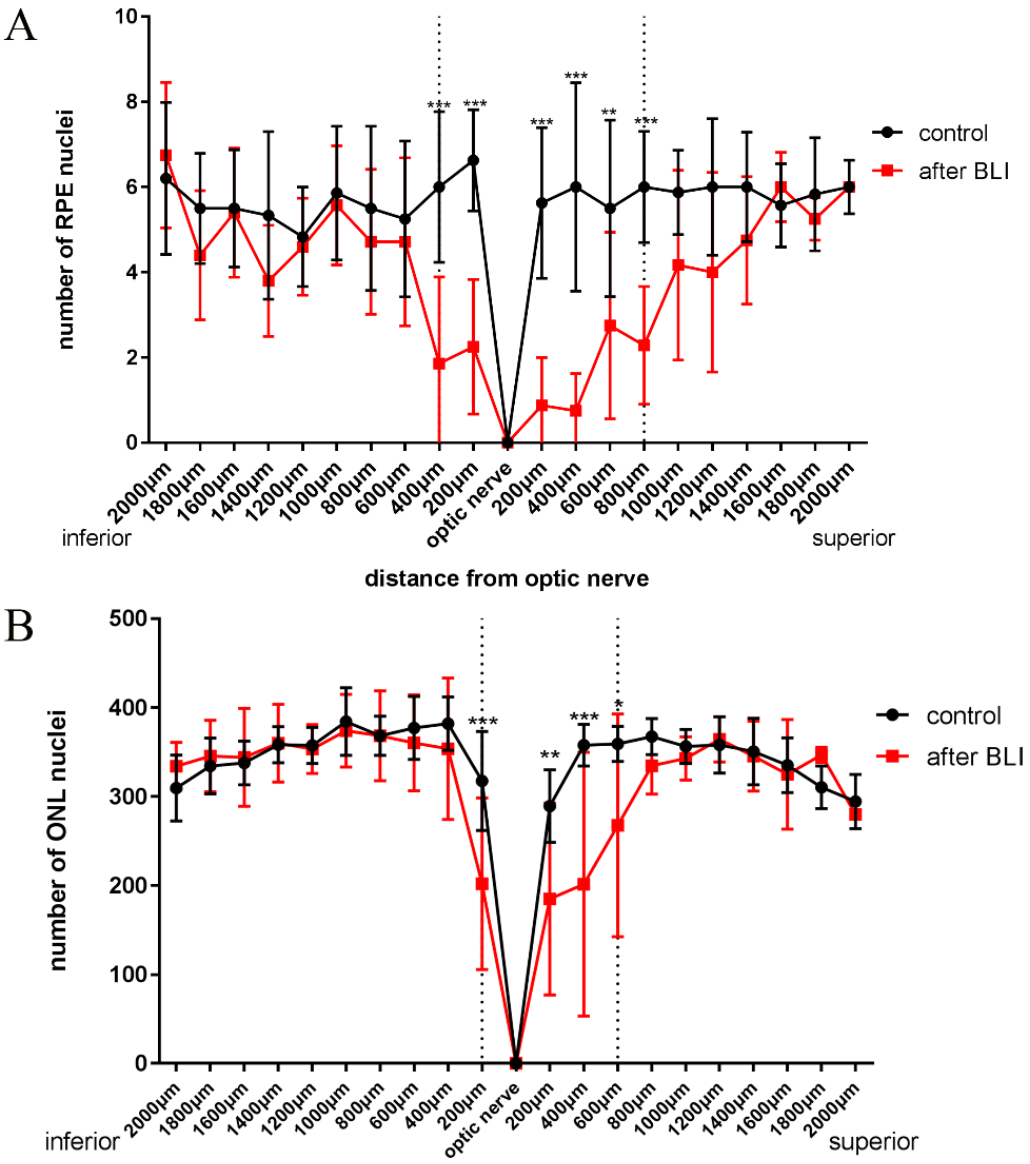

Figure 14. The number of RPE nuclei and photoreceptor nuclei decreased after BLI in 9-month pigmented *Abca4*$^{-/-}$ mice. (**A**) The number of RPE nuclei and (**B**) the number of nuclei in ONL were measured in non-treated (control) pigmented *Abca4*$^{-/-}$ mice and blue light illuminated pigmented *Abca4*$^{-/-}$ mice (after BLI) and plotted as a function of distance from ONH along the vertical axis. The data are expressed as the means (SD), n=8 eyes. Significant differences are analyzed using the unpaired t-test. *P<0.05, **P<0.01, ***P<0.001, control vs. after BLI.

3.1.7 Histological features after BLI in pigmented *Abca4*$^{-/-}$ mice

Blue light-induced degeneration of RPE and photoreceptor cells in pigmented *Abca4*$^{-/-}$ was revealed by using toluidine blue stained semi-thin sections. Retina from non-treated pigmented *Abca4*$^{-/-}$ mice showed no degeneration of

photoreceptors or RPE layer (thickness: 6-8 μm) (Fig. 15A). In accordance with OCT findings, retinal lesions were observed near the ONH. In the peripheral zone of the lesion, aberrant cells with pigment granules were found in the subretinal space, as shown in Fig. 15B, the neighboring RPE cell contained melanin granules at the apical surface and vacuole-like structure at the basal side. In the lesion zone, damaged RPE cells appeared as thinning of RPE layer (thickness<3 μm) with vacuole-like structure (Fig. 15C) or with irregular shaped nucleus (Fig. 15C, E1), increased pigmentation in attenuated RPE cells (Fig. 15E2), multilayers of RPE (Fig. 15E3) and even RPE layer loss (Fig. 15F1-F3). Shortened OS and absence of OS accompanied with RPE atrophy (Fig. 15C), indicating the early photoreceptor degeneration. Blue light damaged photoreceptors and caused progressive thinning of ONL. Aberrant pigmented cells in various amounts accumulated and adhered to Bruch's membrane (Fig. 15D1-D2). The retinal laminar architecture was deformed after blue light, appearing as a rosette-like structure made of ONL and residual IS (Fig. 15E1-E3). The rosette-like structure could extend to OPL (Fig. 15E1-E2) and even intrude into INL (Fig. 15E3) with the presence of different types of RPE atrophy. Aberrant pigmented cells, migrating towards ONL (Fig. 15E1) or adhering to damaged RPE layer (Fig. 15E2-E3), were also observed near to the areas of the rosette-like structure. Furthermore, blue light-induced loss of photoreceptors and RPE cells (Fig. 15F1-F3), which was accompanied by an accumulation of aberrant pigmented cells in the subretinal space in different amounts (Fig. 15F2-F3).

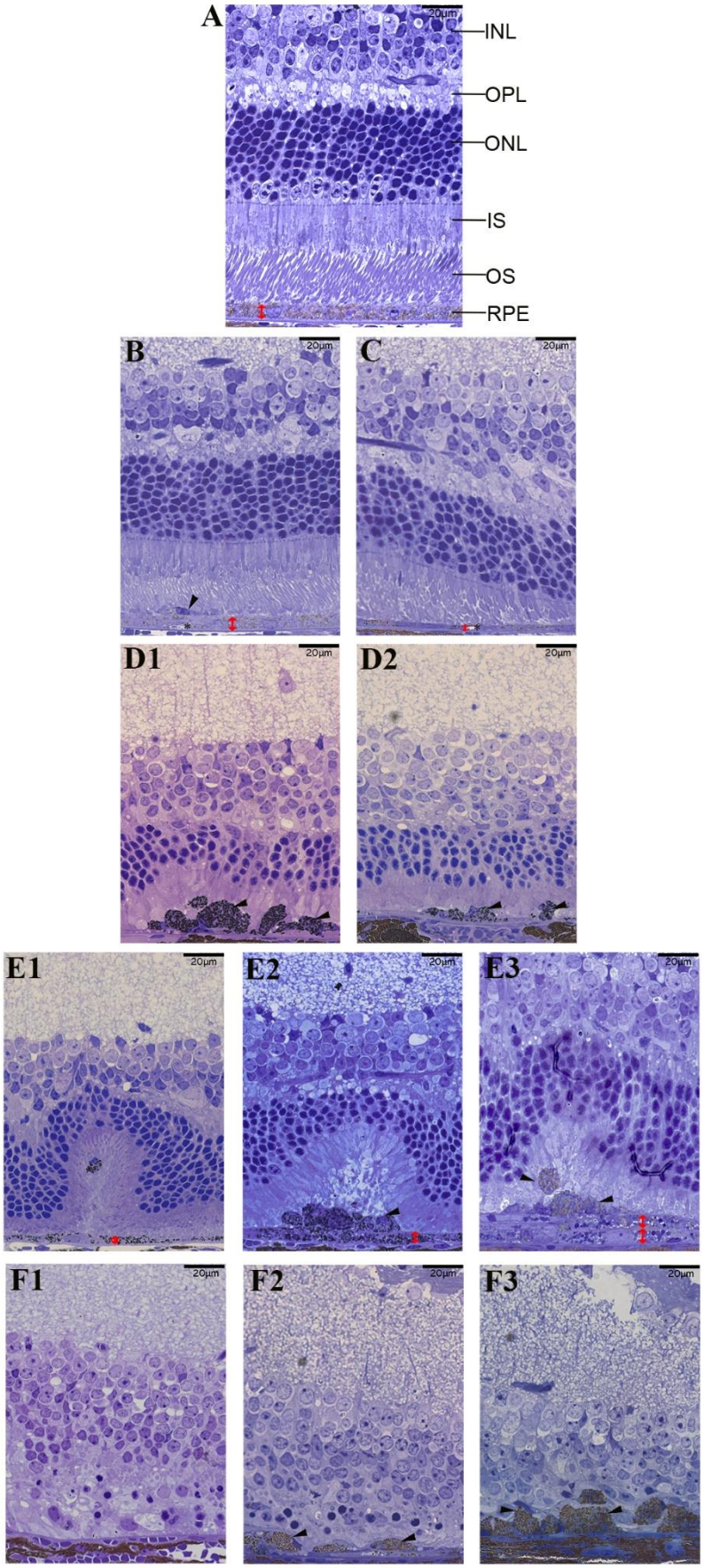
A
20μm
INL
OPL
ONL
IS
OS
RPE
B
20μm
C
20μm
D1
20μm
D2
20μm
E1
20μm
E2
20μm
E3
20μm
F1
20μm
F2
20μm
F3
20μm

Figure 15. Histological features after BLI in 9-month pigmented *Abca4*$^{-/-}$ mice. (A) Representative image of the semi-thin section from the non-treated retina. INL: inner nuclear layer, OPL: outer plexiform layer, ONL: outer nuclear layer, IS: inner segment, OS: outer segment, and RPE: retinal pigment epithelium. (**B-F3**) Representative Images of the damaged retina are recorded at seven days after BLI. (**B**) In the peripheral zone of the lesion, aberrant cells with pigment granules were found in the subretinal space. (**C**) Blue light-induced thinning of RPE layer (thickness<3 μm), vacuole-like structure (*asterisk*), the irregular shaped nucleus in RPE cells. Shortened OS and absence of OS accompanied with RPE atrophy. (**D1-D2**) Blue light caused progressive thinning of ONL accompanied by an accumulation of aberrant pigmented cells (black arrowheads) in various amounts in the subretinal space. (**E1-E3**) Damaged RPE cells appeared as thinning of RPE layer (thickness<3 μm) with abnormal nucleus (**E1**), increased pigmentation (**E2**), multilayers of RPE (**E3**). The retinal laminar architecture was deformed after blue light accompanied by accumulation of pigmented cells. (**F1-F3**) Blue light-induced loss of photoreceptors and RPE cells. Aberrant pigmented cells accumulated in the subretinal space in different amounts.

3.1.8 Ex vivo retinal AF in pigmented *Abca4*$^{-/-}$ mice after blue light illumination

In semi-thin sections of non-treated pigmented *Abca4*$^{-/-}$ mice, AF of lipofuscin in RPE cells was visualized under a fluorescence microscope. With NIR excitation, AF was observed to locate in the RPE layer and choroid. The distribution of NIR-AF mainly corresponded to the melanin pigmentation shown in the bright-field image (Fig.16A). Compared to normal RPE cells, much less lipofuscin with AF presented in the blue light damaged RPE cells in the lesion area. Some damaged RPE cells were depigmented, but some were observed with dense melanosomes showing brighter fluorescence. In the damaged RPE cells, some pigment granules (in white circles) exhibited lipofuscin AF and NIR-AF and appeared as yellow color in the merged image. Nevertheless, the pigment granules (in red circles) were not observed as melanin pigmentation in the bright-field image (Fig. 16B) *(Note: because of the space constraints, it's better to review the images with a computer screen at higher magnification)*. Pigmented cells accumulating in the subretinal space after BLI showed a higher density of melanin pigmentation, hyper AF of lipofuscin and hyper NIR-AF. In the merged image, more pigment

granules (in red/white circles) without melanin pigmentation were found with two types of AF signals in the pigmented cells. In adjacent multilayered RPE cells also contained a few pigment granules which show hyper AF in both modalities (Fig. 16C). Additionally, photoreceptors were not observed with lipofuscin AF or NIR-AF.

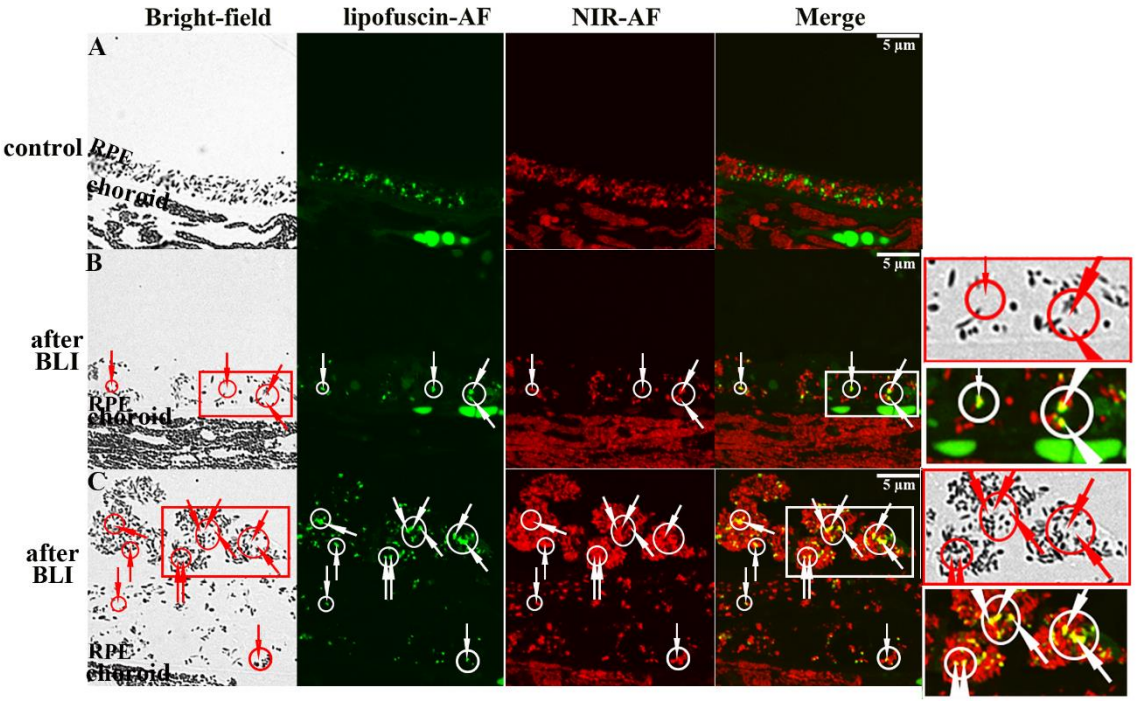

Figure 16. Ex vivo retinal AF in both modalities from non-treated (control) and blue light-illuminated 9-month-old pigmented *Abca4*$^{-/-}$ mice. (**A**) Bright-field image, fluorescence image showing lipofuscin AF (green), NIR-AF image (red) and merged fluorescence image of an unstained semi-thin section from non-treated (control) pigmented *Abca4*$^{-/-}$ mice. Scale bar: 5-µm (**B**) Seven days after BLI, in blue light-damaged RPE cells, some pigment granules (white/red arrows in white/red circle) without melanin pigmentation in the bright-field image, exhibiting lipofuscin AF (green) and NIR-AF (red), appear yellow in the merged image. The areas in the red and white boxes are shown on higher magnification (rightmost). Scale bar: 5-µm. (**C**) After BLI, in the aberrant pigmented cells and multilayered RPE cells, pigment granules (white/red arrows in the white/red circle) without melanin pigmentation, exhibiting lipofuscin AF (green) and NIR-AF (red), were observed with a yellow color in the merged image. The areas in the red and white boxes were shown in the higher magnification (rightmost). Scale bar: 5-µm.

3.1.9 Ex vivo retinal AF in a donor eye with late Stargardt disease

The peri-macular tissue from a 72-year old patient with late Stargardt disease

was investigated for *ex vivo* retinal AF. RPE cells of the peri-macular tissue were packed full of pigment granules, including lipofuscin and melanolipofuscin stained by toluidine blue but bare of melanin (Fig. 17A), as showed by Taubitz, et al. (Taubitz et al., 2018). Fig. 17B and Fig. 17C showed hyper lipofuscin AF and hyper NIR-AF of pigment granules in RPE cells, respectively. Overlay yellow color in merged fluorescence image evidenced that most of the pigment granules were hyperautofluorescent in both modalities (white arrows). Additionally, few pigment granules presented only NIR-AF (red arrowheads) and some only exhibited lipofuscin AF (white arrowheads) (Fig. 17D).

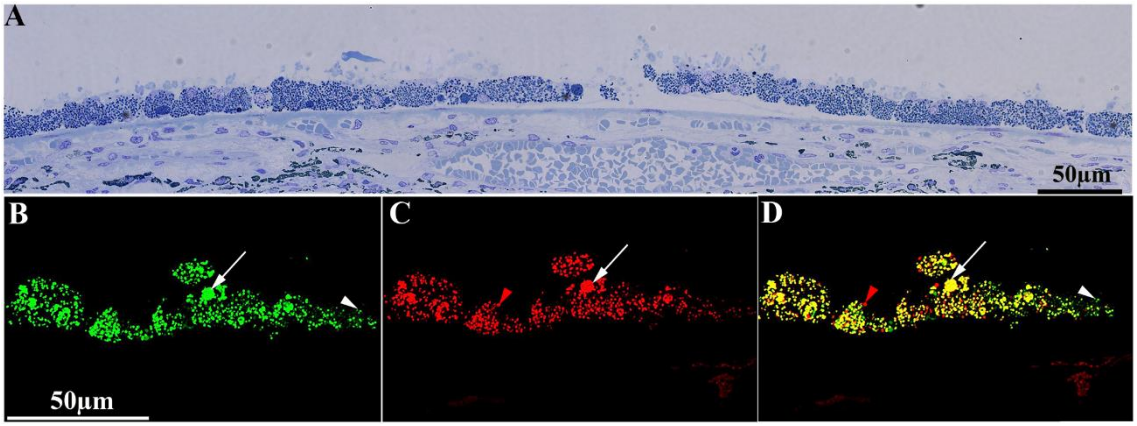

Figure 17. Ex vivo retinal AF in both modalities from a 72-year-old human donor eye with late stage of Stargardt disease. (**A**) Overview of RPE layer from the perimacular tissue of donor eye with late Stargardt disease in toluidine blue stained semi-thin section. (**B**) The fluorescence image shows the distribution of lipofuscin AF in RPE cells from a donor eye with late Stargardt disease. (**C**) The corresponding image of E shows the NIR-AF in RPE cells. (**D**) Merged image of E and F. Overlay areas appear as yellow color (white arrows). Pigment granules only exhibited lipofuscin AF (white arrowheads) and some only exhibited -NIR-AF (red arrowheads).

3.1.10 Correlation among findings of fundus AF, OCT, light microscopy and fluorescence microscopy

To correlate *in vivo* imaging with *ex vivo* imaging, OCT images, and histologic images were captured at the same location and resize to the same scale for alignment. As shown in Fig. 18 (red boxes labelled 1), geographic atrophy was recognized as atrophy of RPE and photoreceptors in OCT and histologic images

with dark patches in fundus AF images. The adjacent area (red boxes labelled 2) with hyper-AF in both modalities (appearing as yellow in the composite image) corresponded to geographic atrophy as well, but with an accumulation of hyperreflective material in OCT. In the microscopic image, abundant aberrant pigmented cells accumulated above Bruch's membrane at the corresponding location.

In Fig. 19A, I observed the orange-colored area in composite AF image (red box 1). The corresponding change appeared as plenty of hyperreflective material adhering to thicker RPE layer, loss of EZ and infolding of IPL in OCT. Relatively, the histologic image showed plenty of pigmented cells accumulated above multilayer of RPE, loss of photoreceptor outer segment (POS), distortion of photoreceptor inner segment (PIS) and rosette-shaped ONL expanding to IPL at the same location (Fig. 19B-C red boxes labelled 1). Under the fluorescence microscope, the pigmented cells in the subretinal space exhibited hyper lipofuscin-like AF and hyper NIR-AF. The multilayered RPE cells, compared with the pigmented cells, emitted weak lipofuscin AF and weak NIR-AF (Fig. 19D-F red box 1). Geographic atrophy was found with few pigmented cells locating in subretinal space (Fig. 19B-C red box 2) and accompanied by loss of autofluorescence both in cSLO (Fig. 19A red box 2) and under the fluorescence microscope (Fig. 19D-F red box 2). The yellow-colored area in AF superimposition (Fig. 19A red box 3) correlated with thinning of RPE layer, accumulation of a few pigmented cells with lipofuscin-AF and NIR-AF in the subretinal space and degeneration of photoreceptors (Fig. 19B-F red box 3). Additionally, the erythrocytes in choroid were autofluorescent under the wavelength that excites lipofuscin autofluorescence.

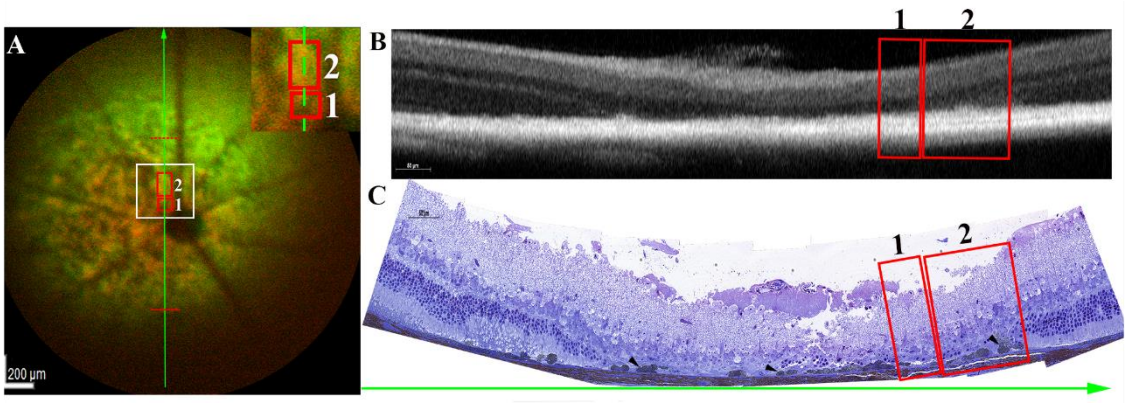

Figure 18. Correlation among images of fundus AF, OCT and light microscopy from a 9-month pigmented *Abca4*$^{-/-}$ mice seven days after BLI. (**A**) The color composition of fundus SW-AF (green-color coded) and NIR-AF (red-color coded) images was recorded at seven days after BLI. top right corner: higher magnification of white box area (**B**) Corresponding B-scan OCT image is acquired along the vertical axis (*green line with arrowhead* in A) and within a defined area (the area between two red dotted lines in A). (**C**) Corresponding histological image recorded from the same eye. Two areas (red boxes labelled 1, red boxes labelled 2) of geographic atrophy appear differently in A, B, C. Pigmented cells (*black arrowheads*) are observed in the subretinal space.

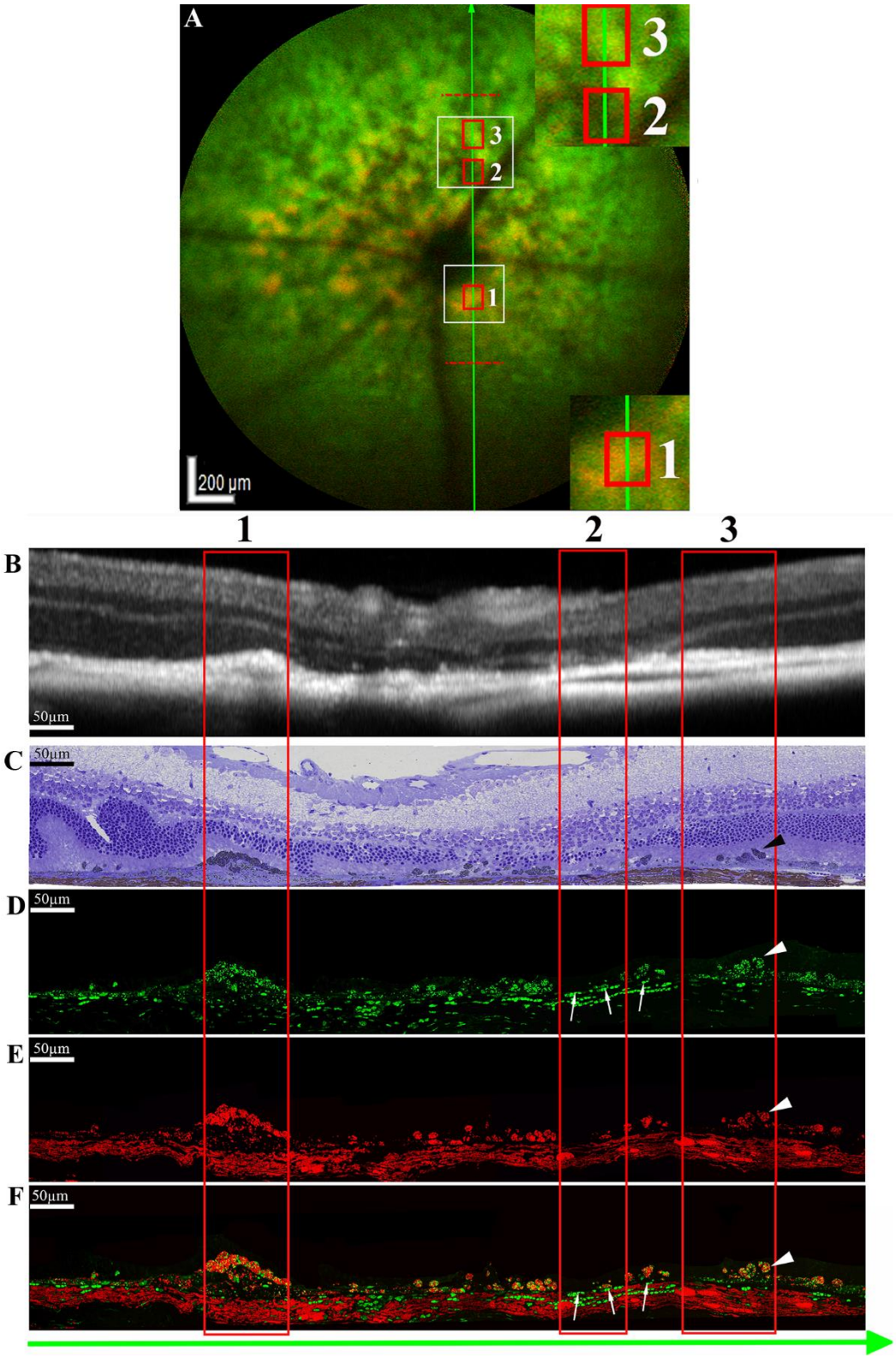

Figure 19. Correlation among images of fundus AF, OCT, light microscopy and fluorescence microscopy from 9-month pigmented *Abca4*$^{-/-}$ mice recorded at seven days after BLI. (**A**) The color composition of fundus SW-AF (green-color coded) and NIR-AF (red-color coded) images was recorded at seven days after BLI. Top right corner and bottom right corner: higher magnification of white box areas. (**B**)

Corresponding B-scan OCT image is acquired along a vertical axis (*green line with an arrowhead* in A) and within a defined area (the area between two red dotted lines in A). (**C**) Corresponding histological image of the OCT image is recorded from the same eye. (**D**) The corresponding image of lipofuscin AF is recorded from the adjacent section. (**E**) The corresponding image of NIR-AF is recorded from the same section of (**C**). (**F**) Merged image of D and E showed colocalization of hyper lipofuscin-like AF and melanin-like AF in pigmented cells. Red boxes 1-3 in A corresponded to the red boxes 1-3 in B-F. Pigmented cells (*black arrowheads,* C) with lipofuscin AF (*white arrowheads,* D) and NIR-AF (*white arrowheads,* E) are observed. The erythrocytes (*white arrows*) in choroid are AF under the wavelength that excites lipofuscin AF.

3.1.11 Ultrastructural changes after BLI in pigmented *Abca4*$^{-/-}$ mice

As reported previously (Taubitz et al. 2018), normal monolayered RPE cells of 9-month-old pigmented *Abca4*$^{-/-}$ mice possessed numerous regular-shaped basal infoldings, mitochondria locating near basal infoldings and well-developed apical microvilli. The features of pigmented *Abca4*$^{-/-}$ RPE cells were also observed with extensive lipofuscin, melanin and melanolipofuscin in the cytoplasm (Fig. 20A). Seven days after blue light illumination, some atrophic RPE cells appeared as thinning RPE containing flattened RPE nuclei, less pigmentation, and reduction of basal infoldings expansion. The vacuole-like structure was also identified in the RPE cytoplasm (Fig. 20B). Numerous undigested phagosomes accumulated and extensively occupied cytoplasm of atrophic RPE cells, accompanied by hypopigmentation and less basal infoldings (Fig. 20C-D). *Abca4*$^{-/-}$ RPE damaged by blue light also exhibited areas of GA where RPE, PIS and POS were absent (Fig. 20E). At the ultrastructural level, spherical-shaped pigmented cells were observed to locate adjacent to atrophic RPE cells in the subretinal space with increased lipofuscin (Fig. 20F), directly cover the Bruch's membrane (Fig. 20G), or float in subretinal space (Fig. 20H). The pigmented cells filled with abundant melanin, lipofuscin, and melanolipofuscin granules. In addition, macrophages with condensed photoreceptor nuclei were observed to locate next to Bruch's membrane (Fig. 20I).

The formation of multilayered RPE cells was induced by blue light. TEM revealed

that compared to the normal RPE cells, the RPE cells forming multilayers contained extensive undigested phagosomes, decreased melanin and lipofuscin in the cytoplasm. Basal infoldings were limited even absent and apical microvilli were not evident. Some RPE cells also lost the apical-basal polarity. Smaller lipofuscin-like granules (<0.3 μm in diameter) instead of mitochondria were observed at the basal side of RPE cells next to Bruch's membrane (Fig. 21).

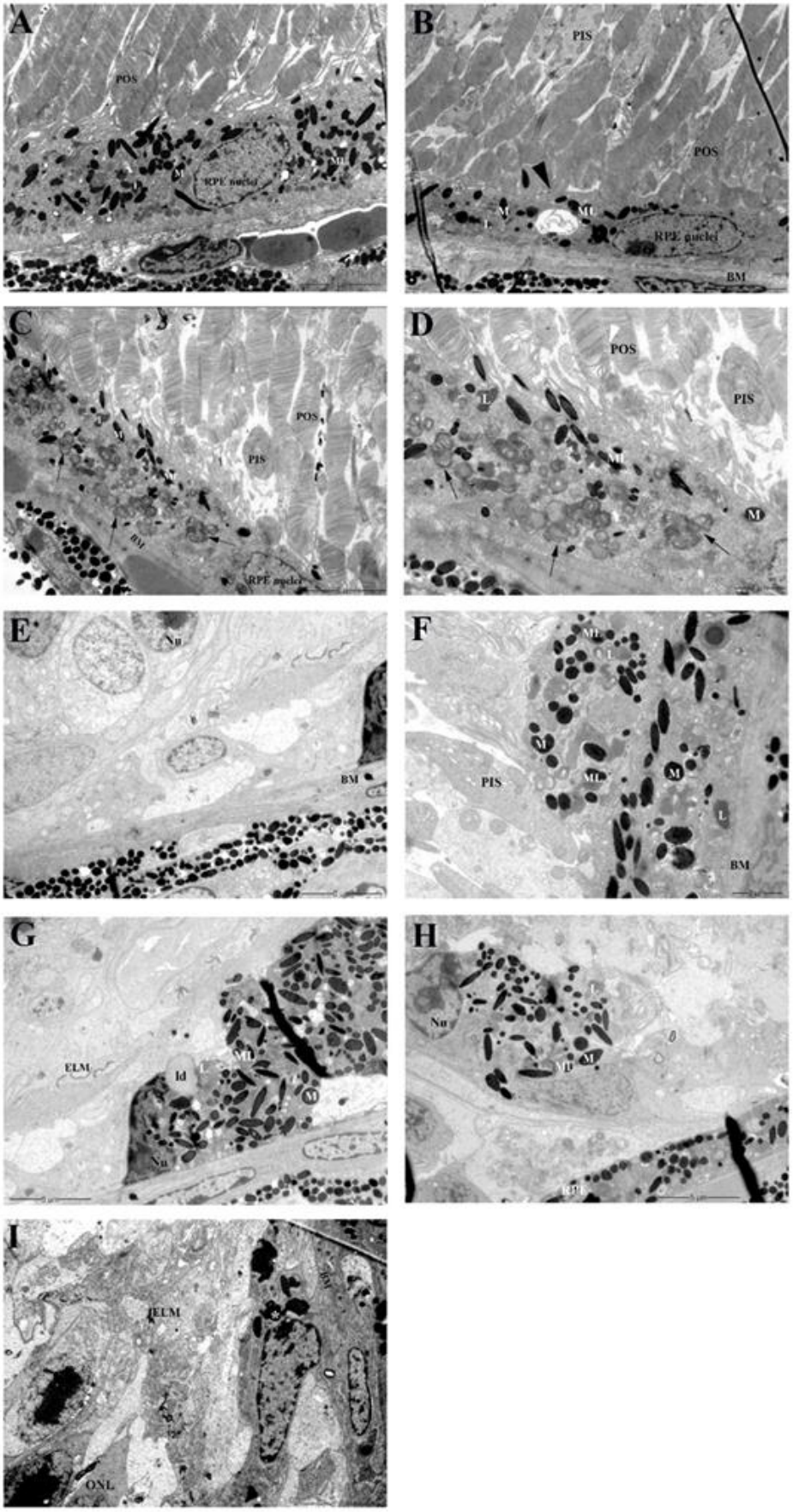
A
POS
RPE nuclei
ML
M
B
PIS
POS
ML
M
RPE nuclei
BM
C
POS
PIS
BM
RPE nuclei
D
POS
PIS
L
ML
M
E
Nu
BM
F
ML
L
M
PIS
BM
G
ELM
Id
ML
M
Nu
H
Nu
ML
M
I
ELM
ONL

Figure 20. Ultrastructure changes in 9-month-old pigmented *Abca4*$^{-/-}$ mice seven days after BLI. (**A**) Normal RPE cells under electron microscopy. (**B**) Seven days after blue light illumination, atrophic RPE cell appears as thinning RPE containing flattened RPE nuclei, less pigment, and reduction of basal infoldings expansion. Vacuole-like structure (black arrowhead) is observed. (**C**) Numerous undigested phagosomes (black arrows) accumulated and extensively occupied cytoplasm of atrophic RPE cells, accompanied by hypopigmentation and less basal infoldings (white arrowheads). (**D**) Higher magnification of the RPE layer area in the red rectangular box in C. (**E**) Blue light-induced areas of GA. (**F**) Spherical-shaped pigmented cells locates in the subretinal space adjacent to atrophic RPE cells, (**G**) directly cover the Bruch's membrane, or (**H**) float in subretinal space. (**I**) Macrophages contain condensed photoreceptor nuclei located next to Bruch's membrane. M: melanin, L: lipofuscin, ML: melanolipofuscin, Nu: nucleus, ONL: outer nuclear layer, ELM: external limiting membrane, POS: photoreceptor outer segment, PIS: photoreceptor inner segment, RPE: retinal pigment epithelium, BM: Bruch's membrane.

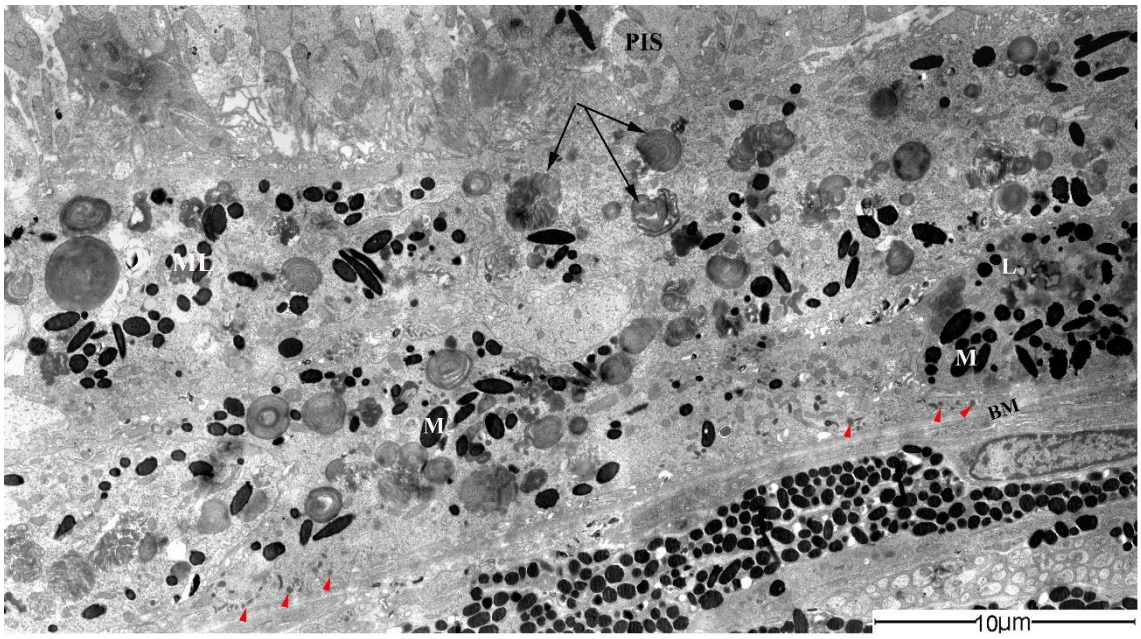

Figure 21. Ultrastructure of multilayered RPE cells seven days after BLI in pigmented *Abca4*$^{-/-}$ mice. Multilayered RPE cells contain extensive undigested phagosomes (black arrows), decreased melanin and lipofuscin in the cytoplasm. Smaller lipofuscin-like granules (red arrowheads) were observed at the basal side of RPE cells next to Bruch's membrane. M: melanin, L: lipofuscin, ML: melanolipofuscin, PIS: photoreceptor inner segment, BM: Bruch's membrane

3.1.12 Immunofluorescence findings

To identify the cell type of the aberrant pigmented cells accumulating in the subretinal space, I immunostained the blue light illuminated-retina with anti-RPE-

65 (used as RPE marker) and anti-Iba1 (a macrophage/microglia marker). Loss of photoreceptors and loss of RPE in the HE-staining section corresponded to the loss of RPE65 expression revealed by immunofluorescence staining. In subretinal space, no expression of RPE65 was observed in the pigmented cells (Fig. 22A-B). Nevertheless, Iba1 positivity of the pigmented cells was evident (Fig. 23A-D). Combining with the results in TEM, it suggested that blue light caused the appearance of macrophages which contained melanin and lipofuscin accumulating in the subretinal space.

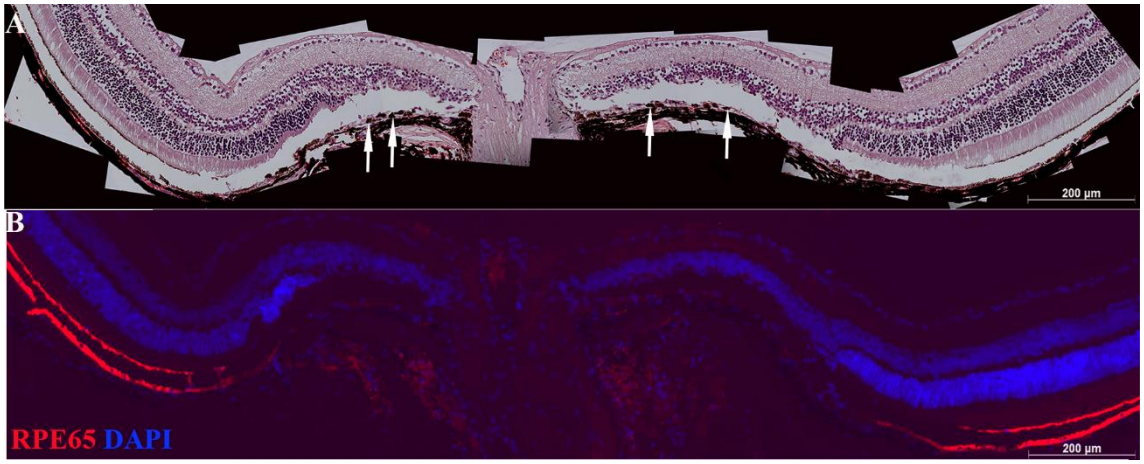

Figure 22. Reduction of RPE-65 expression in pigmented Abca4$^{-/-}$ mice seven days after BLI. (**A**) Representative image of hematoxylin and eosin stained paraffin section is recorded from the blue light-illuminated eye. (**B**) RPE-65 immunostaining (red) and DAPI staining (blue) in the adjacent section shows no evidence of RPE-65 expression in geographic atrophy. No expression of RPE65 was observed in the pigmented cells (white arrows in **A**).

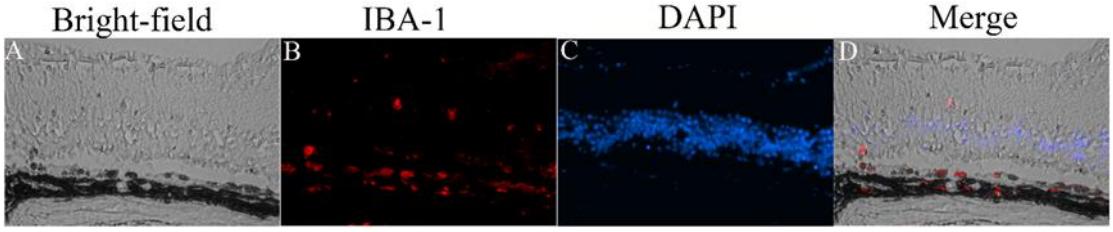

Figure 23. Blue light induced accumulation of macrophages in the subretinal space of pigmented *Abca4*$^{-/-}$ mice. (**A**) Paraffin section under light microscope shows pigmented cells in the subretinal space. (**B**) The pigmented cells are Iba-1 positive. (**C**) The cell nuclei are labeled with DAPI. (**D**) A merged image of **A**, **B** and **C**.

3.1.13 Changes of retinal AF after BLI in albino *Abca4*$^{-/-}$ mice

The albino *Abca4*$^{-/-}$ mice were investigated by using cSLO *in vivo* and

fluorescence microscope *ex vivo* seven days after blue light illumination. Before blue light illumination, 9-month-old albino *Abca4*$^{-/-}$ mice showed hyperfluorescent flecks on SW-AF indicating slight retinal degeneration (Fig. 24A). Due to the absence of melanin, there was no NIR-AF signal in albino *Abca4*$^{-/-}$ mice (Fig 24A). After blue light illumination, much more hyperfluorescent flecks were observed around the ONH on SW-AF (Fig. 24B). Interestingly, some of the flecks were hyperfluorescent on NIR-AF as well and appeared as yellow in composited colour-coded images (Fig. 24B).

As shown in Fig. 24C, accompanied by RPE degeneration and rosette formation of ONL, accumulation of aberrant cells was found in the subretinal space in the blue light illuminated-mice. Under the fluorescence microscope, the aberrant cells and damaged RPE cells exhibited both lipofuscin-related AF and NIR-AF. The merged images revealed that the colocalization of lipofuscin AF and NIR-AF in the pigment granules. I demonstrated that with the absence of melanin, lipofuscin granules contributed to NIR-AF in blue light-illuminated albino *Abca4*$^{-/-}$ mice.

The retinal ultrastructure of blue light illuminated-albino *Abca4*$^{-/-}$ mice was analyzed as well. The aberrant cells fully packed with lipofuscin granules were found in the subretinal space. Some lipofuscin granules showed higher electron density. In the neighboring RPE cells, abundant undigested phagosomes accumulated and occupied the cytoplasm (Fig. 25A). Additionally, I observed smaller granules scattering throughout the cytoplasm of a subretinal cell. However, the origin of these smaller granules is unknown (Fig. 25B).

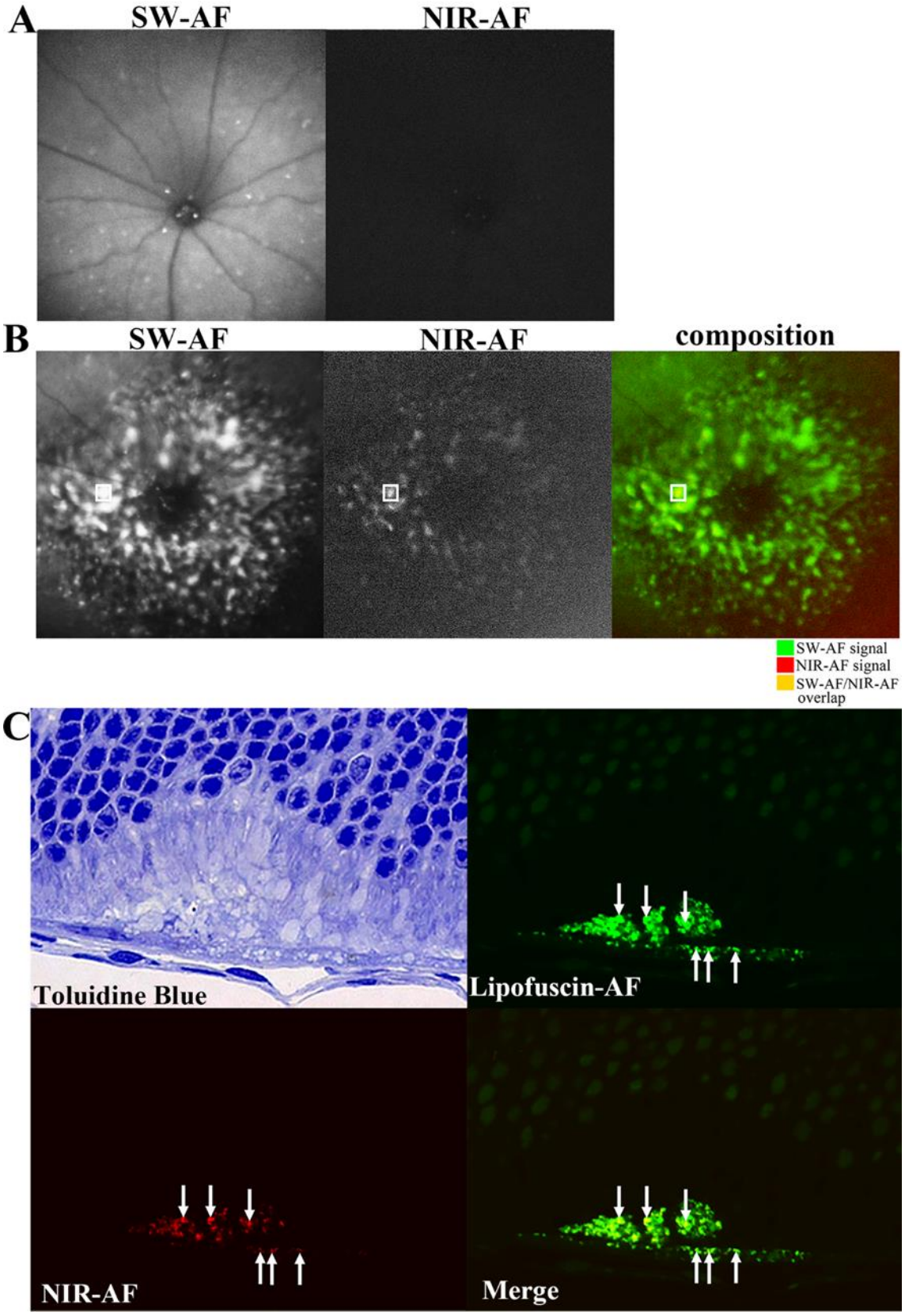

Figure 24. NIR-AF signal was observed in vivo and ex vivo after BLI in albino *Abca4*$^{-/-}$ mice. (**A**) Representative fundus SW-AF (left) and NIR-AF (right) images from an albino *Abca4*$^{-/-}$ mouse before BLI. (**B**) SW-AF and NIR-AF images were correlated in

albino *Abca4*$^{-/-}$ mice after blue light illumination. The green-coded SW-AF image and red-coded NIR-AF image were composited. Boxes: The flecks were hyper autofluorescent in both modalities and appeared yellow on image composition. (**C**) Representative microscopic images of the blue light-illuminated albino *Abca4*$^{-/-}$ mouse. The aberrant cells exhibited lipofuscin AF and NIR-AF. *White arrows*: the pigment granules showed both lipofuscin AF and NIR-AF.

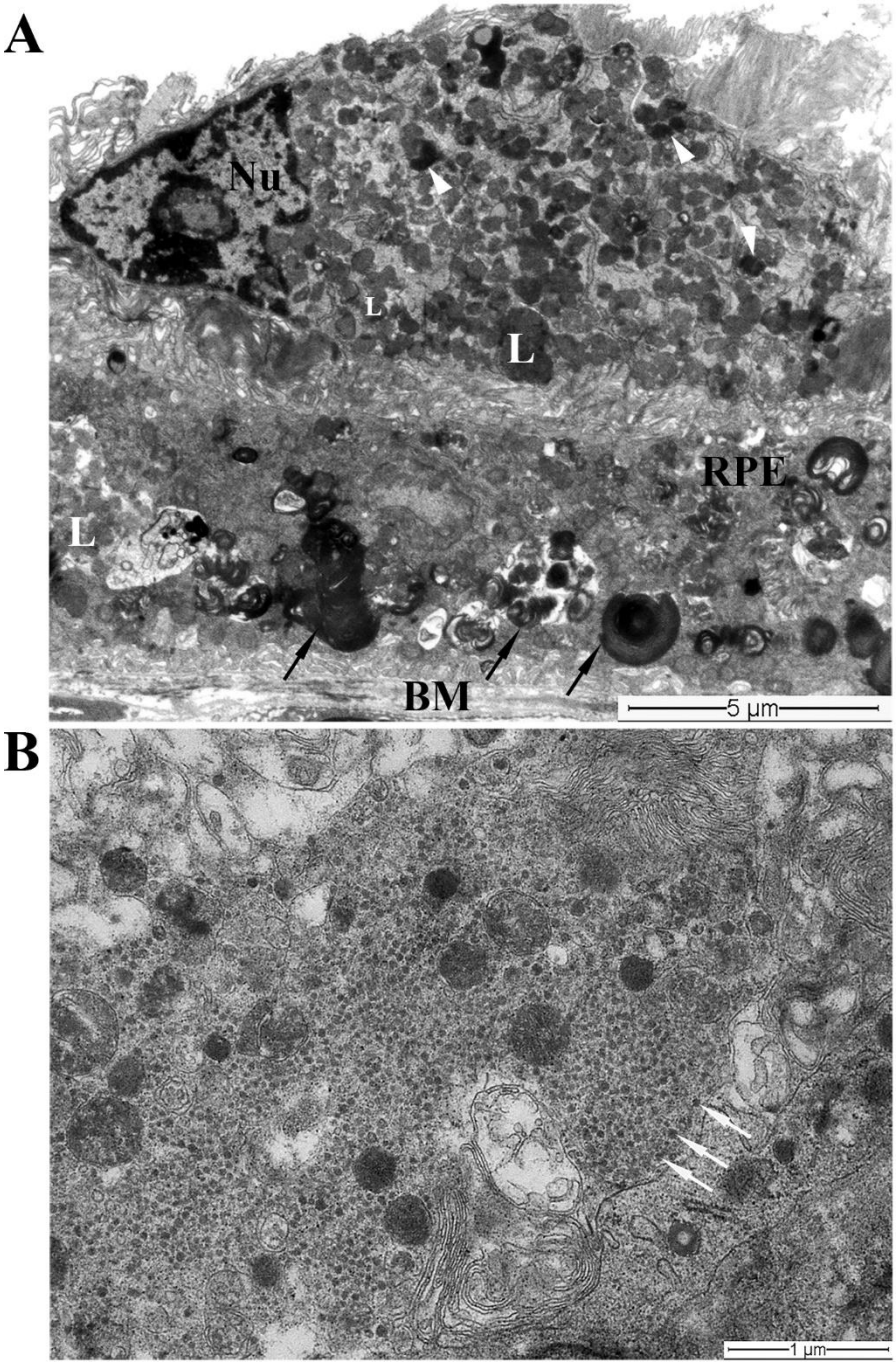

Figure 25. Ultrastructure changes in 9-month-old albino *Abca4*$^{-/-}$ mice seven days after BLI. (A) The aberrant cells fully packed with lipofuscin are located in the subretinal space adjacent to atrophic RPE cells. Some lipofuscin granules were observed with higher electron density. Numerous undigested phagosomes (black arrows) accumulated

and extensively occupied cytoplasm of atrophic RPE cells. **(B)** The suffusion of smaller granules was observed in the cytoplasm of a subretinal aberrant cell. L: lipofuscin, Nu: nucleus, RPE: retinal pigment epithelium, BM: Bruch's membrane.

3.2 Protective effect of Remofuscin® on the retina in pigmented *Abca4*$^{-/-}$ mice after BLI

3.2.1. Treatment with Remofuscin® ameliorated blue light-induced retinal dysfunction

To demonstrate the protective effect of Remofuscin® on retinal function from acute blue light exposure, ERG was performed before treatment, 28 days after intravitreal injection of Remofuscin®/vehicle and seven days after blue light illumination. In non-treated eyes, no change of a-wave and b-wave amplitudes was observed after 28 days (Fig. 26A). By comparison of the ERG amplitudes recorded before intravitreal injection with those recorded 28 days after injection, it was confirmed that treatment with Remofuscin® or vehicle solution showed no toxicity to retina function in pigmented *Abca4*$^{-/-}$ (Fig. 26B-C).

The damage effect of blue light on the eyes was expressed as the percentage of decrease in the amplitudes. As shown in Fig. 27A, treatment with Remofuscin® inhibited blue light-induced reduction of scotopic a-wave amplitudes at the flash intensity of 9.49 cds/m^2 and 25 cds/m^2. After BLI, the differences od a-wave amplitudes between non-treated eyes and Remofuscin®-treated eyes were statistically significant ($n \geq 5$ eyes, $P<0.05$, one-way ANOVA with Bonferroni correction). Blue light decreased the scotopic b-wave amplitudes at the flash intensities from 3 cds/m^2 to 25 cds/m^2 by 70-80% in non-treated eyes and by 59-70% in vehicle-treated eyes, respectively. In the Remofuscin®-treated eyes, the scotopic b-wave amplitudes were decreased by 20-41% at the intensities from 0.095 cds/m^2 to 25 cds/m^2. Treatment with Remofuscin® suppressed the blue light-induced decrease in b-wave amplitudes at the flash intensities from 0.095 cds/m^2 to 25 cds/m^2 markedly ($n \geq 5$ eyes, $P<0.05$, one-way ANOVA with

Bonferroni correction) (Fig. 27B).

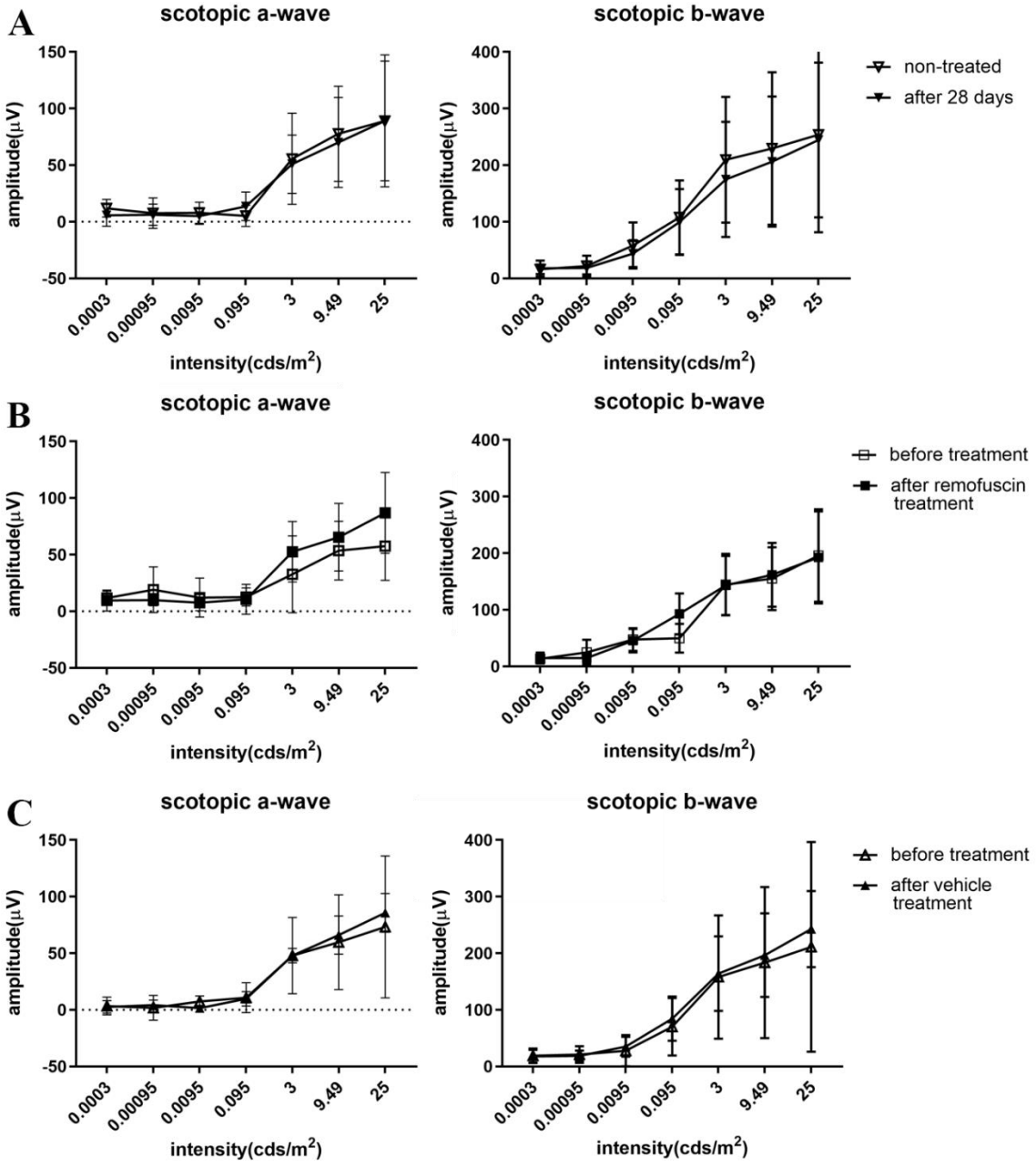

Figure 26. Treatment with Remofuscin® has no toxicity to retina function. (A-C) In non-treated eyes, Remofuscin®-treated eyes and vehicle-treated eyes, no difference of a-wave and b-wave amplitudes were observed between the ERG data recorded before and 28 days after treatment. The data are expressed as the means (SD), $n_{non\text{-}treated}$ = 11 eyes, $n_{Remofuscin}$ = 7 eyes, $n_{vehicle}$ = 6 eyes. Significant differences were calculated with one-way ANOVA with Bonferroni correction.

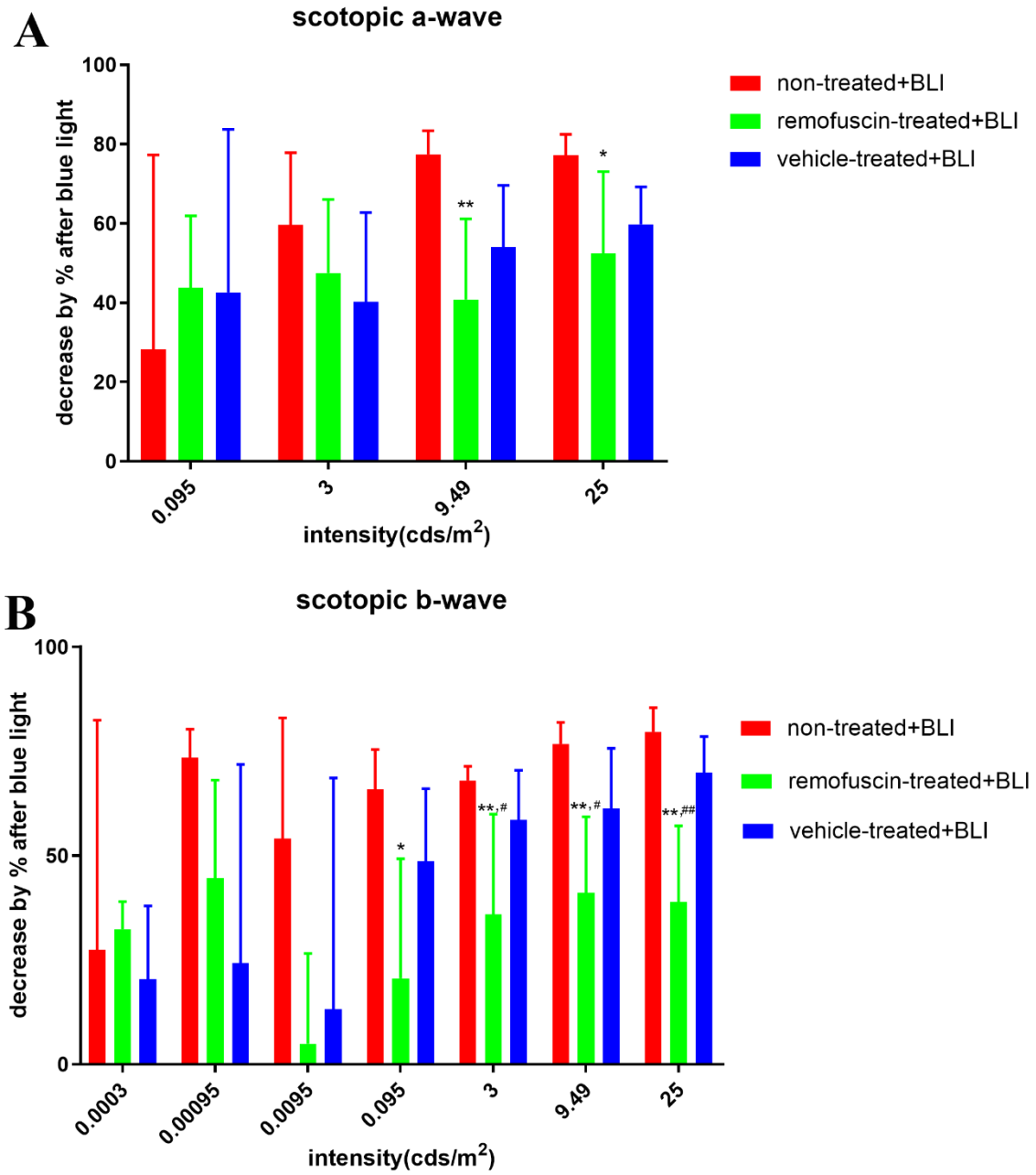

Figure 27. Treatment with Remofuscin® ameliorated blue light-induced retinal dysfunction. (A) After BLI, the percentage of decrease in scotopic a-wave amplitudes of non-treated, Remofuscin®-treated and vehicle-treated eyes were analyzed. **(B)** After BLI, the percentage of decrease in scotopic b-wave amplitudes of non-treated, Remofuscin®-treated and vehicle-treated eyes were analyzed. The data are expressed as the means (SD), n ≥5 eyes. Significant differences were calculated with one-way ANOVA with Bonferroni correction. *P<0.05, **P<0.01, Remofuscin®-treated+BLI vs. non-treated+ BLI. #P<0.05, ##P<0.01, Remofuscin®-treated+BLI vs. vehicle-treated+BLI.

3.2.2. Treatment with Remofuscin® increased blue light-induced reduction

of fundus SW-AF intensity in the mice

Fundus AF was recorded before treatment with Remofuscin®/vehicle and seven days after BLI by using SLO. The mean grey value of nonnormalized SW-AF images was measured and corrected for quantitative analysis of fundus AF as previously mentioned. The results revealed that compared to non-treated and vehicle-treated eyes, Remofuscin®-treated eyes showed a greater reduction in mean intensity of fundus SW-AF after blue light (Fig. 28).

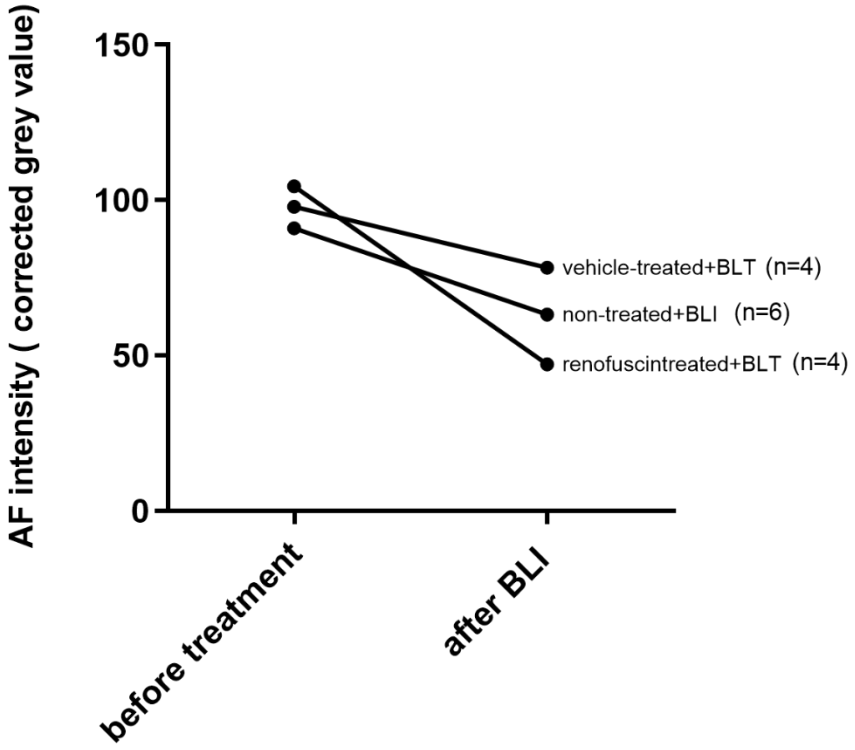

Figure 28. Treatment with Remofuscin® reduced the intensity of fundus AF in mice. The mean intensity of fundus SW-AF was measured in non-treated, vehicle-treated and Remofuscin®-treated eyes before intravitreal injection and seven days after BLI. The data are expressed as the means (SD), n ≥ 4 eyes.

3.2.3. Treatment with Remofuscin® suppressed blue light-induced thinning of the retina in OCT scans

The total retinal thickness of the eyes from each group was measured and plotted from ONH to the superior and the inferior along the vertical axis in OCT images. As previously mentioned, the lesion area induced by blue light was from 400μm

inferior position to ONH and 700μm superior position to ONH along the vertical meridian. Compared to the non-treated eye, the retinal thickness of Remofuscin®-treated eyes increased within the area from 300μm inferior position to ONH and 500μm superior position to ONH along vertical meridian significantly (n≥7 eyes, P<0.05, one-way ANOVA with Bonferroni correction). There was no significant difference between non-treated eyes and vehicle-treated eyes. Above results revealed that treatment with Remofuscin® suppressed blue light-induced retinal thinning (Fig. 29).

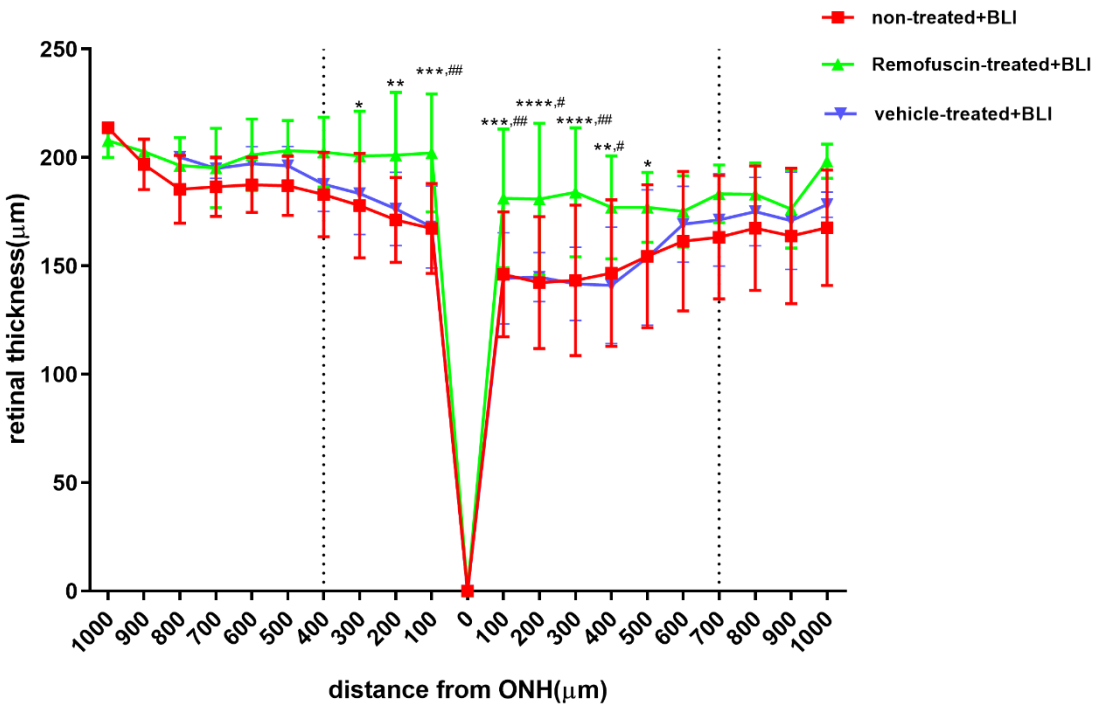

Figure 29. Treatment of Remofuscin® suppressed blue light-induced thinning of the retina in OCT scans. The total retinal thickness of the eyes from each group was measured and plotted from ONH to the superior and the inferior along the vertical axis. No significant difference between non-treated eyes and vehicle-treated eyes. The data are expressed as the means (SD), n≥7 eyes. Significant differences were calculated with one-way ANOVA with Bonferroni correction for multiple comparisons. *P<0.05, **P<0.01, ***P<0.001, ****P<0.0001, Remofuscin®-treated+BLI vs. non-treated+ BLI. $^{\#}$P<0.05, $^{\#\#}$P<0.01, Remofuscin®-treated+BLI vs. vehicle-treated+BLI.

3.2.4. Treatment of Remofuscin® suppressed the blue light-induced loss of RPE and photoreceptors

After BLI, GA was observed in non-treated eyes and vehicle-treated eyes near the ONH, especially in the superior semi-retina (Fig. 30A-B). In Remofuscin®-treated eyes, photoreceptors and RPE cells were preserved. The lamellar structure of retina was deformed by blue light, thus the rosette-like structure of ONL was formed. Accumulation of aberrant pigmented cells in the subretinal space and multilayered RPE cells were observed in Remofuscin®-treated eyes (Fig. 30C).

As previously mentioned, blue light diminished the number of RPE nuclei pronouncedly in the area from 400 μm inferior to ONH and 800μm superior to ONH and reduced number of photoreceptor nuclei dramatically from 200 μm inferior position to 600 μm superior position. To examine the protective effect of Remofuscin® against blue light-induced retinal cell loss, the average of RPE nuclei within each 200 μm interval was measured as a function of distance in the area from 400 μm inferior to ONH and 800μm superior to ONH. The average of photoreceptor nuclei in ONL within each 200 μm interval was quantified as a function of distance in the area from 200 μm inferior to ONH and 600μm superior to ONH. After BLI, compared to non-treated eyes and vehicle eyes, Remofuscin®-treated eyes showed increases in the number of RPE nuclei and photoreceptor nuclei of ONL significantly ($n \geq 4$ eyes, $P<0.05$, one-way ANOVA with Bonferroni correction). The results revealed that treatment with Remofuscin® caused a rescue of RPE and photoreceptor cells from blue light-induced damage (Fig. 30D-E).

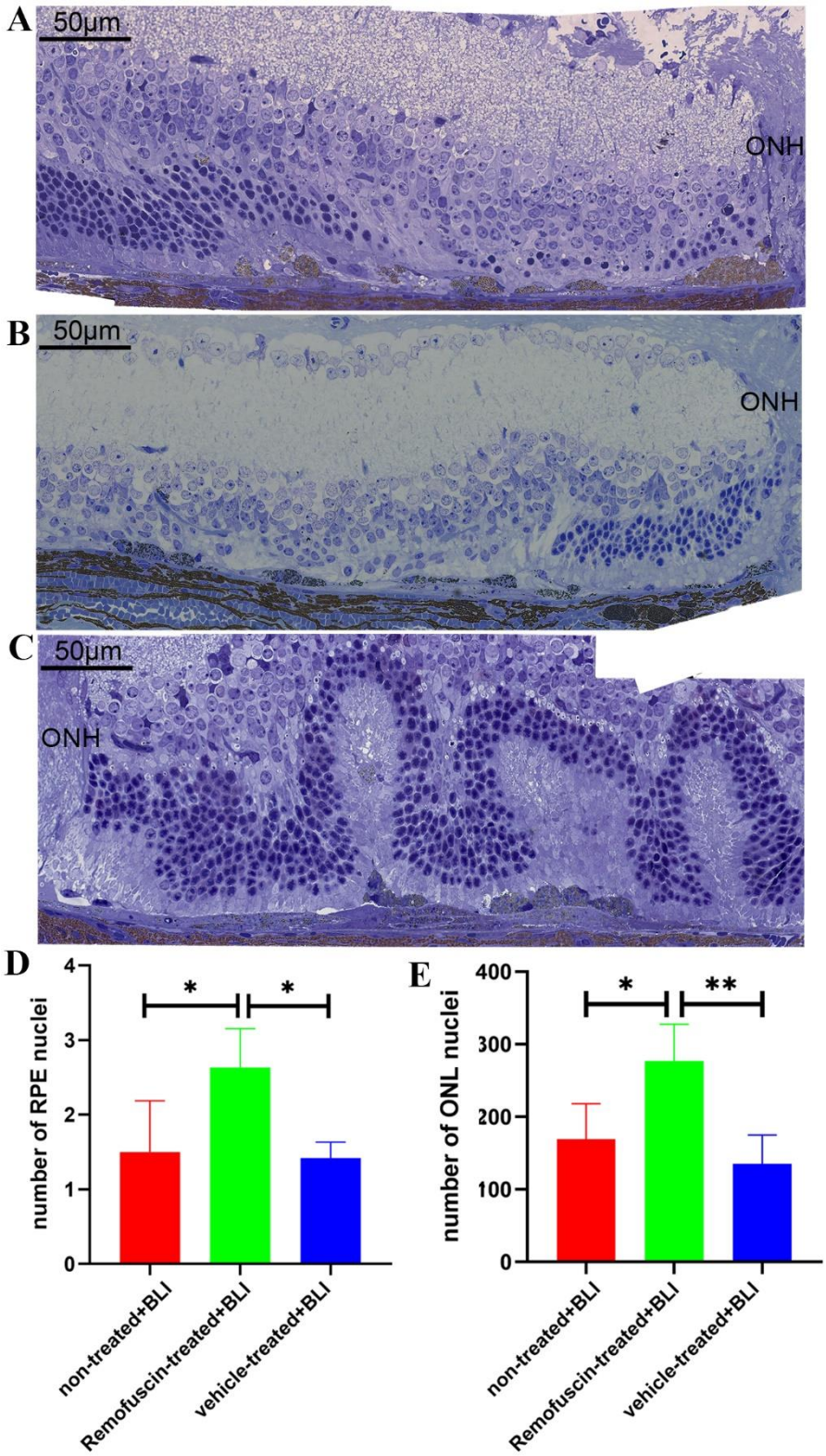

Figure 30. Treatment of Remofuscin® suppressed the blue light-induced loss of RPE and photoreceptors. (A) Representative image of the semi-thin section from a non-treated eye after BLI. **(B)** Representative image of the semi-thin section from a vehicle-treated eye after BLI. **(C)** Representative image of the semi-thin section from a Remofuscin®-treated eye after BLI. **(D)** The average of RPE nuclei within each 200 µm

interval was measured as a function of distance from 400 μm inferior to ONH and 800μm superior to ONH. **(E)** The average of photoreceptor nuclei in ONL within each 200 μm interval was quantified as a function of distance from 200 μm inferior to ONH and 600μm superior to ONH. The data are expressed as the means (SD), n≥4 eyes. Significant differences were calculated with one-way ANOVA with Bonferroni correction for multiple comparisons. *P<0.05, **P<0.01.

4. Discussion

4.1. Blue light-illuminated pigmented *Abca4*$^{-/-}$ mice reflect the advanced Stargardt disease

A correlation has been found between the foveal NIR-AF pattern and vision acuity in Stargardt patients (Parodi et al., 2015). Cideciyan, et al. also have suggested the importance of wide-angle NIR-AF for following the progression of the early-stage of ABCA4-associated retinal disease (Cideciyan et al., 2015). RPE melanin plays a great role in the pathology and diagnosis of Stargardt disease. I induced the retinal degeneration by illuminating the pigmented *Abca4*$^{-/-}$ mice with blue light.

In rodents, RPE cells in the central retina contain a higher level of lipofuscin and a lower level of melanin than in the peripheral retina (Grey et al., 2011, Polosa et al., 2017). In line with the phototoxicity of RPE lipofuscin and antioxidative properties of RPE melanin (Taubitz et al., 2018, Wang et al., 2006), blue light-induced lesions were observed to mainly locate in the central area of the retina of pigmented *Abca4*$^{-/-}$ mice. In this study, quantification of photoreceptor nuclei and RPE nuclei revealed that RPE cells were more susceptible to acute blue light damage than photoreceptors. Moreover, consistent with the observations in Stargardt patients (Greenstein et al., 2015), blue light-induced RPE loss preceded photoreceptor loss. An early study has shown that RPE degeneration is followed by photoreceptor degeneration in blue light-exposed wild-type mice (Nakamura et al., 2018). In *Abca4*$^{-/-}$ mice, abundant bisretinoids increase the risk of blue light-induced RPE degeneration (Wu et al., 2014). Bisretinoids also form

in the OS but remained at a minimum level because of RPE phagocytic function and continuous renewal of OS. The function of RPE is known to support photoreceptor viability. The findings of the present study indicate that blue light initially damages RPE, followed by photoreceptor degeneration in *Abca4*$^{-/-}$ mice.

A longitudinal study of AF in Stargardt patients demonstrated that fleck lesions were increased in SW-AF over time to a peak of hyperAF, and then decreased in SW-AF subsequently and eventually became hypoAF (Cukras et al., 2012). NIR-AF of lesions also changed similarly over time, but the rate of decline in NIR-AF to hypoAF occurred more quickly (Cukras et al., 2012). In this work, both the mean intensities of SW-AF and NIR-AF were reduced in blue light-illuminated pigmented *Abca4*$^{-/-}$ mice. This finding is consistent with the AF changes observed in both modalities in the late stage of Stargardt disease.

I found that blue light-induced abnormalities in SW-AF and NIR-AF were correlated. Correlation between SW-AF and NIR-AF showed three features of fundus AF abnormalities in blue light-illuminated pigmented *Abca4*$^{-/-}$ mice, which are consistent with the observations in Stargardt patients (Cukras et al., 2012, Kellner et al., 2009). First, the majority of lesions showed hyper SW-AF but hypo NIR-AF. Second, the lesions showed hyper-AF in both modalities. Third, the lesions also appeared as dark patches in both modalities.

Blue light-induced lesions were demonstrated by OCT and classified according to the invasion of different retinal layers into 5 Categories. The hyper-reflective material attaching to RPE/Bruch's membrane layer as a common characteristic was observed in the most lesions, except the lesions of Category 2. It is noticeable that dependent on expanding the level of hyper-reflective material, retinal flecks in Stargardt patients showed by SD-OCT have been categorized into distinct groups (Voigt et al., 2010). The expansion of hyperreflective deposits is indicative of stages in the degeneration of surrounding photoreceptor cells and STGD atrophy evaluation (Sparrow et al., 2015, Battaglia Parodi et al., 2019).

In human ABCA4-associated retinal degeneration, the disease sequence has been defined as six stages based on retinal function and structure. Thereinto, Stage Ⅰ is proposed as normal retinal structure and function with normal AF intensity (Cideciyan et al., 2004). While, the pigmented *Abca4*$^{-/-}$ mouse model possesses same characteristics as early stage of the human disease sequence-Stage Ⅱ (increased AF intensity with normal retinal function) (Charbel Issa et al., 2013). Stage Ⅲ and Stage Ⅵ defined respectively as an increase in mean fundus AF intensity and texture, and complete loss of RPE and photoreceptors (Cideciyan et al., 2004) are inconsistent with the observations in this study. Nevertheless, this mouse model mainly reflects the features as shown by advanced stages involving increased fundus AF texture with partial degeneration of photoreceptors (Stage Ⅳ), reduction of mean fundus AF intensity with a further decline of retinal function (Stage Ⅴ).

The histological features in patients with Stargardt disease are not fully studied. The cell components of the hyperreflective deposits are still unclear. In this study, the findings of light and fluorescence microscopy were correlated with fundus AF imaging and SD-OCT scans to interpret the underlying retinal histology of AF abnormalities. First, the sites with hyper SW-AF and hypo NIR-AF (near to background) corresponded to diverse changes in the layers of photoreceptors, such as the loss of IS/OS and reduction or loss of the ONL on OCT. Decreased NIR-AF after blue light can be interpreted by a reduction and loss of melanin in the damaged RPE cells as I observed by electron microscopy (Fig. 20B-C). The damaged cells containing few melanin but abundant undigested phagosomes in the cytoplasm probably caused hyper SW-AF and hypo NIR-AF (Figure 20C-D). Undegraded phagosomes in RPE cells have been reported to exhibit lipofuscin-like fluorescence (Katz et al., 2005). Due to the presence of retinoids in RPE cells, chemical modification in the components of the phagocytosed outer segments

develops lipofuscin-like fluorescence properties (Katz et al., 2005). The accumulation of undegraded phagosomes in RPE cells might be a potential source of SW-AF. The erythrocytes in the choroid without fluorescein labelling were not fluorescent in SLO imaging, although they were autofluorescent under the fluorescence microscope (Wajer et al., 2000). Second, the site with hypo AF in SW-AF and NIR-AF (box 2 in Fig. 19A) showed a reduction of all retinal layers on OCT (box 2 in Fig. 19B). In semithin sections, a reduction of photoreceptors and the absence of RPE cells, resulting in the absence of lipofuscin- AF or the NIR-AF signal, were observed at the corresponding site (box 2 in Fig. 19C-E). Thus, the loss of RPE cells explained the reduction of the mean AF intensity in both modalities. Moreover, photooxidation-induced photodegradation of bisretinoids and photodegradation of melanin caused the loss of bisretinods, melanin and their relevant AF (Ueda et al., 2016, Sarna et al., 2003, Dontsov et al., 2017), which was evident in damaged RPE cells under the fluorescence microscope (Fig. 16B). In Stargardt patients, hypoAF patches associated with poorer visual acuity were prominent in the advanced stage (Kumar, 2017). Third, the sites with hyperAF in SW-AF and NIR-AF (box 1 and box 3 in Fig. 19A) showed hyperreflective material protruding from the RPE/Bruch's membrane layer into the ONL layer (box 1, box3 in Fig. 19B). There was an accumulation of aberrant pigmented cells with highly lipofuscin-derived AF and NIR-AF in the subretinal space at the corresponding site in the semithin section (box 1, box3 in Fig. 19C-E). The presence of hyperreflective lesions in OCT images is a common pathological feature in Stargardt patients. However, its cell components are controversial. Battaglia Parodi, M. et al. suggested that outer retina hyperreflective foci result from the transdifferentiation of RPE cells after the epithelial-mesenchymal transition process (Battaglia Parodi et al., 2019). Paavo et al. suggested that the origin of hyperreflective foci is bisretinoid residing in photoreceptors (Paavo et al., 2018). This work demonstrated that the origin of

hyperreflective lesions is the accumulation of subretinal aberrant pigmented cells. Subretinal aberrant pigmented cells located closer to the inner retina were associated with higher signals in SW-AF and NIR-AF.

In the EM images, two types of pigmented cells were observed in this mouse model: ⅰ) isolated pigmented cells filled with pigment granules (melanin, lipofuscin and melanolipofuscin) in the subretinal space and ⅱ) pigment granule-ladened pigmented cells attaching to Bruch's membrane. The isolated pigmented cells were identified as macrophages by their Iba1 positivity. The presence of macrophages engorged with melanolipofuscin and lipofuscin granules in the outer retina was reported in the donor eyes of a Stargardt patient (Birnbach et al., 1994). However, the isolated pigmented cells in the subretinal space were recognized as migrated RPE cells in Stargardt patients (Bonilha et al., 2016, Birnbach et al., 1994). In addition to immunostaining, RPE cells and macrophages could be distinguished according to their ultrastructure. Atrophic RPE cells and macrophages were both fully packed with pigment granules (melanin, lipofuscin and melanolipofuscin). The features of RPE cells ultrastructure involve cellular junctions, the basal lamina and attachment to Bruch's membrane. However, the macrophages appear to have an irregular cell shape and many extensions of the cell membrane (RYTER, 1985) and no attachment to the Bruch's membrane. Thus, I suggested that the aberrant pigmented cells could be isolated macrophages and atrophic RPE cells attaching to the Bruch's membrane.

Correlative analysis between the distribution of lipofuscin and melanin under the fluorescence microscope revealed the presence of granules with both lipofuscin AF and NIR-AF in the blue light-illuminated mice and donor eye with the late stage of Stargardt disease. It is demonstrated that these granules were lipofuscin or/and melanolipofuscin. In blue light-illuminated albino *Abca4*$^{-/-}$ mice, NIR-AF was observed both *in vivo* by the fundus AF and *ex vivo* by the fluorescence

microscopy. With the absence of melanin, the lipofuscin granules in the subretinal aberrant cells and atrophic RPE cells exhibited both lipofuscin-AF and NIR-AF after blue light illumination. Thus, I suggested that the fluorescence properties of the bisretinoid fluorophores in lipofuscin were modified during the pathological process of blue light damage and Stargardt disease, thus contributing to NIR-AF. The melanolipofuscin granules are considered to be formed by the fusion of lipofuscin and melanin with aging and oxidative stress (Feeney-Burns L Fau - Hilderbrand et al., 1984, Warburton et al., 2007). It is likely that the lipofuscin-like composition (Biesemeier et al., 2011) of melanolipofuscin changed its fluorescence properties and contributed to NIR-AF (Taubitz et al., manuscript in preparation). Additionally, the melanosomes in the subretinal pigmented cells showed brighter NIR-AF than in normal RPE cells. Blue light is known to cause photobleaching enhances the fluorescence intensity of melanosomes (Sarna et al., 2003). Photooxidation is a contributor to age-related changes in melanosome morphology (Sarna et al., 2003, Boulton et al., 1990). Likewise, the increase in the RPE melanin signal was demonstrated in most ABCA4-STGD1 patients (Sears et al., 2017). These findings together indicate that chemical alterations of pigment granules (melanin, lipofuscin, melanolipofuscin) change their fluorescence properties in the late stage of Stargardt disease and this mouse model. Additionally, photoreceptors were not observed with AF in pigmented *Abca4*$^{-/-}$ mice before or after blue light illumination. The outer segments are normally observed without lipofuscin-like AF (Katz et al., 1996). The amount of A2PE in normal *Abca4*$^{-/-}$ OS might be insufficient to cause detectable AF. Interestingly, the lipofuscin-like AF of unphagocytosed outer segments with bisretinoids at a high level was observed in RCS rats and albino *Mertk*$^{-/-}$mice but was not visible in agouti *Mertk*$^{-/-}$ mice (KATZ et al., 1987, Zhao et al., 2018). Thus, the presence of melanin interferes with the AF of OS. The AF (730-nm) of OS only could be seen in the early phase of light exposure (Maeda et al., 2014).

Seven days after blue light illumination, the AF of OS was probably too weak to be detectable in contrast to hyper AF of lipofuscin.

In conclusion, this mouse model reflects the clinical manifestations of advanced Stargardt disease and AMD. Blue light diminished the intensities of fundus SW-AF and NIR-AF. Quantitative analysis of RPE nuclei and photoreceptor nuclei indicated that RPE loss preceded photoreceptor loss after blue light in *Abca4*$^{-/-}$ mice. The correlation of the findings among fundus autofluorescence, SD-OCT, fluorescence microscope and histology can be used to interpret the underlying histological characteristics of fundus AF abnormalities and structural disorders on OCT. Subretinal macrophages phagocytizing RPE debris were proven to be sources of both hyper SW-AF and hyper NIR-AF. Melanin in macrophages with higher NIR-AF, lipofuscin and melanolipofuscin granules expressing SW-AF and NIR-AF indicated chemical alterations of pigment granules after blue light damage. This model could be applied to the preclinical study of therapy strategies for the advanced stage of Stargardt disease.

4.2. Remofuscin® ameliorated retinal degeneration in the mouse model of advanced Stargardt disease

Thus, this mouse model was applied to study the protective effect of Remofuscin® on the retina. Treatment with Remofuscin® showed no toxicity to retina function in ERG assessments. Single intravitreal injection of Remofuscin® reduced the lipofuscin-derived SW-AF efficiently. The results demonstrated that treatment with Remofuscin® ameliorated retinal dysfunction, increased the reduction in fundus SW-AF intensity and rescued of RPE cells and photoreceptors in the mouse model of advanced Stargardt disease. Treatment with Remofuscin® suppressed retinal degeneration in the mouse model which reflected advanced Stargardt disease. Its protective effect on retina resulted from the ability of removal of lipofuscin (Fang Y, et al. IOVS. 2017; ARVO E-Abstract B0287).

What might be the mechanisms of action of Remofuscin®? Even though mature lipofuscin was considered to be undegradable and unremovable from cells by exocytosis (Terman and Brunk, 1998). However, later on, it has been suggested that bisretinoids A2E undergoes photodegradation and photocleavage by quenching the ROS (Wu et al., 2010). Thus, it is hypothesized that with the presence of light, Remofuscin® accumulating within pigment granules of RPE (Fang Y, et al. IOVS. 2017; ARVO E-Abstract B0287) generates reactive oxygen species (ROS) without damage to the retina. Lipofuscin is hydrolyzed and thus broke up into small particles with the participation of ROS. The small particles are likely to be removed by exocytosis of RPE cells and then phagocytosed by macrophages. Then during blue light toxicity, less ROS are formed by lipofuscin, because the amount of lipofuscin has been reduced by Remofuscin®.

These findings indicated that removal of lipofuscin by Remofuscin® is an effective strategy of therapy for Stargardt disease and AMD.

4.3. Limitation of this study

Further analysis of the chemical alteration of pigment granules (lipofuscin, melanolipofuscin and melanin) in RPE cells after blue light is needed. Further study of the mechanisms of the action of Remofuscin® is needed. In this study, the blue light with high intensity reduced the accumulation of lipofuscin and induced severe retinal degeneration. For further study, blue light with low intensity could be applied to study its effect on reducing lipofuscin accumulation.

5. Summary

Stargardt disease (STGD1), known as the most prevalent form of inherited macular dystrophy, is related to ABCA4 mutations. The pigmented *Abca4*$^{-/-}$ mouse strain is considered to be a mouse model of the early phase of Stargardt disease, due to the absence of retinal degeneration. In this study, to induce retinal degeneration in pigmented *Abca4*$^{-/-}$ mice, these mice were illuminated with blue light. By comparing the in vivo assessments including ERG, fundus SW-AF,

fundus NIR-AF and OCT from the mouse model to those from Stargardt patients, I demonstrated that this mouse model reflected the clinical manifestations of advanced Stargardt disease. The results indicated that acute blue light reduced the mean AF intensities of fundus SW-AF and NIR-AF. Additionally, it was indicated that RPE loss preceded the photoreceptor loss in the blue light-illuminated *Abca4*$^{-/-}$ mice. In albino *Abca4*$^{-/-}$ mice, NIR-AF was observed after blue light illumination. Lipofuscin and melanolipofuscin granules were found to contribute to NIR-AF, in the late-stage Stargardt patient and blue light-illuminated *Abca4*$^{-/-}$ mice. It suggested that Stargardt disease and blue light damage in *Abca4*$^{-/-}$ mice shared a common pathological process which changed the fluorescence properties of lipofuscin and melanin. In this mouse model, the correlation between *in vivo* and *ex vivo* assessments revealed histological characteristics of fundus AF abnormalities. The subretinal macrophages fully packed with pigment granules (lipofuscin, melanin, melanolipofuscin) were found as one of the sources of the fundus hyper SW-AF and NIR-AF. This mouse model, which has the phenotypes of advanced STGD1, is important to understand the histopathology of Stargardt disease.

This model also could be used for preclinical study of therapy strategies for the advanced stage of Stargardt disease. Remofuscin®, a remover of lipofuscin, was applied in this mouse model. Single intravitreal injection of Remofuscin® removed lipofuscin from RPE cells thus suppressed blue light-induced retinal degeneration. Remofuscin® is a potential therapeutic drug for lipofuscin-related retinopathies.

6. Zusammenfassung

Die Stargardt Erkrankung (STGD1), bekannt als die häufigste Form der erblich bedingten Makuladystrophie, wird verursacht durch ABCA4 Mutationen. Der pigmentierte *Abca4*$^{-/-}$ Mausstamm ist als Tiermodell nur für die frühe Phase der Stargardt Erkrankung akzeptiert, weil bei diesen Tieren die

Netzhautdegeneration ausbleibt. In dieser Studie wurde bei pigmentierten *Abca4* $^{-/-}$ Mäusen eine Netzhautdegeneration durch Belichtung mit Blaulicht ausgelöst. Durch vergleichende *in vivo* Untersuchungen mit Elektroretinographie (ERG), mit der Messung der Fundusautofluoreszenz im kurzwelligen (SW-AF) und nahem Infrarotbereich (NIR-AF) und mit optischer Kohärenztomograhie (OCT) konnte ich zeigen, dass dieses Mausmodell die klinischen Charakteristika von fortgeschrittener Stargardt Erkrankung hat. Die Ergebnisse zeigten, dass intensive Belichtung mit Blaulicht die mittlere Intensität der Fundusautofluoreszenz im kurzwelligen und nahem Infrarotbereich reduziert.

Zusätzlich zeigte sich, dass in *Abca4*$^{-/-}$ Mäusen nach Toxizität, verursacht durch Blaulicht, retinale Pigmentepithelzellen noch vor den Photorezeptoren geschädigt werden und früher als diese sterben.

In albinotischen *Abca4*$^{-/-}$ Mäusen wurde erstmals NIR-AF im durch Blaulicht geschädigten subretinalen Bereich gefunden.

Lipofuszin- und Melanolipofuszingranula wurden als Verursacher der NIR-Autofluoreszenz bei einem Patentient mit später Stargardt Erkrankung und bei durch Blaulicht geschädigten *Abca4*$^{-/-}$ Mäusen identifiziert. Daher ist es mehr als wahrscheinlich, dass bei Stargardt Erkrankung und durch Blaulicht geschädigten *Abca4*$^{-/-}$ Mäusen ein gemeinsamer pathologischer Process zugrunde liegt, der die Fluoreszenzeigenschaften von Lipofuszin und Melanin verändert. In diesem Mausmodel konnten die *in vivo* Untersuchungen mit histologischen Merkmalen *ex vivo* korreliert werden.

Subretinale Makrophagen, die voll gepackt mit Pigmentgranula (Lipofuszin, Melanin und Melanolipofuszin) waren, wurden als eine der Ursache von Fundus Hyper-Autofluoreszenz im kurzwelligen und nahem Infrarotbereich identifiziert.

Das in dieser Arbeit entwickelte Mausmodell, welches den Phänotyp von fortgeschrittener Stargardterkrankung (STGD1) zeigt, hilft die

histopathologischen Veränderungen bei Stargardt Erkrankung besser zu verstehen.

Außerdem wurde gezeigt, dass die lichtgeschädigte *Abca4*$^{-/-}$ Maus als Modell in präkilischen Studien zur Therapieentwicklung bei fortgeschrittener Stargardt Erkrankung verwendet werden kann.

Dieses wurde durch Behandlung mit Remofuscin®, einem Entferner von Lipofuszin, gezeigt. Eine einzige intravitreale Injektion von Remofuscin® entfernte Lipofuszin aus den RPE Zellen, was durch verminderte Autofluoreszenz gezeigt wurde, und reduzierte die durch Blaulicht verursachte Netzhautdegeneration.

Es wurde gezeigt, dass Remofuscin® ein potentielles Medikament für die Behandlung von durch Lipofuszin verursachten retinalen Erkrankungen ist.

7. Bibliography

Allikmets, R., Singh N Fau - Sun, H., Sun H Fau - Shroyer, N. F., Shroyer Nf Fau - Hutchinson, A., Hutchinson a Fau - Chidambaram, A., Chidambaram a Fau - Gerrard, B., Gerrard B Fau - Baird, L., Baird L Fau - Stauffer, D., Stauffer D Fau - Peiffer, A., Peiffer a Fau - Rattner, A., Rattner a Fau - Smallwood, P., Smallwood P Fau - Li, Y., Li Y Fau - Anderson, K. L., Anderson Kl Fau - Lewis, R. A., Lewis Ra Fau - Nathans, J., Nathans J Fau - Leppert, M., Leppert M Fau - Dean, M., Dean M Fau - Lupski, J. R. & Lupski, J. R. 1997. A photoreceptor cell-specific ATP-binding transporter gene (ABCR) is mutated in recessive Stargardt macular dystrophy. *Nature genetics,* 15.

Amit, M., Carpenter, M. K., Inokuma, M. S., Chiu, C.-P., Harris, C. P., Waknitz, M. A., Itskovitz-Eldor, J. & Thomson, J. A. 2000. Clonally derived human embryonic stem cell lines maintain pluripotency and proliferative potential for prolonged periods of culture. *Dev Biol* 227**,** 271-278.

Anastasakis, A., Fishman, G. A., Lindeman, M., Genead, M. A. & Zhou, W. 2011. SLO-infrared imaging of the macula and its correlation with functional loss and structural changes in patients with Stargardt disease. *Retina,* 31**,** 949-58.

Battaglia Parodi, M., Sacconi, R., Romano, F. & Bandello, F. 2019. Hyperreflective foci in Stargardt disease: 1-year follow-up. *Graefes Arch Clin Exp Ophthalmol,* 257**,** 41-48.

Ben-Shabat, S., Parish, C. A., Vollmer, H. R., Itagaki, Y., Fishkin, N., Nakanishi, K. & Sparrow, J. R. 2002. Biosynthetic studies of A2E, a major fluorophore of retinal pigment epithelial lipofuscin. *J Biol Chem,* 277**,** 7183-90.

Berni, R. & Frarte, A. F. 1992. In vitro interaction of fenretinide with plasma retinol-binding protein and its functional consequences. *FEBS LETTERS,* 308**,** 43-45.

Bhosale, P., Serban, B. & Bernstein, P. S. 2009. Retinal carotenoids can attenuate formation of A2E in the retinal pigment epithelium. *Arch Biochem Biophys,* 483**,** 175-81.

Biesemeier, A., Schraermeyer, U. & Eibl, O. 2011. Chemical composition of melanosomes, lipofuscin and melanolipofuscin granules of human RPE tissues. *Exp Eye Res,* 93**,** 29-39.

Birnbach, C. D., Jarvelainen, M., Possin, D. E. & Milam, A. H. 1994. Histopathology and immunocytochemistry of the neurosensory retina in fundus flavimaculatus. *Ophthalmology,* 101**,** 1211-1219.

Blacharski, P. A. 1988. Fundus flavimaculatus. In: Newsome, D. A. (ed.): Retinal Dystrophies and Degenerations. *New York: Raven Press,* Pp. .

Bonilha, V. L., Rayborn, M. E., Bell, B. A., Marino, M. J., Fishman, G. A. & Hollyfield, J. G. 2016. Retinal Histopathology in Eyes from a Patient with Stargardt disease caused by Compound Heterozygous ABCA4 Mutations. *Ophthalmic Genet,* 37**,** 150-60.

Boulton, M., Docchio F Fau - Dayhaw-Barker, P., Dayhaw-Barker P Fau - Ramponi, R., Ramponi R Fau - Cubeddu, R. & Cubeddu, R. 1990. Age-related changes in the morphology, absorption and fluorescence of melanosomes and lipofuscin granules of the retinal pigment epithelium. *Vision Res,* 30**,** 1291-1303.

Boyer, N. P., Higbee, D., Currin, M. B., Blakeley, L. R., Chen, C., Ablonczy, Z., Crouch, R. K. & Koutalos, Y. 2012. Lipofuscin and N-retinylidene-N-retinylethanolamine (A2E) accumulate in retinal pigment epithelium in absence of light exposure: their origin is 11-cis-retinal. *J Biol Chem,* 287**,** 22276-86.

Charbel Issa, P., Barnard, A. R., Singh, M. S., Carter, E., Jiang, Z., Radu, R. A., Schraermeyer, U. & Maclaren, R. E. 2013. Fundus autofluorescence in the Abca4(-/-) mouse model of Stargardt disease--correlation with accumulation of A2E, retinal function, and histology. *Invest Ophthalmol Vis Sci,* 54**,** 5602-12.

Charbel Issa, P., Singh, M. S., Lipinski, D. M., Chong, N. V., Delori, F. C., Barnard, A. R. & Maclaren, R. E. 2012. Optimization of in vivo confocal autofluorescence imaging of the ocular fundus in mice and its application to models of human retinal degeneration. *Invest Ophthalmol Vis Sci,* 53**,** 1066-75.

Cideciyan, A. V., Aleman, T. S., Swider, M., Schwartz, S. B., Steinberg, J. D., Brucker, A. J., Maguire, A. M., Bennett, J., Stone, E. M. & Jacobson, S. G. 2004. Mutations in ABCA4 result in accumulation of lipofuscin before slowing of the retinoid cycle: a reappraisal of the human disease sequence. *Hum Mol Genet,* 13**,** 525-34.

Cideciyan, A. V., Swider, M., Schwartz, S. B., Stone, E. M. & Jacobson, S. G. 2015. Predicting Progression of ABCA4-Associated Retinal Degenerations Based on Longitudinal Measurements of the Leading Disease Front. *Invest Ophthalmol Vis Sci,* 56**,** 5946-55.

Cukras, C. A., Wong, W. T., Caruso, R., Cunningham, D., Zein, W. & Sieving, P. A. 2012. Centrifugal expansion of fundus autofluorescence patterns in Stargardt disease over time. *Arch Ophthalmol,* 130**,** 171-9.

Delori, F. C., Dorey, K., Staurenghi, G., Arend, O., Goger, D. G. & Writer, J. J. 1995. In Vivo Fluorescence of the Ocular Fundus Exhibits Retinal Pigment Epithelium Lipofuscin Characteristics. *Invest Ophthalmol Vis Sci.,* 36**,** 719-729.

Dobri, N., Qin, Q., Kong, J., Yamamoto, K., Liu, Z., Moiseyev, G., Ma, J. X., Allikmets, R., Sparrow, J. R. & Petrukhin, K. 2013. A1120, a nonretinoid RBP4 antagonist, inhibits formation of cytotoxic bisretinoids in the animal model of enhanced retinal lipofuscinogenesis. *Invest Ophthalmol Vis Sci,* 54**,** 85-95.

Dontsov, A. E., Sakina, N. L. & Ostrovsky, M. A. 2017. Loss of Melanin by Eye Retinal Pigment Epithelium Cells Is Associated with Its Oxidative Destruction in Melanolipofuscin Granules. *Biochemistry (Mosc),* 82**,** 916-924.

Egerton, R. F. 2005a. TEM Specimens and Images. *In:* EGERTON, R. F. (ed.) *Physical Principles of Electron Microscopy-- An Introduction to TEM, SEM, and AEM.* Springer.

Egerton, R. F. 2005b. THE TRANSMISSION ELECTRON MICROSCOPE. *In:* EGERTON, R. F. (ed.) *Physical Principles of Electron Microscopy-- An Introduction to TEM, SEM, and AEM.* Springer.

Feeney-Burns L Fau - Hilderbrand, E. S., Hilderbrand Es Fau - Eldridge, S. & Eldridge, S. 1984. Aging human RPE: morphometric analysis of macular, equatorial, and peripheral cells. *Invest Ophthalmol Vis Sci.,* 25**,** 195-200.

Fishman, G. A. 1976. Fundus flavimaculatus. A clinical classification. *Archives of Ophthalmology,* 94**,** 2061-2067.

Fujinami, K., Lois, N., Davidson, A. E., Mackay, D. S., Hogg, C. R., Stone, E. M., Tsunoda, K., Tsubota, K., Bunce, C., Robson, A. G., Moore, A. T., Webster, A. R., Holder, G. E. & Michaelides, M. 2013a. A longitudinal study of stargardt disease: clinical and electrophysiologic assessment, progression, and genotype correlations. *Am J Ophthalmol,* 155**,** 1075-1088 e13.

Fujinami, K., Lois, N., Mukherjee, R., Mcbain, V. A., Tsunoda, K., Tsubota, K., Stone, E. M., Fitzke, F. W., Bunce, C., Moore, A. T., Webster, A. R. & Michaelides, M. 2013b. A longitudinal study of Stargardt disease: quantitative assessment of fundus autofluorescence, progression, and genotype correlations. *Invest Ophthalmol Vis Sci,* 54**,** 8181-90.

Glazer, L. C. & Dryja, T. P. 2002. Understanding the etiology of Stargardt's disease. *Ophthalmology Clinics of North America,* 15(1)**,** 93-100.

Greenstein, V. C., Schuman, A. D., Lee, W., Duncker, T., Zernant, J., Allikmets, R., Hood, D. C. & Sparrow, J. R. 2015. Near-infrared autofluorescence: its relationship to short-wavelength autofluorescence and optical coherence tomography in recessive stargardt disease. *Invest Ophthalmol Vis Sci,* 56**,** 3226-34.

Grey, A. C., Crouch, R. K., Koutalos, Y., Schey, K. L. & Ablonczy, Z. 2011. Spatial localization of A2E in the retinal pigment epithelium. *Invest Ophthalmol Vis Sci,* 52**,** 3926-33.

Han, Z., Conley, S. M., Makkia, R. S., Cooper, M. J. & Naash, M. I. 2012. DNA nanoparticle-mediated ABCA4 delivery rescues Stargardt dystrophy in mice. *Journal of Clinical Investigation,* 122**,** 3221-3226.

Holz, F. G., Schiitt, F., Kopitz, J., Eldred, G. E., Kruse, F. E., Volcker, H. E. & Cantz, M. 1999. Inhibition of Lysosomal Degradative Functions in RPE Cells by a Retinoid Component of Lipofuscin. *Invest Ophthalmol Vis Sci,* 40**,** 737-743.

Hussain, R. M., Ciulla, T. A., Berrocal, A. M., Gregori, N. Z., Flynn, H. W., Jr. & Lam, B. L. 2018. Stargardt macular dystrophy and evolving therapies. *Expert Opin Biol Ther,* 18**,** 1049-1059.

Julien, S. & Schraermeyer, U. 2012. Lipofuscin can be eliminated from the retinal pigment epithelium of monkeys. *Neurobiology of Aging,* 33**,** 2390–2397.

Katz, M. L., Eldred, G. E. & W. Gerald Robison, J. 1987. Lipofuscin autofluorescence: evidence for vitamin A involvement in the retina. *Mech Ageing Dev.,* 39**,** 81-90.

Katz, M. L., Gao Cl Fau - Rice, L. M. & Rice, L. M. 1996. Formation of lipofuscin-like fluorophores by reaction of retinal with photoreceptor outer segments and liposomes. *Mechanisms of Ageing and Development,* 92**,** 159-174.

Katz, M. L., Wendt, K. D. & Sanders, D. N. 2005. RPE65 gene mutation prevents development of autofluorescence in retinal pigment epithelial phagosomes. *Mech Ageing Dev,* 126**,** 513-21.

Kaufman, Y., Ma, L. & Washington, I. 2011. Deuterium enrichment of vitamin A at the C20 position slows the formation of detrimental vitamin A dimers in wild-type

rodents. *J Biol Chem,* 286**,** 7958-65.

Keilhauer, C. N. & Delori, F. C. 2006. Near-infrared autofluorescence imaging of the fundus: visualization of ocular melanin. *Invest Ophthalmol Vis Sci,* 47**,** 3556-64.

Kellner, S., Kellner, U., Weber, B. H., Fiebig, B., Weinitz, S. & Ruether, K. 2009. Lipofuscin- and melanin-related fundus autofluorescence in patients with ABCA4-associated retinal dystrophies. *Am J Ophthalmol,* 147**,** 895-902, 902 e1.

Kim, S. R., Nakanishi, K., Itagaki, Y. & Sparrow, J. R. 2006. Photooxidation of A2-PE, a photoreceptor outer segment fluorophore, and protection by lutein and zeaxanthin. *Exp Eye Res,* 82**,** 828-39.

Kubota, R., Al-Fayoumi, S., Mallikaarjun, S., Shiva Patil, P., Claes Bavik, P. & Chandler, J. W. 2014. Phase 1, dose-ranging study of emixustat hydrochloride (ACU-4429), a novel visual cycle modulator, in healthy volunteers. *Retina,* 34**,** 603-609.

Kumar, V. 2017. Insights into autofluorescence patterns in Stargardt macular dystrophy using ultra-wide-field imaging. *Graefes Arch Clin Exp Ophthalmol,* 255**,** 1917-1922.

Lambertus, S., Lindner, M., Bax, N. M., Mauschitz, M. M., Nadal, J., Schmid, M., Schmitz-Valckenberg, S., Den Hollander, A. I., Weber, B. H., Holz, F. G., Van Der Wilt, G. J., Fleckenstein, M., Hoyng, C. B. & Foveal Sparing Atrophy Study, T. 2016. Progression of Late-Onset Stargardt Disease. *Invest Ophthalmol Vis Sci,* 57**,** 5186-5191.

Lambertus, S., Van Huet, R. A., Bax, N. M., Hoefsloot, L. H., Cremers, F. P., Boon, C. J., Klevering, B. J. & Hoyng, C. B. 2015. Early-onset stargardt disease: phenotypic and genotypic characteristics. *Ophthalmology,* 122**,** 335-44.

Lenis, T. L., Hu, J., Ng, S. Y., Jiang, Z., Sarfare, S., Lloyd, M. B., Esposito, N. J., Samuel, W., Jaworski, C., Bok, D., Finnemann, S. C., Radeke, M. J., Redmond, T. M., Travis, G. H. & Radu, R. A. 2018. Expression of ABCA4 in the retinal pigment epithelium and its implications for Stargardt macular degeneration. *Proc Natl Acad Sci U S A*.

Lenis, T. L., Sarfare, S., Jiang, Z., Lloyd, M. B., Bok, D. & Radu, R. A. 2017. Complement modulation in the retinal pigment epithelium rescues photoreceptor degeneration in a mouse model of Stargardt disease. *Proc Natl Acad Sci U S A,* 114**,** 3987-3992.

Lin, C. H., Wu, M. R., Li, C. H., Cheng, H. W., Huang, S. H., Tsai, C. H., Lin, F. L., Ho, J. D., Kang, J. J., Hsiao, G. & Cheng, Y. W. 2017. Editor's Highlight: Periodic Exposure to Smartphone-Mimic Low-Luminance Blue Light Induces Retina Damage Through Bcl-2/BAX-Dependent Apoptosis. *Toxicol Sci,* 157**,** 196-210.

Lois, N., Holder, G. E., Bunce, C., Fitzke, F. W. & Bird, A. C. 2001. Phenotypic Subtypes of Stargardt Macular Dystrophy–Fundus Flavimaculatus. *Arch Ophthalmol.,* 119**,** 359-369.

Ma, L., Kaufman, Y., Zhang, J. & Washington, I. 2011. C20-D3-vitamin A slows lipofuscin accumulation and electrophysiological retinal degeneration in a mouse model of Stargardt disease. *J Biol Chem,* 286**,** 7966-74.

Maeda, A., Maeda, T., Golczak, M. & Palczewski, K. 2008. Retinopathy in mice induced by disrupted all-trans-retinal clearance. *J Biol Chem,* 283**,** 26684-93.

Maeda, A., Palczewska, G., Golczak, M., Kohno, H., Dong, Z., Maeda, T. & Palczewski, K. 2014. Two-photon microscopy reveals early rod photoreceptor cell damage in light-exposed mutant mice. *Proc Natl Acad Sci U S A,* 111**,** E1428-37.

Maiti, P., Kong, J., Kim, S. R., Sparrow, J. R., Allikmets, R. & Rando, R. R. 2006. Small Molecule RPE65 Antagonists Limit the Visual Cycle and Prevent Lipofuscin Formation. *Biochemistry* 45**,** 852-860.

Makelainen, S., Godia, M., Hellsand, M., Viluma, A., Hahn, D., Makdoumi, K., Zeiss, C. J., Mellersh, C., Ricketts, S. L., Narfstrom, K., Hallbook, F., Ekesten, B., Andersson, G. & Bergstrom, T. F. 2019. An ABCA4 loss-of-function mutation causes a canine form of Stargardt disease. *PLoS Genet,* 15**,** e1007873.

Marie, M., Bigot, K., Angebault, C., Barrau, C., Gondouin, P., Pagan, D., Fouquet, S., Villette, T., Sahel, J. A., Lenaers, G. & Picaud, S. 2018. Light action spectrum on oxidative stress and mitochondrial damage in A2E-loaded retinal pigment epithelium cells. *Cell Death Dis,* 9**,** 287.

Mata, N. L., Weng J Fau - Travis, G. H. & Travis, G. H. 2000. Biosynthesis of a major lipofuscin fluorophore in mice and humans with ABCR-mediated retinal and macular degeneration. *Proc Natl Acad Sci U S A*.

Mehat, M. S., Sundaram, V., Ripamonti, C., Robson, A. G., Smith, A. J., Borooah, S., Robinson, M., Rosenthal, A. N., Innes, W., Weleber, R. G., Lee, R. W. J., Crossland, M., Rubin, G. S., Dhillon, B., Steel, D. H. W., Anglade, E., Lanza, R. P., Ali, R. R., Michaelides, M. & Bainbridge, J. W. B. 2018. Transplantation of Human Embryonic Stem Cell-Derived Retinal Pigment Epithelial Cells in Macular Degeneration. *Ophthalmology,* 125**,** 1765-1775.

Mihai, D. M. & Washington, I. 2014. Vitamin A dimers trigger the protracted death of retinal pigment epithelium cells. *Cell Death Dis,* 5**,** e1348.

Molday, L. L., Rabin Ar Fau - Molday, R. S. & Molday, R. S. 2000. ABCR expression in foveal cone photoreceptors and its role in Stargardt macular dystrophy. *Nature genetics* 25.

Nakamura, M., Yako, T., Kuse, Y., Inoue, Y., Nishinaka, A., Nakamura, S.,

Shimazawa, M. & Hara, H. 2018. Exposure to excessive blue LED light damages retinal pigment epithelium and photoreceptors of pigmented mice. *Exp Eye Res,* 177**,** 1-11.

Oguchi, Y., Sekiryu, T., Takasumi, M., Hashimoto, Y. & Furuta, M. 2018. Near-infrared and short-wave autofluorescence in ocular specimens. *Jpn J Ophthalmol,* 62**,** 605-613.

Paavo, M., Lee, W., Allikmets, R., Tsang, S. & Sparrow, J. R. 2018. Photoreceptor cells as a source of fundus autofluorescence in recessive Stargardt disease. *J Neurosci Res*.

Parish, C. A., Hashimoto, M., Nakanishi, K., Dillon, J. & Sparrow, J. 1998. Isolation and one-step preparation of A2E and iso-A2E, fluorophores from human retinal pigment epithelium. *Proc. Natl. Acad. Sci. USA,* 95**,** 14609–14613.

Parker, M. A., Choi, D., Erker, L. R., Pennesi, M. E., Yang, P., Chegarnov, E. N., Steinkamp, P. N., Schlechter, C. L., Dhaenens, C. M., Mohand-Said, S., Audo, I., Sahel, J., Weleber, R. G. & Wilson, D. J. 2016. Test-Retest Variability of Functional and Structural Parameters in Patients with Stargardt Disease Participating in the SAR422459 Gene Therapy Trial. *Transl Vis Sci Technol,* 5**,** 10.

Parodi, M. B., Iacono, P., Triolo, G., La Spina, C., Zucchiatti, I., Cicinelli, M. V., Borrelli, E., Manitto, M. P., Martina, E. & Bandello, F. 2015. Morpho-functional correlation of fundus autofluorescence in Stargardt disease. *Br J Ophthalmol,* 99**,** 1354-9.

Polosa, A., Bessaklia, H. & Lachapelle, P. 2017. Light-Induced Retinopathy: Young Age Protects more than Ocular Pigmentation. *Curr Eye Res,* 42**,** 924-935.

Prokopiou, E., Kolovos, P., Kalogerou, M., Neokleous, A., Nicolaou, O., Sokratous, K., Kyriacou, K. & Georgiou, T. 2018. Omega-3 Fatty Acids Supplementation: Therapeutic Potential in a Mouse Model of Stargardt Disease. *Invest Ophthalmol Vis Sci,* 59**,** 2757-2767.

Quazi, F. & Molday, R. S. 2014. ATP-binding cassette transporter ABCA4 and chemical isomerization protect photoreceptor cells from the toxic accumulation of excess 11-cis-retinal. *Proc Natl Acad Sci U S A,* 111**,** 5024-9.

Radu, R. A., Han, Y., Bui, T. V., Nusinowitz, S., Bok, D., Lichter, J., Widder, K., Travis, G. H. & Mata, N. L. 2005. Reductions in serum vitamin A arrest accumulation of toxic retinal fluorophores: a potential therapy for treatment of lipofuscin-based retinal diseases. *Invest Ophthalmol Vis Sci,* 46**,** 4393-401.

Radu, R. A., Hu, J., Yuan, Q., Welch, D. L., Makshanoff, J., Lloyd, M., Mcmullen, S., Travis, G. H. & Bok, D. 2011. Complement system dysregulation and inflammation in the retinal pigment epithelium of a mouse model for Stargardt macular degeneration. *J Biol Chem,* 286**,** 18593-601.

Radu, R. A., Mata, N. L., Bagla, A. & Travis, G. H. 2004. Light exposure stimulates formation of A2E oxiranes in a mouse model of Stargardt's macular degeneration. *Proc Natl Acad Sci U S A,* 101**,** 5928-33.

Radu, R. A., Yuan, Q., Hu, J., Peng, J. H., Lloyd, M., Nusinowitz, S., Bok, D. & Travis, G. H. 2008. Accelerated accumulation of lipofuscin pigments in the RPE of a mouse model for ABCA4-mediated retinal dystrophies following Vitamin A supplementation. *Invest Ophthalmol Vis Sci,* 49**,** 3821-9.

Rattner, A., Smallwood, P. M. & Nathans, J. 2000. Identification and Characterization of All-trans-retinol Dehydrogenase from Photoreceptor Outer Segments, the Visual Cycle Enzyme That Reduces All-trans-retinal to All-trans-retinol. *The Journal of Biological Chemistry,* 275**,** 11034–11043.

Redmond, T. M., Shirley Yu1, E. L., Bok, D., Hamasaki, D., Chen, N., Goletz, P., Ma, J.-X., Crouch, R. K. & Pfeifer, K. 1998. Rpe65 is necessary for production of 11-cis-vitamin A in the retinal visual cycle. *nature genetics,* 20**,** 344-351.

Rotenstreich, Y., Fishman, G. A. & Anderson, R. J. 2003. Visual acuity loss and clinical observations in a large series of patients with stargardt disease. *Ophthalmology,* 110**,** 1151-1158.

Ryter, A. 1985. Relationship between ultrastructure and specific functions of macrophages. *Comp. Immun. Microbiol. infect. Dis. ,* 8**,** 119 133.

Samuel, W., Kutty, R. K., Nagineni, S., Vijayasarathy, C., Chandraratna, R. A. & Wiggert, B. 2006. N-(4-hydroxyphenyl)retinamide induces apoptosis in human retinal pigment epithelial cells: retinoic acid receptors regulate apoptosis, reactive oxygen species generation, and the expression of heme oxygenase-1 and Gadd153. *J Cell Physiol,* 209**,** 854-65.

Sarna, T., Burke, J. M., Korytowski, W., Rozanowska, M., Skumatz, C. M., Zareba, A. & Zareba, M. 2003. Loss of melanin from human RPE with aging: possible role of melanin photooxidation. *Exp Eye Res,* 76**,** 89-98.

Schmitz-Valckenberg, S., Holz, F. G., Bird, A. C. & Spaide, R. F. 2008. Fundus autofluorescence imaging: review and perspectives. *Retina,* 28**,** 385-409.

Schwartz, S. D., Regillo, C. D., Lam, B. L., Eliott, D., Rosenfeld, P. J., Gregori, N. Z., Hubschman, J.-P., Davis, J. L., Heilwell, G., Spirn, M., Maguire, J., Gay, R., Bateman, J., Ostrick, R. M., Morris, D., Vincent, M., Anglade, E., Del Priore, L. V. & Lanza, R. 2015. Human embryonic stem cell-derived retinal pigment epithelium in patients with age-related macular degeneration and Stargardt's macular dystrophy: follow-up of two open-label phase 1/2 studies. *The Lancet,* 385**,** 509-516.

Sears, A. E., Bernstein, P. S., Cideciyan, A. V., Hoyng, C., Charbel Issa, P., Palczewski, K., Rosenfeld, P. J., Sadda, S., Schraermeyer, U., Sparrow, J. R.,

Washington, I. & Scholl, H. P. N. 2017. Towards Treatment of Stargardt Disease: Workshop Organized and Sponsored by the Foundation Fighting Blindness. *Transl Vis Sci Technol,* 6**,** 6.

Sieving, P. A., Chaudhry, P., Kondo, M., Provenzano, M., Wu, D., Carlson, T. J., Bush, R. A. & Thompson, D. A. 2001. Inhibition of the visual cycle in vivo by 13-cis retinoic acid protects from light damage and provides a mechanism for night blindness in isotretinoin therapy. *Proc Natl Acad Sci U S A,* 98**,** 1835-1840.

Simon, W. A., Herrmann, M., Klein, T., Shin, J. M., Huber, R., Senn-Bilfinger, J. & Postius, S. 2007. Soraprazan: setting new standards in inhibition of gastric acid secretion. *J Pharmacol Exp Ther,* 321**,** 866-74.

Sparrow, J. R. & Boulton, M. 2005. RPE lipofuscin and its role in retinal pathobiology. *Exp Eye Res,* 80**,** 595-606.

Sparrow, J. R., Gregory-Roberts, E., Yamamoto, K., Blonska, A., Ghosh, S. K., Ueda, K. & Zhou, J. 2012. The bisretinoids of retinal pigment epithelium. *Prog Retin Eye Res,* 31**,** 121-35.

Sparrow, J. R., Marsiglia, M., Allikmets, R., Tsang, S., Lee, W., Duncker, T. & Zernant, J. 2015. Flecks in Recessive Stargardt Disease: Short-Wavelength Autofluorescence, Near-Infrared Autofluorescence, and Optical Coherence Tomography. *Invest Ophthalmol Vis Sci,* 56**,** 5029-39.

Sparrow, J. R., Nakanishi, K. & Parish, C. A. 2000. The Lipofuscin Fluorophore A2E Mediates Blue Light– Induced Damage to Retinal Pigmented Epithelial Cells. *Invest Ophthalmol Vis Sci,* 41**,** 1981–1989.

Sparrow, J. R., Vollmer-Snarr, H. R., Zhou, J., Jang, Y. P., Jockusch, S., Itagaki, Y. & Nakanishi, K. 2003. A2E-epoxides damage DNA in retinal pigment epithelial cells. Vitamin E and other antioxidants inhibit A2E-epoxide formation. *J Biol Chem,* 278**,** 18207-13.

Stargardt, K. 1909. Ueber familiare progressive Degeneration in der Makulagegend des Augues. . *Albrecht V Graefes Arch Opthamology,* 71**,** 534–550.

Taubitz, T., Tschulakow, A. V., Tikhonovich, M., Illing, B., Fang, Y., Biesemeier, A., Julien-Schraermeyer, S. & Schraermeyer, U. 2018. Ultrastructural alterations in the retinal pigment epithelium and photoreceptors of a Stargardt patient and three Stargardt mouse models: indication for the central role of RPE melanin in oxidative stress. *PeerJ,* 6**,** e5215.

Terman, A. & Brunk, U. T. 1998. On the degradability and exocytosis of ceroid/lipofuscin in cultured rat cardiac myocytes. *Mechanisms of Ageing and Development,* 100**,** 145-156.

Teussink, M. M., Lambertus, S., De Mul, F. F., Rozanowska, M. B., Hoyng, C. B., Klevering, B. J. & Theelen, T. 2017. Lipofuscin-associated photo-oxidative stress during fundus autofluorescence imaging. *PLoS One,* 12**,** e0172635.

Thao, M. T., Renfus, D. J., Dillon, J. & Gaillard, E. R. 2014. A2E-mediated photochemical modification to fibronectin and its implications to age-related changes in Bruch's membrane. *Photochem Photobiol,* 90**,** 329-34.

Trapani, I., Toriello, E., De Simone, S., Colella, P., Iodice, C., Polishchuk, E. V., Sommella, A., Colecchi, L., Rossi, S., Simonelli, F., Giunti, M., Bacci, M. L., Polishchuk, R. S. & Auricchio, A. 2015. Improved dual AAV vectors with reduced expression of truncated proteins are safe and effective in the retina of a mouse model of Stargardt disease. *Hum Mol Genet,* 24**,** 6811-25.

Ueda, K., Zhao, J., Kim, H. J. & Sparrow, J. R. 2016. Photodegradation of retinal bisretinoids in mouse models and implications for macular degeneration. *Proc Natl Acad Sci U S A***,** 6904–6909

Van Der Burght, B. W., Hansen, M., Olsen, J., Zhou, J., Wu, Y., Nissen, M. H. & Sparrow, J. R. 2013. Early changes in gene expression induced by blue light irradiation of A2E-laden retinal pigment epithelial cells. *Acta Ophthalmol,* 91**,** e537-45.

Van Huet, R. A., Bax, N. M., Westeneng-Van Haaften, S. C., Muhamad, M., Zonneveld-Vrieling, M. N., Hoefsloot, L. H., Cremers, F. P., Boon, C. J., Klevering, B. J. & Hoyng, C. B. 2014. Foveal sparing in Stargardt disease. *Invest Ophthalmol Vis Sci,* 55**,** 7467-78.

Voigt, M., Querques, G., Atmani, K., Leveziel, N., Massamba, N., Puche, N., Bouzitou-Mfoumou, R. & Souied, E. H. 2010. Analysis of retinal flecks in fundus flavimaculatus using high-definition spectral-domain optical coherence tomography. *Am J Ophthalmol,* 150**,** 330-7.

Von Ruckmann, A., Fau, F. F. & Bird, A. C. 1995;. Distribution of fundus autofluorescence with a scanning laser ophthalmoscope. *British Journal of Ophthalmology* 79**,** 407-412.

Wajer, S. D., Taomoto, M., Mcleod, D. S., Mccally, R. L., Nishiwaki, H., Fabry, M. E., Nagel, R. L. & Lutty, G. A. 2000. Velocity measurements of normal and sickle red blood cells in the rat retinal and choroidal vasculatures. *Microvasc Res,* 60**,** 281-93.

Wald, G. 1968. Molecular basis of visual excitation. *Science,* 162**,** 230-239.

Wang, Z., Dillon, J. & Gaillard, E. R. 2006. Antioxidant properties of melanin in retinal pigment epithelial cells. *Photochem Photobiol,* 82**,** 474-9.

Warburton, S., Davis, W. E., Southwick, K., Xin, H., Woolley, A. T., Burton, G. F.

& Thulin, C. D. 2007. Proteomic and phototoxic characterization of melanolipofuscin: Correlation to disease and model for its origin. *Molecular Vision,* 13**,** 318-29

Wassell, J., Davies S Fau - Bardsley, W., Bardsley W Fau - Boulton, M. & Boulton, M. 1999. The Photoreactivity of the Retinal Age Pigment Lipofuscin. *Journal of Biological Chemistry,* 274**,** 23828–23832.

Watson, M. L. 1958a. Staining of tissue sections for electron microscopy with heavy metals. *J Biophys Biochem Cytol.,* 4**,** 475-478.

Watson, M. L. 1958b. Staining of tissue sections for electron microscopy with heavy metals. II. Application of solutions containing lead and barium. *J Biophys Biochem Cytol. ,* 4**,** 727-730.

Weng, J., Mata, N. L., Azarian, S. M., Tzekov, R. T., Birch, D. G. & Travis, G. H. 1999. Insights into the Function of Rim Protein in Photoreceptors and Etiology of Stargardt's Disease from the Phenotype in abcr Knockout Mice. *Cell,* 98**,** 13-23.

Wu, L., Ueda, K., Nagasaki, T. & Sparrow, J. R. 2014. Light damage in Abca4 and Rpe65rd12 mice. *Invest Ophthalmol Vis Sci,* 55**,** 1910-8.

Wu, Y., Fishkin, N. E., Pande, A., Pande, J. & Sparrow, J. R. 2009. Novel lipofuscin bisretinoids prominent in human retina and in a model of recessive Stargardt disease. *J Biol Chem,* 284**,** 20155-66.

Wu, Y., Yanase, E., Feng, X., Siegel, M. M. & Sparrow, J. R. 2010. Structural characterization of bisretinoid A2E photocleavage products and implications for age-related macular degeneration. *Proc Natl Acad Sci U S A,* 107**,** 7275-80.

Zhao, J., Ueda, K., Riera, M., Kim, H. J. & Sparrow, J. R. 2018. Bisretinoids mediate light sensitivity resulting in photoreceptor cell degeneration in mice lacking the receptor tyrosine kinase Mer. *J Biol Chem,* 293**,** 19400-19410.

Zhou, J., Jang, Y. P., Kim, S. R. & Sparrow, J. R. 2006. Complement activation by photooxidation products of A2E, a lipofuscin constituent of the retinal pigment epithelium. *Proc Natl Acad Sci U S A,* 103**,** 16182-7.

Zhou, J., Kim, S. R., Westlund, B. S. & Sparrow, J. R. 2009. Complement activation by bisretinoid constituents of RPE lipofuscin. *Invest Ophthalmol Vis Sci,* 50**,** 1392-9.

Zhou, J., Ueda, K., Zhao, J. & Sparrow, J. R. 2015. Correlations between Photodegradation of Bisretinoid Constituents of Retina and Dicarbonyl Adduct Deposition. *J Biol Chem,* 290**,** 27215-27.

8. Declaration of Contributions

The dissertation work was carried out at the division of experimental vitreoretinal surgery, center for ophthalmology, institute of ophthalmic research under the supervision of Prof. Dr. rer. nat. Ulrich Schraermeyer.

The study was designed by Prof. Ulrich Schraermeyer and PD Dr. rer. nat. Sylvie Julien-Schraermeyer.

ERG and cSLO/OCT were carried out by me with the assistance of Dr. Alexander Tschulakow. The blue light model was carried out by me with the assistance of Tatjana Taubitz. I carried out the rest of the experiments independently. Statistical analysis was carried out independently by me.

I confirm that I wrote the thesis myself under the supervision of Prof. Ulrich Schraermeyer.

Signed_____

on _____ in Tübingen

9. Acknowledgment

Hereby I want to express my immense gratitude to my supervisor Prof. Dr. Ulrich Schraermeyer for giving me the opportunity to work on the project and supervising me as well as being kindly open for discussion. I also would like to thank PD Dr. Sylvie Julien-Schraermeyer, who planned and supervised the project as well. They give me continuous encouragement and help me a lot in life and work.

Biggest thanks to Tatjana Taubitz, who helps me a lot and has been a wonderful colleague and advisor. I am very grateful to Dr. Alexander Tschulakow for all the assistance he offered during my period in the lad.

Special thanks to Monika Rittgarn, Dr. Barbara Illing and Antonina Burda for their excellent technical assistance. Thanks to Dr. Antje Biesemeier for her guidance of experimental safety and her technical supports. I am also grateful to Judith Birch, who help me a lot in the paper work. Many thanks to Shan Liu for her great support in both professional and personal life.

Again, thanks to all the above from the Division of Experimental Vitreoretinal Surgery for the warm and friendly environment in the lab and making me feel at home.

I would like to thank the China Scholarship Council for its financial support.

My special thanks to my family (my parents, my sister, my brother-in-law and my niece) for giving me support all the time. They all keep encouraging me to keep up my spirit. Thanks to my friend Kshitij Agarwal, Wang min, Xiaomin, Leilei, Chenhao, Gaoji, Yapeng, Yanjun……for their support and company.

I love you all.